Metamorphism in the Contact Aureole of the Eastern Limb of the Bushveld Complex, South Africa

Philani Knowledge Mavimbela

Submitted for a degree of Master of Science in the Faculty of Agriculture and Natural Science

Department of Geology

University of Pretoria

Supervisors

Dr. James Robert

Dr. Gelu Costin

Dr. Martin Rigby

2013

UNIVERSITEIT VAN PRETORIA
UNIVERSITY OF PRETORIA
YUNIBESITHI YA PRETORIA

Declaration of originality

I Philani Knowledge Mavimbela fully declare that this thesis is my own original work. Where other people's work has been used (either from a printed source, internet, or any other source), this has been properly acknowledged and referenced in accordance with the departmental requirements.

I have not used work previously produced by another student or any other person to hand in as my own.

I have not allowed, and will not allow, anyone to copy my work with the intention of passing it off as his or her own work.

Signature……

Dedication

I dedicate this work to uLwazi lweMvelo my sons, all my siblings and my extended family.

"We must remember that intelligence is not enough. Intelligence plus character-that is the goal of true education. The complete education gives one not only power of concentration, but worthy objective upon which to concentrate. "

Martin Luther King, Jr.

"Science investigates and religion interprets. Science gives man knowledge, which is power; religion gives man wisdom which is control. Science deals mainly with facts; religion deals with values. The two are not rivals."

Martin Luther King, Jr.

Acknowledgements

There are a lot of people that deserve to be thanked for their contributions in completing this study. I am indebted to God almighty and everyone else for help and encouragements during the course of this thesis. First of all, I will start by thanking Dr. Rigby who initiated this study. Dear Martin, it has to be said that your enthusiasm provided a highly stimulating and motivating atmosphere for scientific research. Many thanks also goes to Dr. Roberts, who even though this study was outside of his field of expertise but still provided guidance and corrections/ suggestions for improvements of the draft chapters over the course of the project. My sincere gratitude also goes to Dr. Costin, who helped me with restructuring this work, corrections/ suggestions and guidance in the later stages of this study, not forgetting all the late hours we had in the lab with Kea. Your insightful knowledge and enthusiasm in elucidating geological processes was very inspiring. I very much enjoyed all the days I spent in Grahamstown, you had no reason to help me but you still did anyway and I will be forever grateful for that. Thank you for your warm hospitality and entertaining evenings together with Lolly and Kea.

Denni and Yolande Raubenheimer accompanied me during my field visit; I thank Denni again for sharing old sources of the study area. Thanks also go to the previous and current stoneman team at the University of Pretoria for their assistance with polished thin-section preparation, EPMA, XRF and XRD.

Dr. Zeh and Gerdes are also thanked for preparation of Lu-Hf analysis from garnets used in chapter 3.

I will also like to thanks the Postgraduate Mentorship Bursary for financial support during the first two years of this study and Prof Eriksson for additional financial support and motivation during the course of the study. Discussions on various topics with Mokete, Mimi, Keorapetse and Thembelani during our honours year also motivated me to pursue a Master's degree, not forgetting various discussions which I have had with Montasir, since 2011. I thank Mrs de Swart and Mrs Rajab for their administrative support, Philemon Tsela for technical support. Prof Merkle is thanked for ploughing the seed during my undergraduate days. I will like to thank all my colleagues at the Department of Geology (UP) for their various contributions to this thesis.

Lastly but not least, I will like to thank my family, especially my wife (Mojabeng) for encouragement and support in so many ways to the accomplishment of this dissertation.

ABSTRACT

The 2.06 to 2.054 Ga Bushveld Igneous Complex intruded into the sedimentary rocks of the Transvaal Supergroup and generated an extensive contact metamorphic aureole mainly developed in the upper Pretoria group. The studied samples represent the Silverton Daspoort and Timeball Hill formations and are divisible into garnet bearing hornfels (DY918, DY954 and DY956) and garnet-free staurolite-bearing metapelites (DY916, DY982 and DY987). The garnet-bearing hornfelses marks the garnet zone within the aureole and the garnet formation is controlled by different reactions forming from 490 to 630 ^{0}C. On the other hand, the garnet free staurolite-bearing Fe-Al rich metapelites define the staurolite zone restricted to the Timeball Hill formation. The recorded P-T conditions in G0 and G1 garnets of the DY954 hornfels imply that the two garnets formed under different conditions indicating two stages of metamorphism. However, the Lu-Hf isotope systematics of these garnets records a 2061 Ma age for all garnet porphyroblasts in both the DY918 and DY954 hornfelses, which support co-genetic garnet growth regardless of their stratigraphic positions. Therefore, the 2061 Ma garnet age denote the emplacement age of the Lower Zone and Critical Zone magmas which was synchronous with the extrusion of the Rooiberg Group volcanics. The fact that all analysed garnets do not record the 2059 – 2054 intrusion of the Main Zone and Upper Zone magmas probably means that the crystallisation temperatures of the later magma pulse was not significant enough to shift the Lu-Hf isotopic signatures. Euhedral staurolites are widespread within the Fe-Al rich metapelites with grain sizes of up 4mm; texturally the majority of them have been altered or overgrown by biotite and chloritoid. The alteration or of these staurolite porphyroblasts is due to isobaric cooling during uplift, and the St-Bt assemblage represent the peak equilibrium conditions and marks the upper stability limit of the Chl-Ctd assemblage.

Table of Contents

List of tables

List of figures

Thesis structure

Chapter 1

- Provides a brief review of the published metamorphic studies in the BC contact aureole, which includes a compilation of some of the published P-T conditions in the Eastern Bushveld contact aureole
- Aims and objectives of the project
- Sampling
- Methodology

Chapter 2

- Dating of garnet crystallisation to constrain the age of the contact metamorphism and indirectly brackets the emplacement age of the Rustenburg Layered Suite, using Lu-Hf isotopic systematics of garnets from the underlying Silverton and Daspoort formation of the Pretoria Group

Chapter 3

- Estimates the P-T conditions of garnet bearing hornfels using pseudosection approach (garnet isopleth thermobarometry) and classical geothermobarometry.

Chapter 4

- Discusses the P-T-X evolution of garnet and andalusite free staurolite-bearing Fe-Al rich metapelites using pseudosection and classical geothermobarometry.
- This include inferring staurolite forming reactions

Chapter 5

- Discussion and conclusion remarks of all chapters

Chapter 1

A brief review of metamorphism in the Bushveld Complex contact aureole

1.1 Introduction

The ~ 2.06 Ga Bushveld Igneous Complex (BC) famously contains the world's largest layered mafic-ultramafic intrusion, termed the Rustenburg Layered Suite (RLS), which in turn is host to the world's largest ore reserves of platinum group elements, chromium and vanadium (Cawthorn and Walraven, 1998; Cawthorn et al., 2006). Additionally, the BC contains arguably the world's most voluminous body of felsic volcanics and associated granitoid intrusive rocks, which are subdivided into three distinct groups known as the Rooiberg Group, Rashoop Granophyre Suite and Lebowa Granite Suite as shown in figure 1-1 (SACS, 1980; Robb et al., 1994; Hatton & Schweitzer, 1995; Cawthorn et al., 2006).

According to Hall (1932) the metamorphic effect of the complex are so vast and so intense in more or less profoundly changing the appearance of the Transvaal sediments (predominantly Pretoria group) through thousands of meters in thickness, such that no description of the Bushveld Complex will be complete without taking into account the metamorphism which it gave rise to.

Metamorphic studies of the BC contact aureole can provide constraints on the thermal history and can also help bracket the emplacement time of the intrusion. Furthermore, studies of mineral assemblages of rocks from the aureole will help determine the different metamorphic zones developed within the aureole. This chapter attempt to review the currently published P-T database with a view of comparing them to the result obtained from this study.

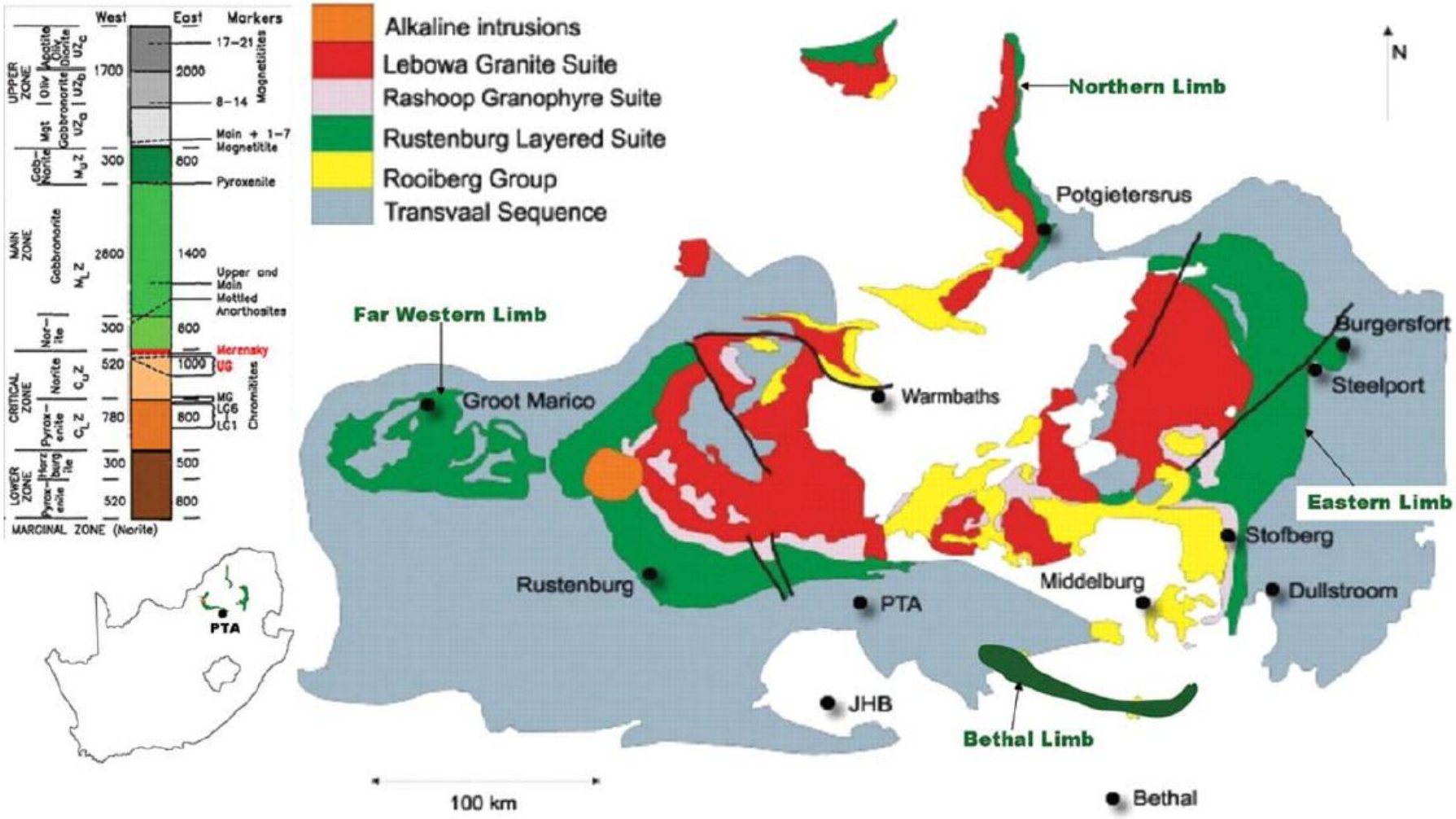

Figure 1-1. A map showing the geology of the Transvaal Supergroup and the Bushveld Complex (Campbell, 2011)

1.2 Geologic background

The Bushveld Complex (BC) occurs in the northern Kaapvaal Craton, north eastern part of South Africa (Figure 1-1) and covers an area of ~ 65, 000 km^2 produced by an estimated magma volume of ~0.38 M km^3 (Eales and Cawthorn, 1996; Cawthorn and Walraven, 1998). The Bushveld magmatism is stratigraphically represented by five successive discrete groups of rocks from the base upward; (1) the 2.046 - 2.042 Ga mafic sills which intrude the country rock sediments, (2) the 2.059 - 2.054 Ga ultramafic to mafic Rustenburg Layered Suite (RLS), (3) the 2.055 - 2.053 Ga Rashoop granophyre suite, (4) the 2.054 Ga Lebowa granite suite, and (5) the 2.06 – 2.061 Ga acidic Rooiberg group volcanic suite (SACS, 1980; Schweitzer et al., 1997; Rajesh et al, 2013 and references herein). The BC outcrops are then represented by five compartments; the eastern, western, northern/Potgiesterus, south-eastern/ Bethal and far western limbs (Du plessis and Walraven, 1990). Furthermore, the RLS can be subdivided into five zones; the Marginal, Lower, Critical, Main and the Upper zones (Figure 1-1) (Hall, 1932). The BC is likely to have consisted of three main episodes of magmatism; the ~2.061-2.060 Ga, ~2.059-2.054 Ga and ~2.046-2.042 Ga (Rajesh et al., 2013). The second pulse which represent the 7-9 km thick, shallow dipping, interconnected sheet of layered ultramafic to mafic rocks of the RLS, enjoyed a much longer period of magmatism forming as a series of consecutive sub magma pulses that enjoyed a temperature range of 1300 ^{0}C to 1160 ^{0}C (Cawthorn and Walraven, 1998; Rajesh et al., 2013). Rajesh et al. (2013) further postulate that two sub magma pulses were responsible for the layered ultramafic to mafic RLS with the first pulse forming the Lower Zone to lower Critical Zone and Upper Critical to lower Main Zone while upper Main Zone and Upper Zone represent the intrusion of the last magma pulse.

The RLS intruded into the upper part of the pre-existing Transvaal basin-fill during below the Rooiberg group volcanic suite (Eriksson et al., 1999 and references therein). The intrusion resulted into a development of an extensive but poorly exposed metamorphic contact aureole at the base of the RLS, more predominantly within the Pretoria group sediments (Johnson et al., 2003). The strata of the argillaceous and arenaceuos Pretoria group rocks comprises of Timeball Hill, Daspoort, Silverton, Magaliesburg, Vermont and Lankenvalei formations from stratigraphic base upwards as shown in figure 1-2 (Johnson et al., 2003).

The Pretoria group overlies the carbonaceous Chuniespoort group which is strongly thermally metamorphosed in the northern limb (Buick et al., 2004) due to the variable exposure of the floor rocks in the northern limb. The contact aureole is the thickest in the eastern limb and extends for ~ 25 km along strike from the contact, which corresponds to a true distance of ~ 5 km from the contact (Johnson et al., 2003). In the western limb where the Pretoria Group as well as the underlying dolomite experienced the thermal effects of the intrusion, the extent of the aureole is unknown (Saggerson and Turner, 1995). The true width of the northern limb where the thermal metamorphic effects reaches the underlying Archean basement is also unknown (Saggerson and Turner, 1995).

According to Waters and Lovegrove (2002), the bulk X_{Mg} [molar Mg/ (Mg+Fe)] of the Pretoria Group metapelites shows a systematic increase towards the contact and is represented by a change from andalusite to cordierite dominated assemblages. The Timeball Hill formation can be divided into three major units; the lower pelitic/shale unit, Klapperkop quartzite member and upper pelitic/shale unit with a thickness of about 1400, 100 and 180 m respectively (Nell, 1984; Uken, 1998 etc.). The two pelitic members are made of Fe and Al rich graphitic shale, mudstone and siltstone (Nell, 1984). The lower Timeball Hill pelitic rocks are highly enriched in Al_20_3 and slightly enriched in Fe_20_3 (t), accompanied by depletion in Mg0, Ca0 and Na_20 (Reczko, 1994). The upper pelitic member also exhibits relative enrichment in Al_20_3 and depletion of Mg0, Ca0 and Na_20 with a slight enrichment in P_20_5 content as compared to the lower pelitic member (Reczko, 1994).

Porphyroblasts (up to 5mm) of staurolite are common together with some biotite flakes which are visible on hand specimen (Uken, 1998). The metamorphic grade increases upward with the lower pelitic unit characterised by chloritoid associated with an andalusite-staurolite-biotite assemblage (Nell, 1984, 1985). The upper pelitic units are characterised by high grade mineral assemblages of cordierite-garnet (almandine)-biotite-sillimanite-spinel and minor corundum (Nell, 1984, 1985 and Uken, 1998). According to Nell (1984, 1985) the presence of sillimanite and garnet in the upper unit may imply melting.

The Boshoek formation overlying the Timeball hill consists of basal conglomerate and diamictite (Button, 1973) and it immediately underlies the Hekpoort andesite formation. Overlying the former is the Dwaalheuwel quartzite formation consisting of basal conglomerate, quartzite and intercalated thin layer of shale (Nell, 1984). The Strubenkop formation comprises of shale and mudstone (metapelites) which exhibit a pronounce enrichment in Al_20_3 and Fe_20_3 accompanied by moderate to strong depletion of $Si0_2$, Mg0, Mn0, K_2O, Ca0 and Na_20 (Nell, 1984; Reczko, 1994).

The Strubenkop formation is characterised by a mineral paragenesis of andalusite-fibrolite-biotite-chlorite-cordierite-Kfeldspar which exhibit an increasing metamorphic grade upward (Nell, 1984, 1985; Uken, 1998).

The Silverton shale formation is subdivided into three units; the basal Boven shale, middle Machadodorp and upper Lydenburg shale members (Eriksson et al., 2001). These members preserves a 500 m thick pelitic rocks, 10-30 m thick calc-silicates rocks with occasional graphite rich pelites at the base and 400 m pelitic rocks respectively (Uken, 1998). The Boven shale member is chiefly made up of a chiastolite-fibrolite-biotite-andalusite assemblage and is enriched in $Si0_2$ but depleted in Fe_20_3 (t), Mn0, Mg0, Ca0 and K_20 compared to an average shale estimate and this is also true for the Lydenburg shale member (Reczko, 1994 and Uken, 1998). Furthermore, a mineral assemblage of cordierite-antophyllite-cummingtonite has been noted together with a development of andalusite-Kfeldspar-orthopyroxene-clinopyroxene assemblage with increasing metamorphic grade towards the intrusion (Nell, 1984, 1985 and Uken 1998). The pyroxenes are more common where the formation is in contact with the RLS and are accompanied by the development of a migmatite texture (Nell, 1984, 1985 and Uken 1998).

The 200 – 300 m thick Magliesburg quartzite forms the immediate floor to the RLS in some areas and passes gradational upwards into a succession of pelitic and semi-pelitic rocks of the 300 m thick Vermont formation which is about (SACS, 1980). The semi-pelitic and pelitic units exhibit development of migmatite texture with a common cordierite-fibrolite assemblage and an occasional development of high grade orthopyroxene bearing pelites. Lastly the uppermost noticeable unit in the Pretoria group is the Lakenvalei quartzite formation (Uken, 1998).

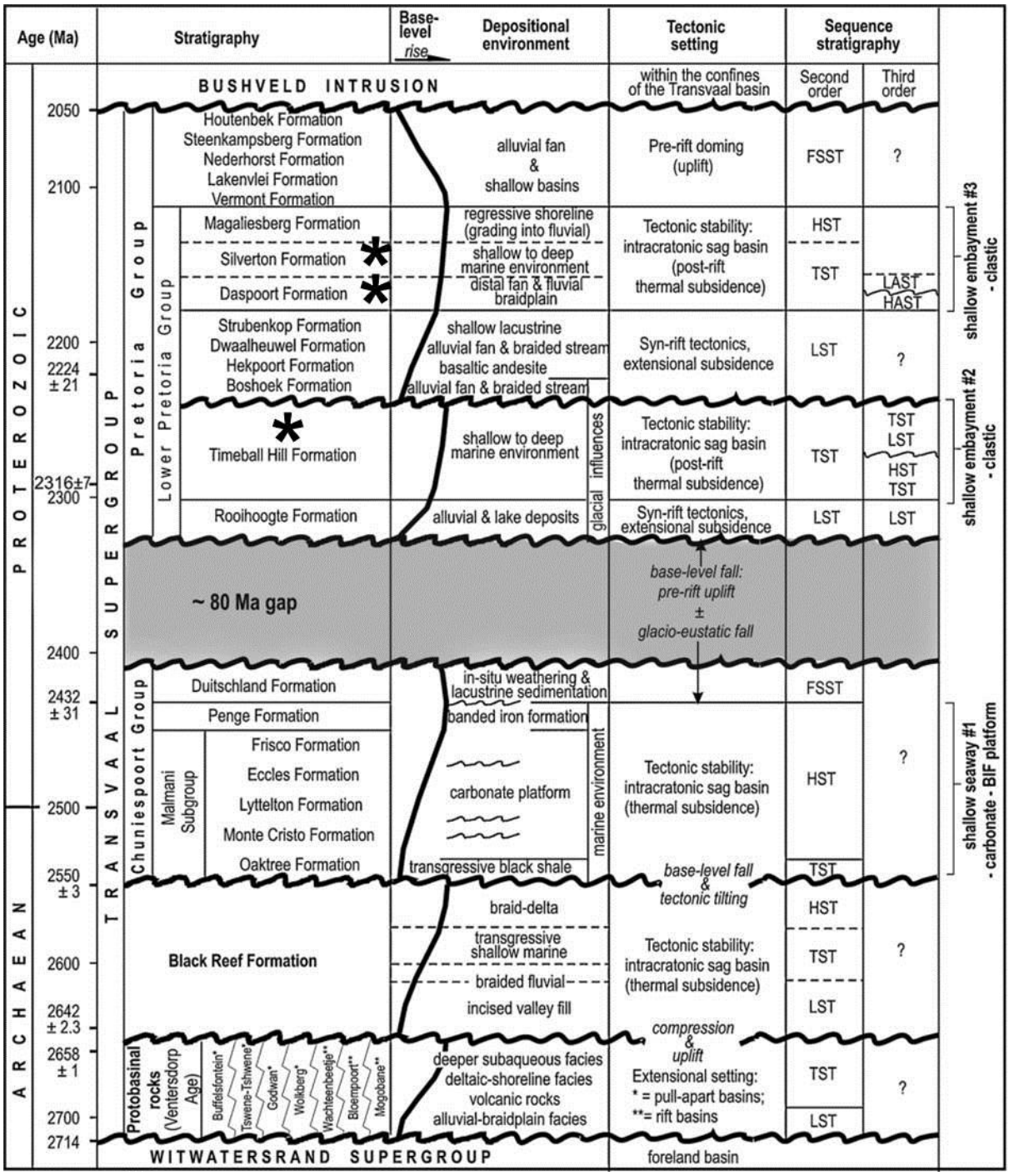

Figure1-2. Summarized stratigraphy of the Transvaal Supergroup (Eriksson et al., 2001), the stars represent formation which were sampled (see figure 1-3 for the actual position of the samples.

1.3 A brief overview of metamorphism in the contact of the Bushveld Complex

The majority of the studies of the contact aureole have focused on the eastern limb owing to its greater thickness as compared to the other two limbs.

Human (1975) suggested a poly-metamorphic history for the contact by arguing that the high grade sillimanite-bearing assemblages in the Havercroft area, NW of Penge (NE Bushveld) were produced by pre-Bushveld mafic sills and only the albite-epidote to hornblende hornfels facies assemblages were produced as a consequence of intruding mafic magmas associated with the RLS. Based on constructed P-T grids and the presence of staurolite and cordierite in the lower grade rocks, Human (1975) concluded that the peak metamorphism caused by the BC occurred at temperatures of 500-530 ± 10 ºC and pressures between 1-2 kbar.

Hulbert and Sharpe (1981) noted that the pressure in the eastern limb varies from around 4 kbar near Lydenburg up to a maximum of 5.3 kbar in areas immediately adjacent to Burgersfort. Furthermore, using garnet-biotite and cordierite-biotite Fe-Mg exchange thermometry they inferred isotherms of 500, 600 and 700 ^{0}C (reaction 1 and 2). Utilizing the same equilibria Sharpe (1982) expanded on the earlier work and obtained various P-T estimates from eastern limb ranging from 500-1150 ^{o}C and 3.5-5.3 kbar (Figure 1-3).

Plagioclase = garnet + sillimanite + quartz (Ghent, 1976) (1)

Cordierite = garnet + sillimanite + quartz (Wood and Fraser, 1976) (2)

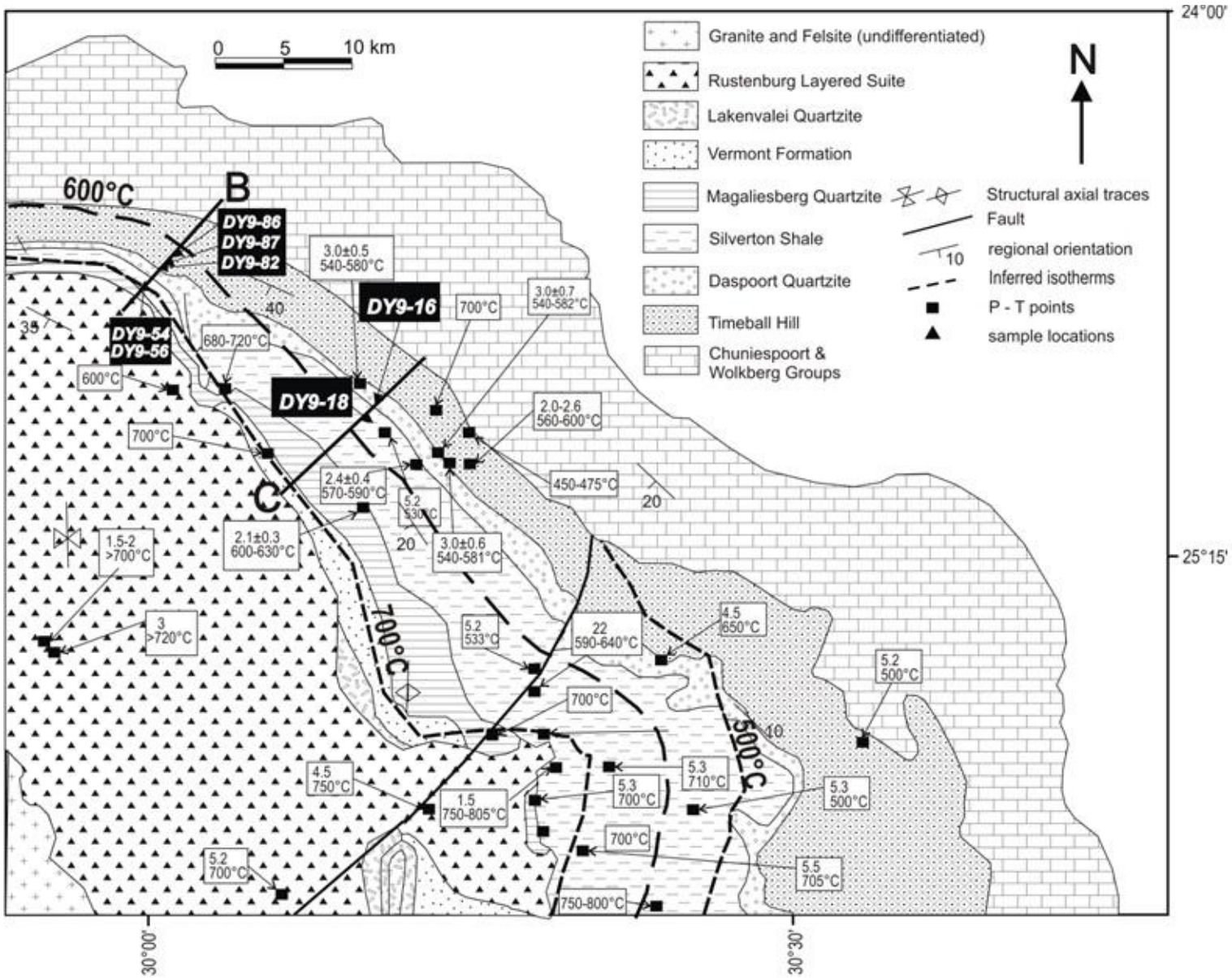

Figure 1-3. A map showing the eastern limb contact aureole, several published P-T data and postulated isotherms (after Sharpe and Chadwick, 1982; Harris et al., 2003).

Hartzer (1987) estimated metamorphic conditions recorded in argillaceous and calc-silicate rocks of the Crocodile River Fragment present in the western BC contact aureole) (Figure 1- 1). He identified two mineral assemblages, useful for thermobarometric inferences, in the argillites; (1) muscovite + quartz + chlorite + K-feldspar and (2) andalusite, biotite + muscovite + quartz. These assemblages yielded temperatures of 470-620 ^{0}C at 0.25 kbar. Additionally, for the calc-silicates, he inferred the operation of the following two reactions;

$$3 \text{ dolomite} + 4 \text{ quartz} + H_2O = 1 \text{ talc} + 3 \text{ calcite} + 3\ CO_2 \quad (3)$$

$$5 \text{ talc} + 6 \text{ calcite} + 4 \text{ quartz} = 3 \text{ tremolite} + 6\ CO_2 + 2\ H_2O \quad (4)$$

Reaction (3) occurred from 400 to 490ºC and 520 ºC at 1 and 2.5 kbar respectively. Reaction (4) occurred at temperatures between 450-530 ºC at 0-2.5 kbar. However, based on the absence of diopside, he inferred a temperature range between 470-530 ºC. These reactions were based on earlier work by Winkler (1976).

Miyano et al. (1987) suggested that the amphibolite sills in the Penge Iron Formation, post-date the peak metamorphism caused by the intrusion of the RLS. This proposal was based on the discovery of a hornblende-clinopyroxene-fayalite assemblage that appear to overprint an earlier grunerite-bearing assemblage which formed in response to the intrusion of the different zones in the RLS.

A two-stage metamorphic history corresponding to discrete thermal events related to the intrusion of the different zones in the RLS was inferred by Walmach et al. (1989). They suggested that peak temperatures in calc-silicate xenoliths in the RLS near Steelpoort (NE Bushveld) had exceeded 1200 ºC and pressures of 0.6-1.6 kbar and 1.1-2.4 kbar (Figure 1-1). The low pressure range was interpreted to represent the emplacement of the Critical Zone, whilst the latter was attributed to the emplacement of the Main Zone.

Kaneko and Miyano (1990) calculated pressure and temperature estimates for two stratigraphic levels containing metapelites of the Pretoria Group near. Stratigraphically these two levels occur 1.7 and 2.9 km below the BC- Pretoria Group contact, respectively. The pressure estimates were based on the following equilibrium reaction:

$$\text{Anorthite} = \text{grossular} + \text{andalusite} + \text{quartz} \quad (5)$$

The method of Newton and Haselton (1981) was employed along with the experimental dataset of Koziol and Newton (1988) to yield pressures of 2.0-2.3 kbar for the shallower stratigraphic level and ~2.6 kbar for the deeper level. The temperature estimates were based on the following equilibria;

$$\text{Almandine} + \text{phlogophite} = \text{pyrope} + \text{Fe-cordierite} + H_2O \qquad (9)$$

$$\text{Almandine} + \text{Mg-cordierite} = \text{pyrope} + \text{Fe-cordierite} \qquad (10)$$

The method of Hodges and Spear (1982) was utilized for Reaction 6 and produced temperatures of 560 - 570 ºC for the shallower stratigraphic level and 540 ºC for the deeper level. For Reaction 10, the method of Thompson (1976) was used and recorded similar temperature estimates to Reaction 9.

Uken (1998) worked on the northern portion of the eastern Bushveld aureole (Figure 1-3), where he applied garnet-biotite (Thompson, 1976; Holdaway and Lee, 1977; Ferry and Spear, 1978) and garnet-cordierite thermometry (Thompson, 1976; Wells, 1976; Holdaway and Lee, 1977; Wells, 1979), garnet-staurolite barometry (Perchuk, 1977) and the petrogenetic grid of Dymoke and Sandiford (1992). The assemblage of cordierite - staurolite - biotite - muscovite - quartz recorded equilibrium P-T conditions of 535-563 ºC at 2.8-3.2 kbar.

Mizumo et al. (1999) studied melt textures in orthopyroxene bearing hornfels sampled within the Vermont formation about 1.5 km from the intrusion. They inferred that these samples experienced temperature of about 700^0C since they occurred close to the 700^0C isotherm estimated by Sharpe and Chadwick (1981). In a study of micro-structures and mineral chemistry of metapelitic rock from the Timeball Hill formation north of Burgersfort; Kaneko et al. (2000) reported an occurrence of andalusite and staurolite ghost and pseudo-morphs structures in a mineral assemblage of biotite-garnet-staurolite-andalusite-plagioclase-muscovite-chlorite-quartz. They concluded that these pseudomorphs and ghost structures which are restricted to the Timeball Hill formation formed by the consumption of Al-bearing minerals at the same time as the staurolite and andalusite poikiloblasts were forming. They further noted zoning in garnet exhibiting Fe-Mn enriched cores and Ca-Mg enriched rims.

Pitra and de Waal (2001), while working on the metapelitic rock from the marble hall Fragment reported a two stage LP-HT metamorphism. This was based on the occurrence of distinct mineral paragenesis forming under different conditions; (1) chiastolite-andalusite-cordierite-biotite-garnet-quartz which equilibrated at 550 - 600 ^{0}C during the intrusion of the multiphase RLS.

The intrusion of the hot Nebo granite marked the peak metamorphism which transformed the assemblage to (2) garnet-cordierite-biotite-K-feldspar-quartz, sillimanite-cordierite-K-feldspar-quartz and quartz under-saturated cordierite-spinel symplectite which replaced the chiastolite porphyroblast. Using the KFMASH pseudosection they concluded that these assemblages were formed by rapid heating at constant pressure and temperature of about 720 ^{0}C which was not associated with widespread fluid absent melting.

Waters and Lovegrove (2002) studied the staurolite-biotite-cordierite hornfelses of the Eastern Limb contact aureole in an attempt to gain insight on the relative timing of porphyroblast and metamorphic reactions that took place. They used mineral microstructures, phase equilibrium relations and calculated mineral nucleation rates; upon which they concluded that the formation of andalusite and staurolite from the muscovite, chlorite and chloritoid breakdown reactions was as a result of critical temperature overstepping (30-40 ^{0}C).

Harris et al. (2003) studied the migmatite zone of the eastern Bushveld aureole and reported the occurrence of granite sheets and veins which formed due to fluid enhanced, incongruent biotite melting of the underlying Silverton formation during prograde metamorphism of temperature exceeding 700 ^{0}C. In another study of the migmatite zone in the eastern contact aureole, Johnson et al. (2003) noted that migmatites beneath the BC preserved evidence for water under-saturated and saturated melting. This was evident from leucocratic patches and macroscopic discordant leucosomes which formed by incongruent melting of biotite and congruent melting that was catalysed by a structurally controlled H_2O rich volatile derived from underlying dehydrating rock respectively. Furthermore, Johnson et al. (2004) performed a detail study of migmatised andalusite and symplectite bearing metapelitic rock sampled in the Phepane dome in the north eastern part of the BC aureole. They reported that spinel- cordierite partially replaces andalusite in their studied metapelitic rocks, and with the aid of a MnNCKFMASHT pseudosection, they concluded that fluid absent melting reactions consuming andalusite and biotite were responsible for the formation of cordierite moats surrounding andalusite. The reaction proceeded until quartz was completely consumed and at around 720 ^{0}C spinel started growing together with cordierite.

Kaneko et al. (2005) studied the crystal size distribution of garnets in the eastern BC aureole and reported that the crystal size distribution shapes of these garnets showed a log normal to a qausi-log normal distribution. Based on this they concluded that these garnets were formed by decaying-rate nucleation and surface controlled growth rather than the Ostwald ripening, which was to be expected in an aureole that experienced a relatively long lived thermal history. Using several geothermometers and the GASP geobarometer, they estimated a temperature increase from 440 - 490 ^{0}C along the margins to 800 - 840 ^{0}C close to the contact. Furthermore they noted that the geothermal gradient vertical to the strike of the Pretoria Group sediments is 60 to 90 ^{0}C/km.

Nell (1985) suggested two stages of metamorphism are preserved near Potgietersrus (southern part of Northern Limb) (Figure 1-3). He determined that initial maximum temperatures of 750 ºC were reached at 1.5 kbar based on cordierite - olivine - orthopyroxene ± spinel ± quartz assemblages. The inferred second stage of metamorphism, occurring at approximately 850-900 ºC and 4 to 5 kbar was deduced from Reaction 4-5:

Garnet + cordierite + orthopyroxene + biotite (3)

Clinopyroxene + plagioclase + quartz (4)

Cordierite + spinel ± sillimanite ± corundum ± orthopyroxene ± olivine (5)

He interpreted these two stages of metamorphism to be reflecting two major magma pulses; the first low pressure event corresponding to the emplacement of the Lower Zone, whilst the higher pressure phase corresponds to the emplacement of the Critical, Main and Upper Zones.

Johnson et al. (2010) integrated field work, petrography and bulk rock composition with pseudosection modeling to investigate metamorphic evolution of quartz absent Fe rich aluminous metapelitic xenoliths. The xenoliths occur within the Platreef (Northern Limb) magmatic rocks and are assumed to represent remnants of Timeball Hill formation sediments. They subdivided the xenoliths into low and high grade; the low grade rocks includes metastable low grade hydrous phase (chlorite, muscovite, chloritoid) which were rapidly heated and resulted in a formation of corundum and / spinel rich micro-diatexite. The rapid partial melting caused the xenolith composition to be depleted of K_2O and H_2O and accounted for more than 50% melt loss (Johnson et al., 2010). The cores of the xenoliths record\ slow temperature increase, resulting from prograde continuous equilibration and subsequent loss of fluids due to subsolidus dehydration reactions (Johnson et al., 2010).

Engelbrecht (1976) studied the metamorphic aureole in the area north-east of Zeerust, along the far-western (Nietverdiend) limb of the BC and identified that the mineral assemblages are characteristic of the hornblende-hornfels facies formed under 530-630 ^{0}C at < 2.5 kbar. From the western-most lobe, Engelbrecht (1990) gave thermobarometric evidence for peak metamorphic conditions between 646 - 760 ^{0}C and 2.1 - 3.2 kbar. The pressure estimates were obtained from orthopyroxene-garnet-cordierite-biotite-plagioclase-quartz assemblages by applying the barometers of Bowlen et al. (1983), Newton and Perkins (1982), Perkins and Chipera (1985) and Powell and Holland (1988). The temperature estimates were calculated from garnet - biotite pairs, according to the method of Ferry and Spear (1978), as well as by garnet - cordierite thermometry outlined by Thompson (1976), Ferry and Spear (1978), Holdaway and Lee (1977) and Perchuk et al. (1981).

1.4 Metamorphic zoning in the BC contact aureole

One of the first characterizations of the metamorphic zoning within the BC contact aureole was proposed by Willemse (1959) using whole-rock geochemical data phase equilibrium and metamorphic facies principles (e.g. Eskola 1939).

Hammerbeck (1986) subdivided the aureole of the south-western part of the Western limb (Figure 1-1) into four zones (A-D) based on rock types and characteristic minerals. Zone A consists of 'slate' that contains modally abundant chiastolite and biotite with moderate amounts of epidote and cordierite. Zone B, the largest area of outcrop, consists of blue, grey and green biotite- and chiastolite-bearing slates, which are similar to those of Zone A, except that cordierite is absent. Zone C is reportedly characterised by primary andalusite growths that are, in part, pseudomorphed by quartz and sericite. Finally, Zone D is characterised by spotted slates with characteristic anhedral biotite and completely altered andalusite/chiastolite.

Furthermore, Hammerbeck (1986) defined five zones (A-E) in the aureole of the eastern limb. Zone A occurs in the region of Malipsdrif (NE Bushveld) (Figure 1-1) and is reported to record regional metamorphism. This zone is bound in the south and north-west by shear zones and consists of cordierite- and sillimanite-bearing schists. Zone B is restricted to the north of Burgersfort characterised by a fine-grained, dark-coloured, cordierite-bearing metapelites, which are interpreted to have formed as a result of contact metamorphism (Figure 1-1).

Zone C stretches over most of the eastern Bushveld Complex aureole and contains a variety of assemblages including chiastolite-muscovite-biotite, garnet-staurolite-biotite and chiastolite-staurolite-biotite metapelites. At lower grades, Zone D is characterised by chloritoid-bearing metapelites. Zone E consists of chiastolite-bearing 'spotted slates'. Furthermore, he described the metamorphic rocks along the north-western margin of the BC surrounding; in this area the metapelites of the Silverton Formation are characterised by fine-grained, dark-grey, cordierite-bearing hornfelses.

Saggerson and Turner (1995) inferred the metamorphic zoning of the aureole based on classic metamorphic facies principle and grade of metamorphism using previously published data on the aureole. They noted that the grade of metamorphism ranges from localised sanidinite hornfels facies through pyroxene hornfels facies, to hornblend hornfels facies and lower grade albite-epidote hornfels facies in metapelitic and some carbonate rocks (Figure 1-4). These facies scheme was defined using various observed mineral assemblages (e.g. Table 2)

Table. 1- 1 Pelitic mineral assemblages and associated contact facies within the BC contact aureole (after Saggerson and Turner, 1995).

Contact metamorphic Facies	Pelitic mineral assemblage
Albite-epidote hornfels facies	Qtz-Bt-Chl
Hornblende hornfels facies	Bt-Crd-Ms Bt-And-Ms Bt-And-Ctd-Crd Bt-Gt-St-And
Pyroxene hornfels facies	Bt-Gt-Crd-Sill Bt-Crd-Kfs Bt-Hyp-Crd Bt-Hyp-Crd-And
Sanidinite hornfels facies	Crn-Spl Crn-Cd-Pl-Ru Crd-Mul-Spl-Cor Pl-Crn-Spl-Spr

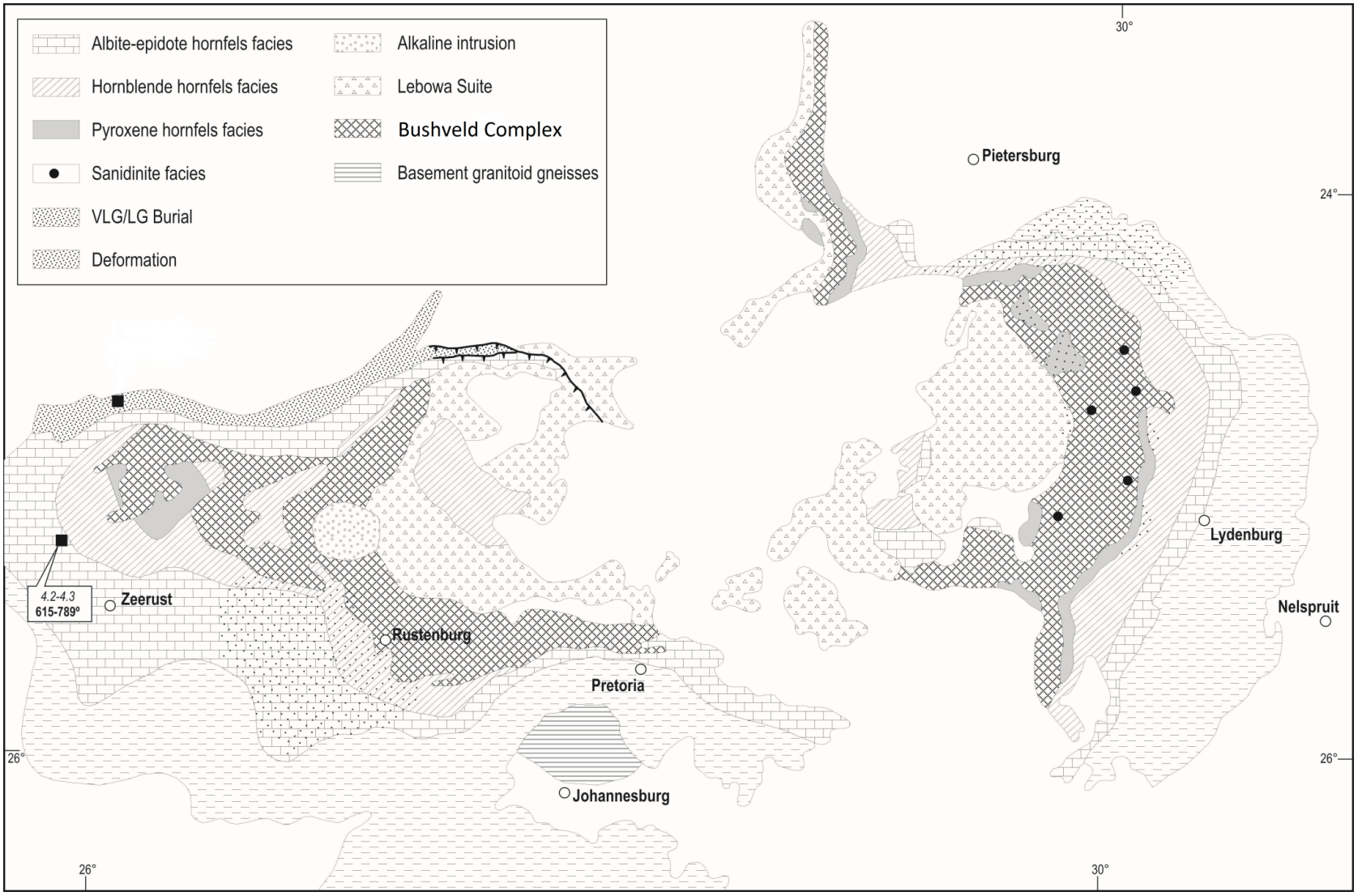

Figure 1-4. Metamorphic facies zonation of the Bushveld Complex contact aureole (Saggerson and Turner, 1995).

1.5 Discussion

Interpreting and evaluating the current P-T database mainly in the eastern Bushveld aureole shows that the variations of P-T conditions (see figure 1-3 and Table 1-2) of the earlier studies were large and the estimates started to be more consistent in the early 90's. The vast majority of published P-T data from the BC aureole is derived from the use of various conventional thermo-barometers, including several calibrations of the same equilibria and most of these studies exhibit large errors. In recent years conventional thermo-barometry has been superseded by a pseudosection approach (Powell & Holland, 1998). Pseudosection studies on these rocks and better calibrated thermobarometers have the capability of minimising these error margins. Better constrained P-T conditions in combination with mineral micro-textures can be used to better describe the metamorphic zones within the aureole. Due to the variable thickness of the Pretoria Group formations the metamorphic zones will be different from different locations

Table 1-2. Summary of P-T estimates within the BC contact aureole (after Raubenheima, 2012)

PRESSURE (kbar)	TEMPERATURE (°C)	METHOD	Mineral assemblage	AUTHOR	LOCATION
2.1-4.2*	700-750#	Inferred	Ak-Mtc-Wo	Willemse (1959)	Steelpoort area
1.0-2.0	500-530, ± 10	PT-grids	Bio-St-Gt-And-Crd	Human (1975)	Havercroft-Streatham andalusite deposit (near Penge)
<2.5	530-630	PT-grids	A) And-Bt-Ms-Chiastolite; B)Anth-Bt-Crd; C) And-Ms-Qtz; D) Gt-And-Bt-Ms-Qtz; E) Alm-Amph-Gru; F) Crd-Bt-Kfls-Ms-And-Pl-Qtz; G) Gt-Bt-Ms-Kfs-Qtz; H) Hbl-Crd-Bt-Kfs-Ms-Czo-Pl-Qtz; I) Hbl-Cum-Bt; J) Di-Pl-Hbl-Cal-Czo; 11) Dio-Scp-Hbl-Czo	Engelbrecht (1976)	North-east of Zeerust
A) 5.3, B) 5.3, C) 5.2, D) 5.2, E) 4.5 and F) 4.0	A) 500, B) 710, C) 530, D) 700, E) 1200# and F) 600	Geothermobarometry	Bt-Gt-Crd-Sill-Pl-Qtz	Hulbert and Sharpe (1981)	Eastern BCaureole. A) S 24.69° E 30.49°, B) S 24.65° E 30.41°, C) Burgersfort: S 24.34° E 30.20°, D) S 24.77° E 30.10°, E) S 24.98° E 30.13° and F) S 25.26° E 30.09°.
3.5*	535 and 589 respectively	Geothermobarometry	Gr-Cpx	Sharpe and Fortsch (1981)	Eastern BC contact areole on farms Klipbankspruit and Houtenbek near Belfast.
A) 5.2, B) 5.3, C) 5.5, D) 5.2, E) 4.5#, F) 4.5# and G) 3.5	A) 500, B) 700, C) 705, D) 533, E) 1150#, F) 1150# and G) 575	Geothermobarometry	Bt-Gt-Crd-Sill-Pl-Qtz	Sharpe (1982)	Eastern BC contact aureole, samples collected around Burgersfort
1.5 (first stage) and 4-5 (second stage)	~750 (first stage) and 850-900 (second stage)	Geothermobarometry	A) Gt-Opx-Crd-Bt; B) Cpx-Pl-Qtz; C) Ol-Cor-Crd-Sp-Sill-Opx	Nell (1984)	North of Potgietersrus
<2.5 *	A) >650 and B) 470-530,	Geothermobarometry	A) Ms-Kfs-Chl-Qtz; B) And-Bt-Ms-Qtz	Hartzer (1987)	Western BC contact aureole, Crocodile River Fragment. A) Metapelite; B) Calc-sillicates
0.6-1.6 and 1.1-2.4	>1200#	P-T grid	A) Cal- Ak -Mtc; B) Cal - Fo-Mtc; C) Ak-Di - Mtc; D) Di - Fo - Mtc; E) Cal- Per -Mtc	Wallmach *et al*. (1989)	Eastern BC contact aureole, near Steelpoort
2.1-3.2	646-760	Geothermobarometry	Opx-Gt-Crd-Bt-Pl-Qtz	Engelbrecht (1990)	Westerm BC contact aureoleNear Nietverdiend
A) 2.0 - 2.3 and B) 2.6	A) 560-570 and B) 540	Geothermobarometry	Gt-Bt-Crd-And-Pl-Qtz	Kaneko *et al*. (1990a)	Eastern BC contact aureole, Near Penge. A) shallow and B) deeper level
-	550-650 (fibrolite formation)	Geothermobarometry	Gt-Bt-Crd-And-Fibrolite-Pl-Qtz	Kaneko *et al*. (1990b)	Eastern Bushveld Complex aureole.

PRESSURE (kbar)	TEMPERATURE (°C)	METHOD	Mineral assemblage	AUTHOR	LOCATION
-	≤800	Geothermobarometry	A) Gt-Bt-Crd-Ms-Pl-And-Qtz; B) Cpx-Grs-Pl-Hbl-Preh-Tr; C) Hbl-Pl	Hartzer (1994)	Eastern BC contact aureole; Crocodile River, Dennilton and Marble Hall Dome, Rooiberg and Stavoren Fragment
<1.5	1100-1200#	P-T grid	A) Cal - Di - Ak - CO_2; B) Cal- + Ak Mtc + CO_2	Wallmach et al. (1995)	Eastern limb close to Roossenekal and north-west of Steelpoort
A) 2.8-3.2 and B) 3.2-4.8	(A) 535-563 and (B) 460-619	B) Geothermobarometry and A) Petrogenic grid	St -Qtz- Ms -Bt- Gt- And-Gt-Pl + H2O	Uken (1998)	North-Eastern BC contact aureole; 29°30' and 29°08' east and 24°08' and 24°30' south.
1.8*	700-780	Geothermobarometry	Opx-Kfls-Bt-Pl-Crd	Mizuno and Miyano (1999)	Just southeast of Steelpoort and northwest of Burgersfort
1.5-2.5 (first and second stage)	550-600 (first stage) and >720 (second stage)	P-T pseudosections	A) Chiastolite-And-Crd-Bt-Gt-Qtz; 2) Gt-Crd-Bt-Kfls-Qtz; 3) Sill-Crd-Kfls-Qtz	Pitra and De Waal (2001)	Marble Hall Fragment
3.0 ± 0.5	-	Mineral micro-structures, phase equlibrium relations and nucleation rates	A) Ms- Qtz-Kfls-And/Sill-H_2O; B) Ms- Bt-Qtz-Crd- Ksp-H_2O C) Bt-And/Sill - Qtz- Crd-Ksp- H_2O	Waters and Lovegrove (2002)	Eastern BC contact aureole; West of Penge: M32) S 24.31° E 30.20°, M33) S 24.36° E 30.25° and DLB-9) S 24.37° E 30.26°
-	>700	PT-pseudosection	Bt-Pl-Sill-Qtz	Harris *et al*. (2003)	Eastern BC contact aureole, samplessamples collected around Lydenburg
3.5 ± 1.5	750 ± 100, 600-650 and 650-800 (from garnet-bearing granofels) as well as ~680-690 and ~720 (from lower grade migmatites and higher grade migmatites respectively)	Geothermobarometry and Pseudosection	Bt-Gt-Crd-Sill-Pl-Qtz	Johnson *et al*. (2003)	Eastern BC contact aureole Metatexites: S24°37•35' E30°21•07' and S24°37•31' E30°21•03', leucosomes: S24°19•41' E30°02•68' and S24°21•56' E30°42•57' and diatexite: S24°21•56' E30°42•57'.
3 (first stage) and 1.5-2 (second stage)	>720 (first stage) and >700 (second stage)	Pseudosections	Crd-And-Sp-Qtz	Johnson *et al*. (2004)	Phepane Dome north of Burgersfort
A)-C) 1.5 ; D) 1.5-2.5; E)2.2- 3.1 ; F) 1.5 - 2.5; G) 2.4; H) 2.1	A) 750-805, B) 755-820, C) 740-790, D) 550-595, E) 635-665, F) 450-475, G) 570 ± 20 and H) 600 ± 30	Geothermobarometry and Petrogenic grid	A) Bt-Crd-Opx-Kfs-Pl-Qtz; B-C) Bt-Gt-Crd-Chl-Ms-Pl-Qtz-Ilm; D) Bt-Gt-Chl-Ms-Pl-Qtz-Ilm; E) ;F) Bt-Gt-Chl-Qtz-Ilm; G) And-Bt-St-Grt-Chl-Ms-Pl-Qtz-Ilm; H) And-Bt-Crd-Grt-Chl-Ms-Pl-Qtz-Ilm	Kaneko *et al*. (2005)	Eastern Bushveld Complex aureole: A&B) S 24.74° E 30.38°, C) S 24.90° E 30.19°, D) S 24.43° E 30.28°; S 24.36° E 30.21° and S 24.40° E 30.26°; E) S 24.48° E 30.16°; F) S 24.33° E 30.28°; G) S 24.36° E 30.23° and H) S 24.42° E 30.18°.

Notes: # P-t estimates on xenolith. * assumed P-T conditions

1.6 Aims and Objectives of the study

- Provide a brief review on metamorphism in the Bushveld contact aureole and compile a list of published P-T conditions in the Eastern Bushveld contact aureole
- Constrain the age of the Bushveld contact metamorphism which will indirectly provide the emplacement time of the Rustenburg Layered Suite and the minimum cooling period, using Lu-Hf isotope systematics of garnets bearing hornfels present in the contact.
- Estimate the P-T conditions of the garnet bearing hornfels using garnet isopleth thermo-barometry pseudosection approach and classical geothermobarometry and compare the result to the published P-T from the Bushveld contact.
- Furthermore, evaluate the metamorphic evolution of Gt-And free staurolite bearing Fe-Al rich metapelites

1.7 Sampling and Methodology

A total of 86 fresh samples were collected around the north eastern BC contact aureole and polished thin sections were prepared at the Council for Geosciences (Pretoria). Six of the samples were studied in detail and were collected along the Silverton shale, Daspoort and Timeball Hill formations.

Hand specimen descriptions were done using a hand lenses and rocks were classified according to the IUGS classification scheme. Petrographic analyses of 86 polished thin sections were carried out using a polarizing microscope in order to determine their mineral assemblages and their microstructural relationship. Three of the samples are garnet bearing hornfels and the rest are biotite-staurolite-plagioclase hornfels.

1.7.1 Hand specimen descriptions

Figure 1-5. Photographs of Sample DY916

DY916
Formation: Daspoort
Colour: dark greenish
Texture: fine to medium grained
Minerals: greenish chlorite and black biotite flakes
Name: Hornfels
Inferred protolith: Mudrock

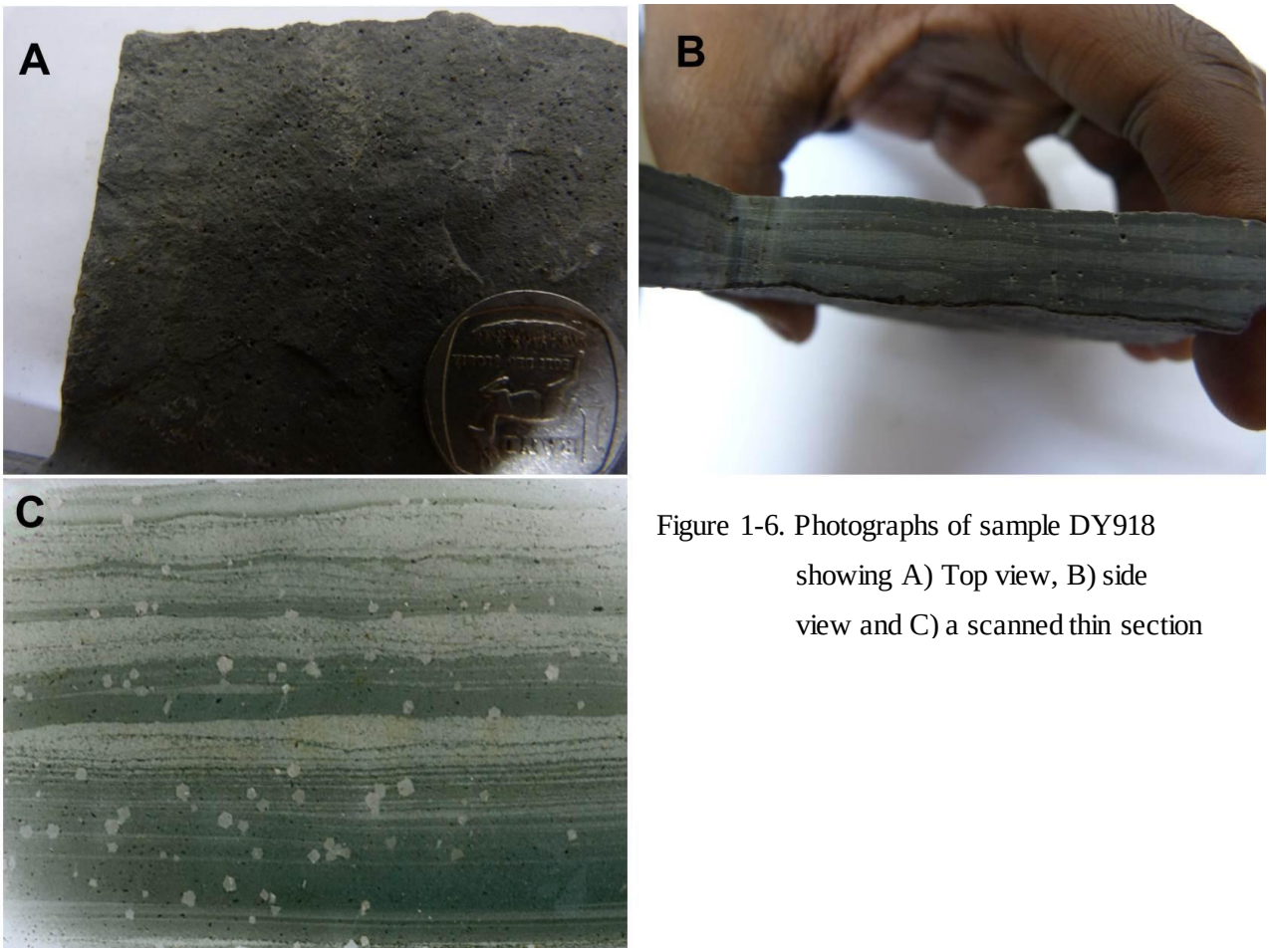

Figure 1-6. Photographs of sample DY918 showing A) Top view, B) side view and C) a scanned thin section

DY918
Formation: Daspoort
Colour: dark coloured top view and the side view shows an interlayering of lighter and darker domains
Texture: fine grained with reddish-brown spots of garnet
Minerals: Only garnet which constrained within the darker domain is clearly visible and the rest is a homogenous dark colour. The lighter domain contains Qtz+Pl
Name: Spotted garnet hornfels
Inferred Protolith: organic rich mudstone/black shale

DY954
Formation: Silverton
Colour: dark coloured rock
Texture: fine grained with pinkish Andalusite porphyroblasts and small reddish brown garnets
Minerals: Bt flakes, tabular andalusite porphyroblast, rounder reddish brown garnet
Name: Gt-And hornfels
Inferred Protolith: organic rich mudrock/ black shale

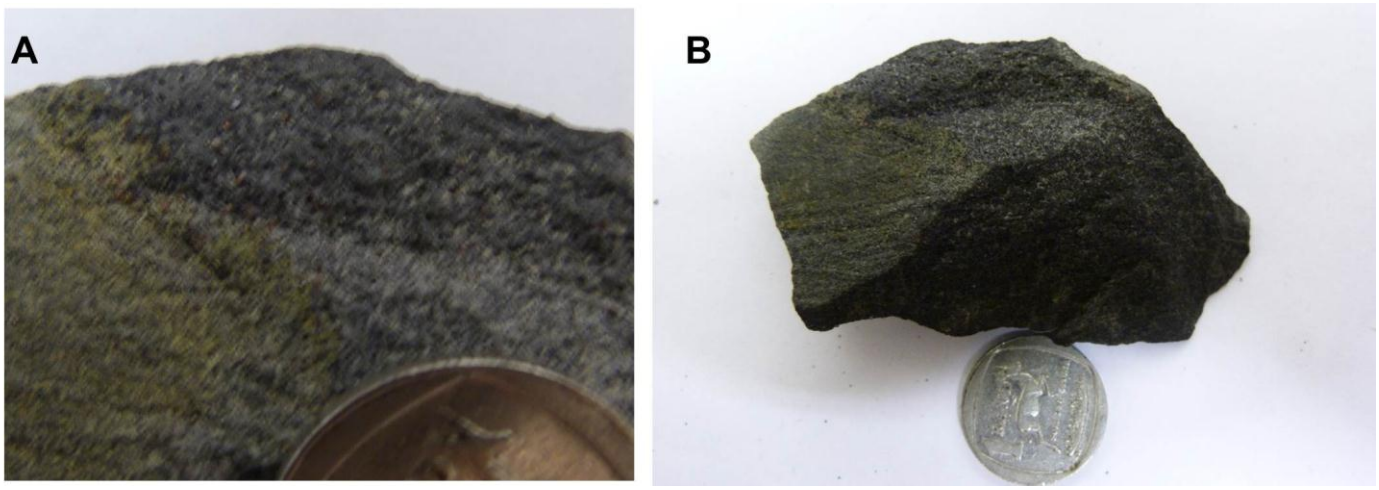

Figure 1-7. Photographs of sample DY954

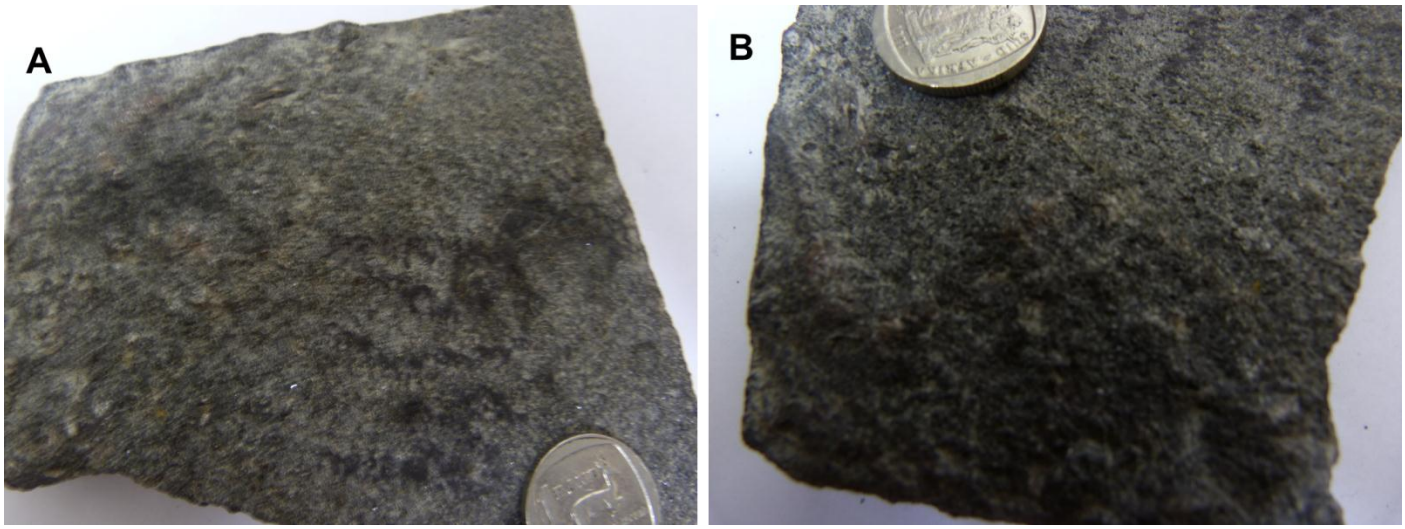

Figure 1-8. Photographs of sample DY956

DY956
Formation: Silverton
Colour: dark coloured
Texture: fine grained with andalusite porphyroblast
Minerals: shiny black flakes of biotite – tabular andalusite
Name: Andalusite hornfels
Inferred Protolith: black shale/ organic rich mudrock

Figure 1-8. Photograph of sample DY982

DY982
Formation: Timeball Hill
Colour: Light coloured with dark spot of Bt and St
Texture: fine-medium grained with Bt and St porphyroblasts
Minerals: shiny black flakes of biotite – yellowish St-white patches of Pl and Qtz
Name: Bt-St hornfels
Inferred Protolith: Mudrock

DY987
Formation: Timeball Hill
Colour: dark coloured with thin light layers
Texture: fine grained with Bt and St porphyroblasts, well preserved sedimentary layering
Minerals: shiny black flakes of biotite – yellowish St-white patches of Pl and Qtz
Name: Bt-St hornfels
Inferred Protolith: Mudrock

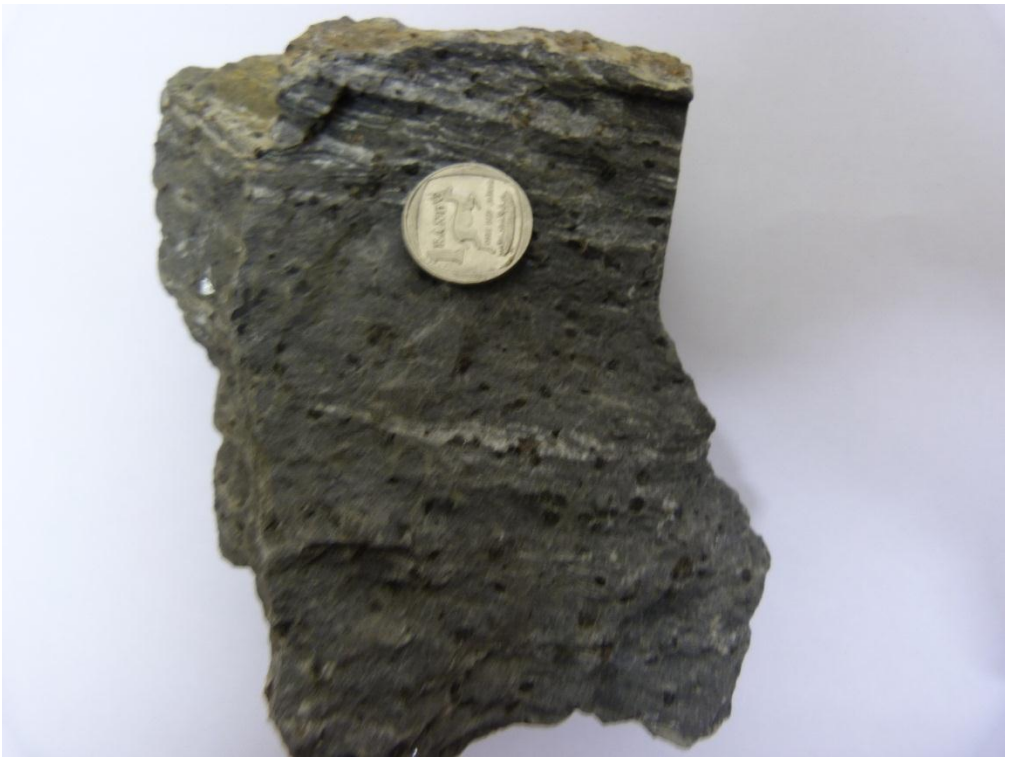

Figure 1-9. Photograph of sample DY987

1.7.2 Whole rock geochemical analysis

X-ray fluorescence (XRF) analysis was used to determine the bulk rock composition which was carried out using an ARL9400XP+ spectrometer at the University of Pretoria, to determine major elements compositions of twenty samples.

The samples were crushed and grounded to < 75 µm in a tungsten carbide milling vessel, roasted at 1000 ^{0}C to determine loss on ignition (LOI) and thereafter fused into glass beads by adding 1g sample to 6g $Li_2B_4O_7$. Another aliquot of the samples were pressed in a powder briquette for trace element analyses. The obtained Fe_2O_3 was converted to FeO by assuming that 90% of the present iron is Fe^{2+} (e.g. Fe^{2+} [(Fe_2O_3 x ((2 x 71.84))/159.69) x 0.9]) (Chmielowski, 2009).

1.7.3 Electron microprobe analysis (EPMA)

The first set of the mineral chemical analysis were determined by wavelength-dispersive spectrometry (WDS) using a CAMECA SX-100 electron microprobe at the University of Pretoria, with an accelerating voltage of 15 kV and a beam current of 20 nA. Analyses were performed with a beam diameter at ~1–2 µm. Element concentrations were calculated from relative peak intensities using the internal PAP-correction software of Pouchou and Pichoir (1991).

Garnet, staurolite and plagioclase compositions were taken across the grains to determine whether they displayed any chemical zonation.

Owing to technical difficulties at the University of Pretoria EPMA lab, additional analyses were carried out at Rhodes University but the obtained analyses do correlate with the earlier analysis (See Appendix C). The mineral chemistries were obtained using a wavelength dispersive JEOL JXA 733 Super probe (ZAF correction) at Rhodes University with 15 kV acceleration potential and beam currents of 20 nA with a beam diameter of 2 μm.

1.7.4 Lu-Hf garnet isotope analysis

Three metapelitic hornfels containing garnet porphyroblasts were selected for Lu-Hf analysis. The selected rock samples were crushed in a jaw crusher and then sieved. The garnet grains fractions of 400-600 mg were handpicked under a binocular microscope; most of the garnet porphyroblasts in these samples were inclusion free and hence they would not have a negative effect on the Lu-Hf systematics and produce biased isochrons. The Lu-Hf analysis was carried out at Frankfurt University in Germany, using the method described in Millonig et al. (2008). To selectively dissolve the garnet fractions while leaving zircon as the main Hf-bearing contaminant intact, the fractions were digested in closed Teflon® vials on a 1200 ^{0}C hotplate rather than in high-pressure Parr® bombs (Lagos et al., 2007; Schmidt et al., 2008). After rinsing with Milli-Q H_2O, the mineral separates were spiked with a mixed ^{176}Lu - ^{180}Hf tracer for Lu and Hf concentration determinations, and then digested as follows. The minerals were decomposed in HF-HNO_3-$HClO_4$ and then 10M HCl, drying down at high temperature (fuming $HClO_4$) between the steps (Lagos et al., 2007).

Separation of Lu and Hf was achieved on an ion-exchange column containing Eichrom Ln-Spec resin (Münker et al., 2001). Lu and Hf isotope ratios were measured on a Finnigan Neptune MC-ICP-MS system equipped with a Cetac ARIDUSTM sample introduction system at Goethe University Frankfurt.

This instrumental setup ensured high sensitivity, allowing the precise measurement of the Hf isotope compositions of samples having as little as 10 ng of Hf at a signal intensity of ~350 mV of ^{176}Hf for a 10 ppb Hf solution.

Because only 50 - 80% of the Yb was separated from Lu using the purification technique employed here, a correction was necessary for the interference of ^{176}Yb on ^{176}Lu (Blichert-Toft et al., 1997). The Yb interference was monitored by measuring two interference-free Yb isotopes (^{173}Yb and ^{171}Yb).

Their ratio was used to apply an instrumental mass bias correction to the measured $^{176}Lu/^{175}Lu$ values, assuming a $^{173}Yb/^{171}Yb$ of 1.129197 and the exponential law (Vervoort et al., 2004). This mass bias correction was also applied to the $^{176}Yb/^{171}Yb$ used for correcting the ^{176}Yb interference on ^{176}Lu. In-run statistics for the measured and corrected $^{176}Lu/^{175}Lu$ range from 0.006 to 0.01% 2 SE. Mass bias on the Hf isotope ratios was corrected for using $^{179}Hf/^{177}Hf = 0.7325$ and the exponential law. The Hf fractions were virtually free of any Yb and Lu, but contained variable amounts of Ta and W. All isobaric interferences on Hf isotopes were monitored and corrected using the mass bias corrected $^{173}Yb/^{176}Yb$, $^{175}Lu/^{176}Yb$, $^{180}Ta/^{181}Ta$, and $^{183}W/^{180}W$ values. In-run analytical uncertainty for $^{176}Hf/^{177}Hf$ was typically around ~ 0.3 ε or better. For the calculation of the mineral isochrons the ISOPLOT program (Ludwig, 2007) was used with $^{176}Lu = 1.867 \times 10^{-11}$ (Scherer et al., 2001; Söderlund et al., 2004). For the $^{176}Hf/^{177}Hf$ uncertainties, quadratic additions of the reproducibility of the JMC-475 ($2\sigma = 0.6\varepsilon$) and the in-run precisions (2σ errors) were used. Uncertainties on $^{176}Lu/^{177}Hf$ were propagated from the reproducibility of the Lu standard and the uncertainty in the spike calibration (0.15%), and multiplied by an error magnification factor that depends on the measured $^{176}Lu/^{175}Lu$. Resulting uncertainties for the $^{176}Lu/^{177}Hf$ values are between 0.26% and 0.35%. Repeated blank measurements yielded < 540 pg for both Lu and Hf.

1.7.5 Thermodynamic modelling

P-T pseudosections were calculated for six samples; DY918, DY954, DY956 DY916, DY982 and DY987 to calculate rock specific equilibrium assemblages. Simplified model systems of MnO-Na_2O-CaO-K_2O-FeO-MgO-Al_2O_3-SiO_2 +H_2O, Na_2O-CaO-K_2O-FeO-MgO-Al_2O_3-SiO_2-+ H_2O and K_2O-FeO-MgO-Al_2O_3-SiO_2-+ H_2O were chosen for these calculations. The pseudosections were calculated using the Theriak-Domino software collection programs written by C. de Capitani. For more information on these different programs and their applications the reader is referred to de Capitani and Petrakakis (2010 and references herein).

The above chemical systems were chosen based on major oxides that best describe the observed mineral assemblages. Based on petrography and literature, it was postulated that the samples could represent a medium grade metamorphism and therefore, a P-T range of 1-4 kbar and 400-700 ^0C was explored in these calculations. The garnet modes and compositions were successfully modelled in the domino program, creating P-T graphs depicting the changes in composition of the mineral phases with respect to P-T conditions for a given bulk rock composition (e.g. moles almandine, spessartine, grossular and pyrope).

The P-T conditions for the complete growth of garnet were constrained from the isopleths intersection (e.g. X_{alm} and X_{prp}) corresponding to the compositions measured by microprobe for the rim to the core. The internally consistent thermodynamic database "tcdb55c2d" (Holland and Powell 1998) was used in Theriak-Domino version 01.08.09. Solid solution models of: garnet, phengite, biotite, chlorite, omphacite and orthopyroxene: site mixing and Margules parameters; staurolite and chloritoid: ideal mixing and Margules parameters; spinel and talc: site mixing were used. Δ G of H_2O is according to Holland and Powel (1998).

Two classical geothermobarometers were used namely, garnet-biotite-plagioclase-quartz [(GBPQ) Wu et al., 2004] and garnet-muscovite-plagioclase-quartz [(GMPQ) Wu and Zhao, 2006]. The GBPQ barometry is based on the balanced reactions shown below (reaction 11 and 12) (e.g. Hoisch, 1990 and 1991) and yields a random error of 1.2 kbar. The Holdaway (2000) thermometer uses activity models of garnet and biotite due to its lower random error of ~ 25 ^{0}C and also an Al-avoidance plagioclase activity model of Fuhrman & Lindsley (1988).

$$Mg_3Al_2Si_3O_{12} + 2Ca_3Al_2Si_3O_{12} + 3K(Mg_2Al)(Si_2Al_2)O_{10}(OH)_2 + 6SiO_2$$

pyrope grossular eastonite quartz (11)

$$= \tfrac{1}{4}6CaAl_2Si_2O_8 + 3KMg_3(AlSi_3)O_{10}(OH)_2$$

anorthite phlogophite

and

$$Fe_3Al_2Si_3O_{12} + 2Ca_3Al2Si_3O_{12} + 3K(Fe_2Al)(Si_2Al_2)O_{10}(OH)_2 + 6SiO_2$$

almandine grossular siderophyllite quartz (12)

$$= \tfrac{1}{4}6CaAl_2Si_2O_8 + 3KFe_3(AlSi_3)O_{10}(OH)_2$$

anorthite annite

The GMPQ barometer is based on the Fe-Mg end member's equilibrium reactions below (Reaction 13 and 14) (e.g. Hoisch, 1990, 1991; Wu et al., 2004a) and yields random errors of 15 ^{0}C and 1.5 kbar for the GM and GMPQ thermometer and barometer. For more information the reader is referred to Wu and Zhao, 2006;

$$Mg_3Al_2Si_3O_{12} + 2Ca_3Al_2Si_3O_{12} + 3KAl_2(AlSi_3)\ O10(OH)_2 + 6SiO_2$$

pyrope grossular muscovite quartz

$$= ¼\ 6CaAl2Si_2O_8 + 3K(MgAl)\ Si_4O_{10}(OH)_2 \quad (13)$$

anorthite Mg-celadonite

and

$$Fe_3Al_2Si_3O_{12} + 2Ca_3Al_2Si_3O_{12} + 3KAl_2(AlSi_3)\ O_{10}(OH)_2 + 6SiO_2$$

almandine grossular muscovite quartz (14)

$$= ¼\ 6CaAl_2Si_2O_8 + 3K(FeAl)\ Si4O10(OH)_2$$

anorthite Fe-celadonite

Chapter 2

Lu-Hf garnet geochronologic constraints from the Bushveld Complex contact aureole, South Africa

2.1 Introduction

The age of the contact metamorphism which resulted from the intrusion of Bushveld Igneous Complex (BC) has up to so far not been well constrained. Moreover, the relationship between the relative timing of magmatic crystallization and garnet growth has not been successfully investigated. Integration of the magmatic crystallization and garnet growth could help put constraints on the relationship between magmatism, metamorphism and tectnonism (Castro, et al., 1998). Furthermore, by constraining the relative timing of contact aureoles using garnets crystallization ages and even zircons from anatectic melts could help to elucidate the effects of pre, syn and post intrusions (Scherstén et al., 2000). Garnet geochronology has recently been applied to date prograde metamorphic and thermal events, using Sm-Nd and Lu-Hf isotopic systems (Wolf et al., 2010 and references herein).

In this chapter, Lu-Hf garnet ages of two samples located on two distinct locations within the aureole are presented.

2.2 A brief overview of the geochronology of the BC contact aureole

Buick et al. (2001) worked on the calc -sillicate xenoliths within the RLS characterised by a mineral assemblage of vesuvianite- wollastonite-garnet which was first described by Walmach (1989 and 1995). The Upper Zone of the eastern BC preserves cal-sillicate xenoliths (~1200 ^{0}C) which were hydrothermally metasomatised by retrograde fluids. Using U-Pb analysis on titanites they obtained a 2058.9 ± 0.8 Ma age and suggested that this it's represent 600 – 700 ^{o}C hydrothermal alteration during the cooling of the RLS.

The timing of the deformation and low grade regional metamorphism developed in the Transvaal Supergroup especially in the uppermost Pretoria Group, has not been dated up until the early 2000's (e.g. Tankard et al.,1982; McCarthy et al.,1986; Andreoli, 1988 a and b; Bumby et al., 1998; Gibson et al.,1999). Alexandre et al., (2006) carried out single grain ^{40}Ar/^{39}Ar dating of white micas from slates and phyllites of the Pretoria Group, developed in the western BIC contact aureole. They obtained two distinct ages, 2.15 Ga and ~2042.1 ± 2.9 Ma and interpreted the latter to represent a post BC extensive fold and thrust belt known as the Transvaalide fold and thrust belt present in the central Kaapvaal craton.

More recently, a Re/Os age of 2322 ± 16 Ma from lower Timeball Hill mudrocks (Hannah et al., 2004) and a SHRIMP U–Pb detrital zircon age of 2324 ± 17 Ma, also from the Timeball Hill Formation (Dorland et al., 2004), have been obtained from near the base of the group.

Other attempts to constrain the emplacement of the BIC indirectly from garnets in the contact aureole were deemed to be unsuccessful (J. Kruger, cited as pers. comm., 2000, in Buick et al., 2001).

Scoates et al. (2012) studied 8 samples from the RLS and the roof rocks of the complex utilising chemical abrasion IDTIMS U-Pb zircon results. The two samples collected from the Merensky Reef at the top of the Upper critical zone in the Western and Eastern limb (Figure 3-1) recorded a 2055.30 ± 0.61 and 2056.13 ± 0.70 Ma. Below the Meresnky Reef and the UG2 chromite layers two samples from different locations of the footwall pyroxenite recorded older ages of 2060.5 ± 1.4 Ma and 2059.8 ± 1.2 Ma. The felsic rock collected in the roof of the Complex just above the UZ diorite which include a granodiorite mixed with hornfels (“leptite”), a granophyre from the Rashoop Granophyre Suite, and a granite from the Nebo/Lebowa granites recorded ages of 2054.83 ± 0.86, 2055.70 ± 1.0 and 2054.23 ± 0.79 Ma respectively. These results suggest an ~5Ma time gap between the intrusion of the LZ to CZ and the MZ to UZ, also implying a cogenetic evolution for the ultramafic-mafic and felsic rocks of the complex (Scoates et al., 2012)

According to Rajesh et al. (2013), the emplacement of the Bushveld LIP at 2061 Ma produced different magma pulses with a related geochronological history. The period from 2063 to 2030 was characterised by three major magma pulses which commenced with the 2.061 - 2.060 Ga (Walraven, 1997) Rooiberg Group volcanic Suite, followed by a 2.059 - 2.054 Ga (Scoates et al., 2012) associated with the sub pulses that produced the RLS and coeval felsic intrusions in the roof rocks and completed by the 2.046 - 2.042 Ga intrusions of ultramafic to mafic (e.g. Uitkomst Complex and associated intrusions) and the intrusion sills (e.g. Thabazimbi sills). The emplacement of this LIP had a profound effect on the Pretoria Group sediments such that these ages and effects might be recorded by the metamorphic rocks within the BC contact aureole. For instance the ages constrained by Buick et al. (2001) and Alexandre et al., (2006) records 2.059 - 2.054 and 2.046 - 2.042 Ga events respectively.

2.3 Sample description

Two garnet bearing hornfels rocks namely sample DY918 and DY954 were collected in the Daspoort and Silverton formation of the North Eastern limb contact aureole occurring 4.5km and 500 m from the RLS respectively (Figure 3-1 and Table 3-1). Sample DY9-18 is defined by darker and lighter chemical domains layers composed of a matrix assemblage of garnet, chlorite, plagioclase, biotite, quartz and ilmenite. The 0.2 - 1.4 mm garnet porphyroblasts are constrained within the phyllosilicate rich layers. The majority of the garnet porphyroblasts are fractured with no apparent chemical zoning on thin section scale and in rare cases ilmenite inclusions are noted.

Sample DY9-54 has a matrix assemblage of garnet, biotite, staurolite, muscovite, andalusite, ilmenite, plagioclase and quartz. The garnet porphyroblast ranges in size from 0.05 – 1 mm in diameter, exhibiting euhedral to rounded grain shapes and contains ilmenite and quartz inclusions at times. The average garnet end member composition is ~79% X_{alm}, ~8% X_{sps}, ~7% X_{prp} and ~5%X_{grs} for sample DY9-54, and ~82%X_{alm}, ~7%X_{sps},~9%X_{prp} and~6%X_{grs} for sample DY9-18(see Appendix B).

Table 2-1. Sample locations and mineral assemblages

Sample	DY918	DY954
Co-ordinates	$24^0$33.179' S $24^0$20.998' E	30^0 20.554'S $29^0$97.972' E
Formation	Daspoort	Silverton
Mineral assemblage		
Bt	+	+
Chl	+	+
Pl	+	+
Gt		+
Ms		+
St		+
And		+
Qtz	+	+
Ilm	+	+

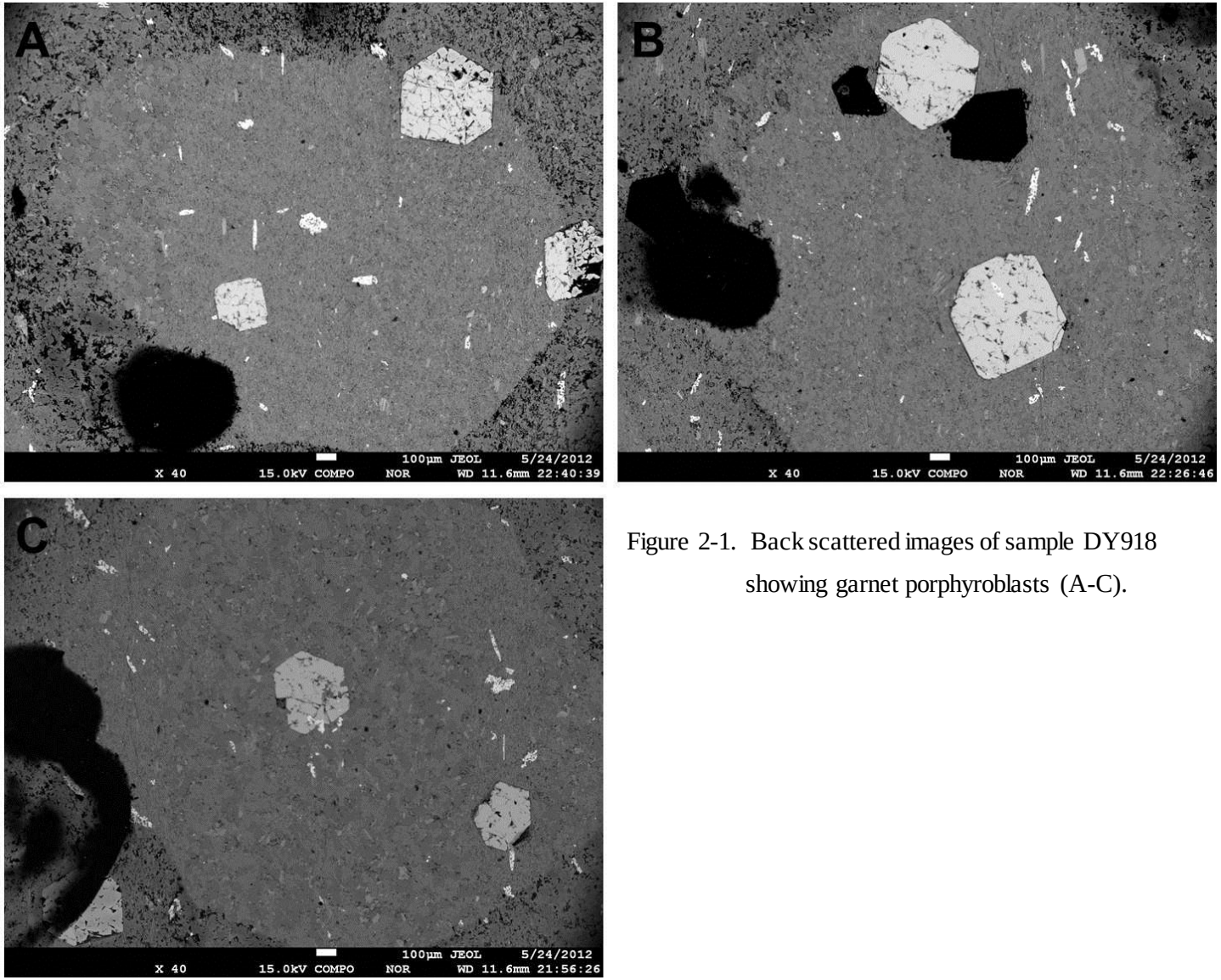

Figure 2-1. Back scattered images of sample DY918 showing garnet porphyroblasts (A-C).

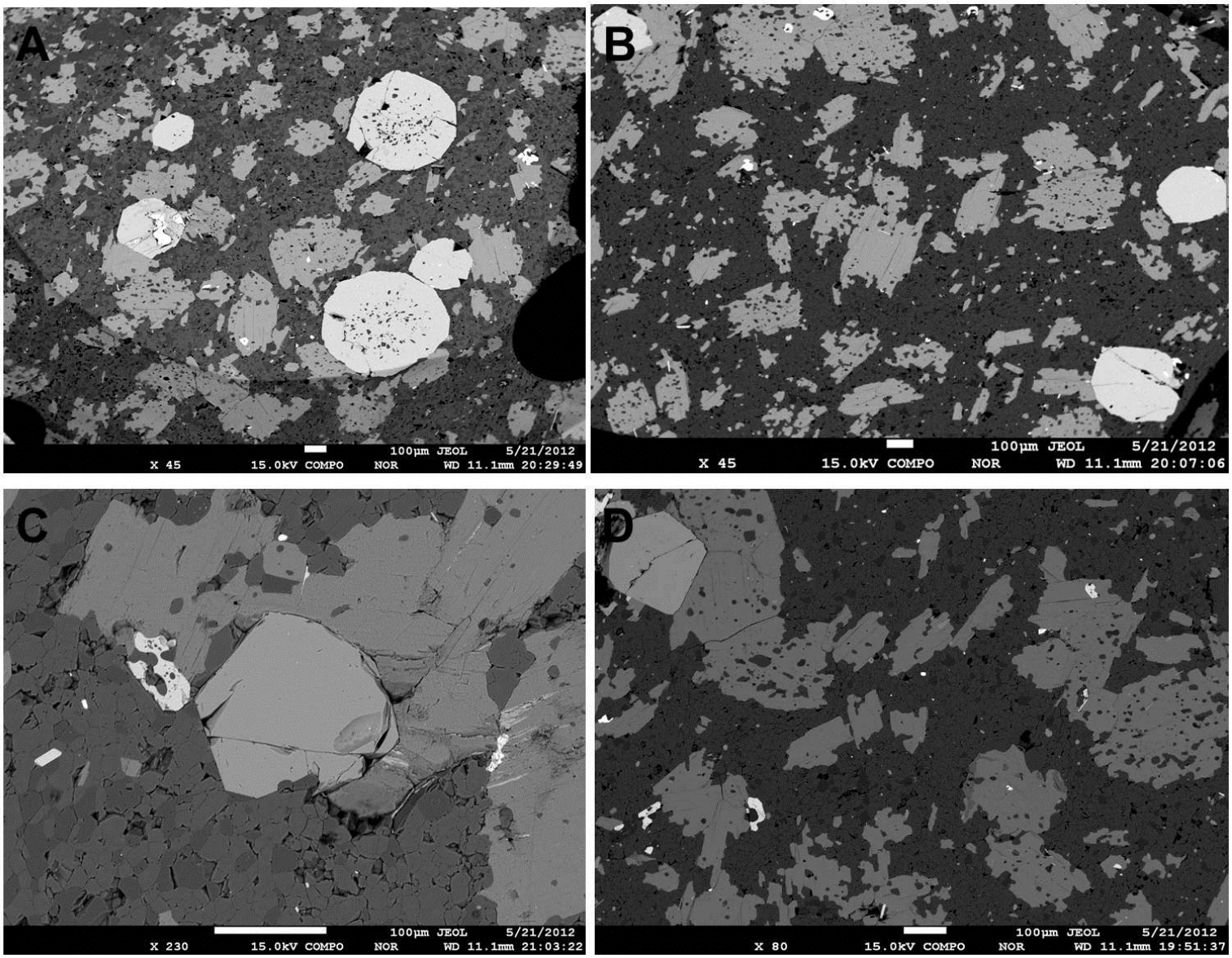

Figure 2-2. Back scattered images of sample DY954 showing garnet porphyroblasts (A-D).

2.4 Results

The Lu-Hf analysis results are presented in Table 3-1 and Figure 3-3. The garnet Lu-Hf isochrons provide isochrons at 2061.5 ± 5.1 Ma (MSWD=1.4) and 2061.4 ± 3.5 Ma (MSWD=2.2) for DY9-54 and DY9-18 samples respectively. These isochrons were obtained from bulk rock chemistry and garnet fractions; the ratios of $^{176}Lu/^{177}Hf$ for the garnet fractions ranges from 0.33 to 0.98 (Table 3-1). The low $^{176}Lu/^{177}Hf$ ratios in the garnet fractions can be due to the minor ilmenite inclusions within the garnets (Wolf et al., 2010).The average age of the two samples, is 2061 Ma with a MSWD of 1.8. Since zircon inclusions are absent in garnets from both samples the Lu-Hf systematics were assumed to be homogeneous. All the garnet separates for the two samples exhibit a perfect fit on their respective isochrons within their analytical uncertainties. In addition, the smaller MSWD values indicate high quality of the data with a very small degree of analytical uncertainties.

Table 2-2. Lu-Hf elemental and radiogenic isotope data of sample DY918 and DY954.

Fraction	Lu (ppm)	Hf (ppm)	$^{176}Lu/^{177}Hf$	±2 SD(abs)	$^{176}Hf/^{177}Hf$	±2 SD(abs)
Sample DY954						
D54-Grt1	5.8	2.2	0.37303	0.00093	0.295942	0.00003
D54-Grt2	5.2	2.2	0.33335	0.00083	0.294321	0.00003
D54-Grt3	5.6	2.2	0.35920	0.00090	0.295346	0.00003
D54-Bt	0.17	3.7	0.00649	0.00002	0.281517	0.00003
D54-wr	0.36	3.7	0.01387	0.00003	0.281815	0.00003
Sample DY918						
D18-Grt1	7.5	1.2	0.92386	0.00231	0.317487	0.00003
D18-Grt2	8.0	1.2	0.98314	0.00246	0.319847	0.00003
D18-Grt3	7.7	1.3	0.86319	0.00216	0.315005	0.00003
D18-wr	0.55	5.2	0.01494	0.00004	0.281800	0.00003

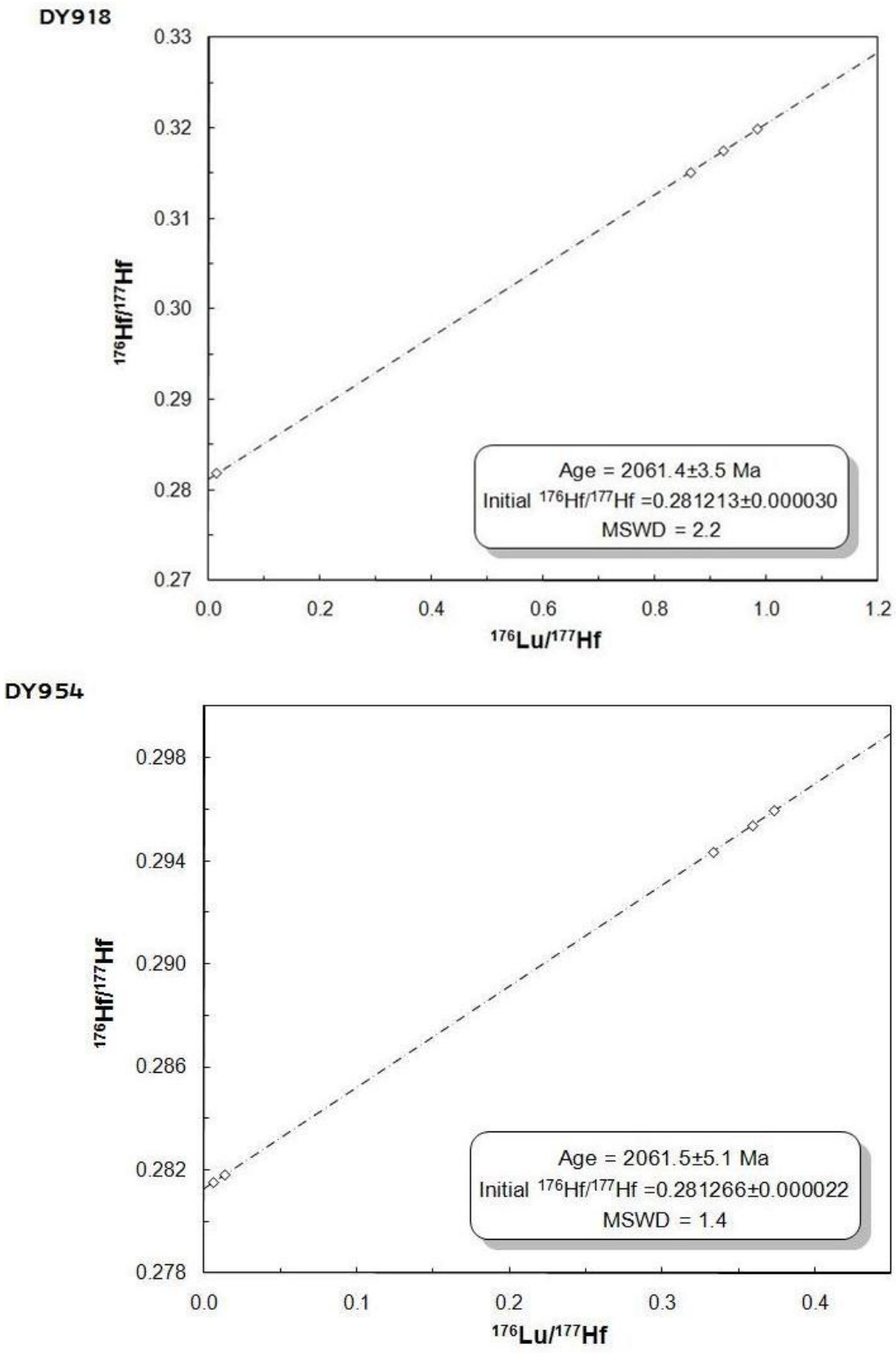

Figure 2-3. Concordia diagrams showing Lu-Hf garnet data from sample DY918 and DY954 collected on the Bushveld contact aureole.

2.5 Discussion

These ages provides a more precise timing of the hornblende hornfels facies metamorphism developed in the eastern BC proper contact aureole. The closure temperature of garnet for Lu-Hf isotopic system is between 700 and 800 ^{0}C and requires higher temperatures and longer sustained thermal activity in order to mobilise the elements by diffusion (Wolf et al., 2010 and references herein). Based upon the observed mineral assemblages and rock texture these rocks equilibrated at temperatures below this range. These robust Lu-Hf isochrons do in fact support a co-genetic garnet growth for both hornfelses regardless of their distance apart (see table 3-1 and figure 3-1). Taking Rajesh et al. (2013) into consideration, the 2061 Ma age records the 2061- 2060 Ma (Walraven, 1997) magma pulse which represent the Rooiberg Group Volcanic suite and not the 2059-2054 RLS sub pulses (Rajesh et al., 2013). However, the 2061-2060 Ma magma pulse does not solely represent the extrusion of the Rooiberg Group felsic rocks but also the coeval sub pulse of ultramafic LZ and CZ magmas (Scoates et al., 2012). Therefore, the 2061 Ma garnet age denote the crystallisation age of this sub pulse and not that of the Rooiberg group volcanic suite. These further support the 2 stage evolution of the RLS (e.g. Nell, 1984; Scoates et al., 2012) and ~7Ma time interval for the BC proper magmatism (Scoates et al., 2012). Assuming the validity of this argument, how do we then explain that the Lu-Hf garnet isotope systematics did not record the 2059-2054 magma pulse associated with the MZ to UZ intrusion? This can probably be explained by temperature differences between these sub pulses; the first sub pulse had more thermal effects on the aureole than the second pulse such that the second pulse lower temperatures could not affect the isotopic signatures to reflect it thermal history.

Chapter 3

P-T-X evolution of garnet bearing hornfelses from the north-eastern BC contact aureole: Constraints using garnet isopleth thermobarometry and classical geothermobarometry

3.1 Introduction

The investigation of P-T-X conditions of mineral assemblages is a very important aspect of understanding the metamorphic evolution of rocks (Spear, 1993; Gaides et al., 2006 and references herein). Elucidating the P-T-X history of contact aureoles with help define the isotherms and metamorphic zonation within the aureole. This can further provide more insight on the emplacement history of the plutons and associated tectonic events based on the mineral micro textures (Barboza and Bergantz, 2000).

Classical geothermobarometry and the pseudosection approach are two well accepted techniques used to constrain the P-T conditions of metamorphic rocks (Powell and Holland, 2008 and references herein). Even though the pseudosection approach has gained momentum over the last decade due to additional capabilities that are absent in conventional thermobarometry; the latter may still provide useful information for rocks with different chemical domains which cannot be separately analysed by XRF, and in cases where pseudosections predict larger P-T stability fields of certain mineral assemblages (Powell and Holland, 2008). Therefore, a combination of these two methods may provide more robust results about the P-T-X evolution of metamorphic rocks.

The behaviour of garnet end-members namely almandine, spessartine, grossular and pyrope in P-T-X space enables estimation of P-T condition at which the garnet equilibrated (Tracy and Robinson 1976) which denotes the peak metamorphic conditions experienced by the rock (Bestel et al., 2009). The points at which two or more garnet compositional isopleths intersect record the actual P-T conditions that the rock was subjected to (Evans, 2004; Gaides et al., 2006; Bestel et al., 2009). The choice of garnet as an important mineral to apply this technique is based on the number of properties that the mineral possesses and are described in more detail by Evans (2004).The majority of the published P-T data (Table 1-2) in the BC contact aureole were estimated using conventional geothermobarometry and few pseudosection studies (e.g. Pitra and de Waal, 2001; Harris et al., 2003; Johnston et al., 2003 and 2004). In this study both classical geothermobarometry and pseudosection approach will be utilised and compared to the already published data.

.

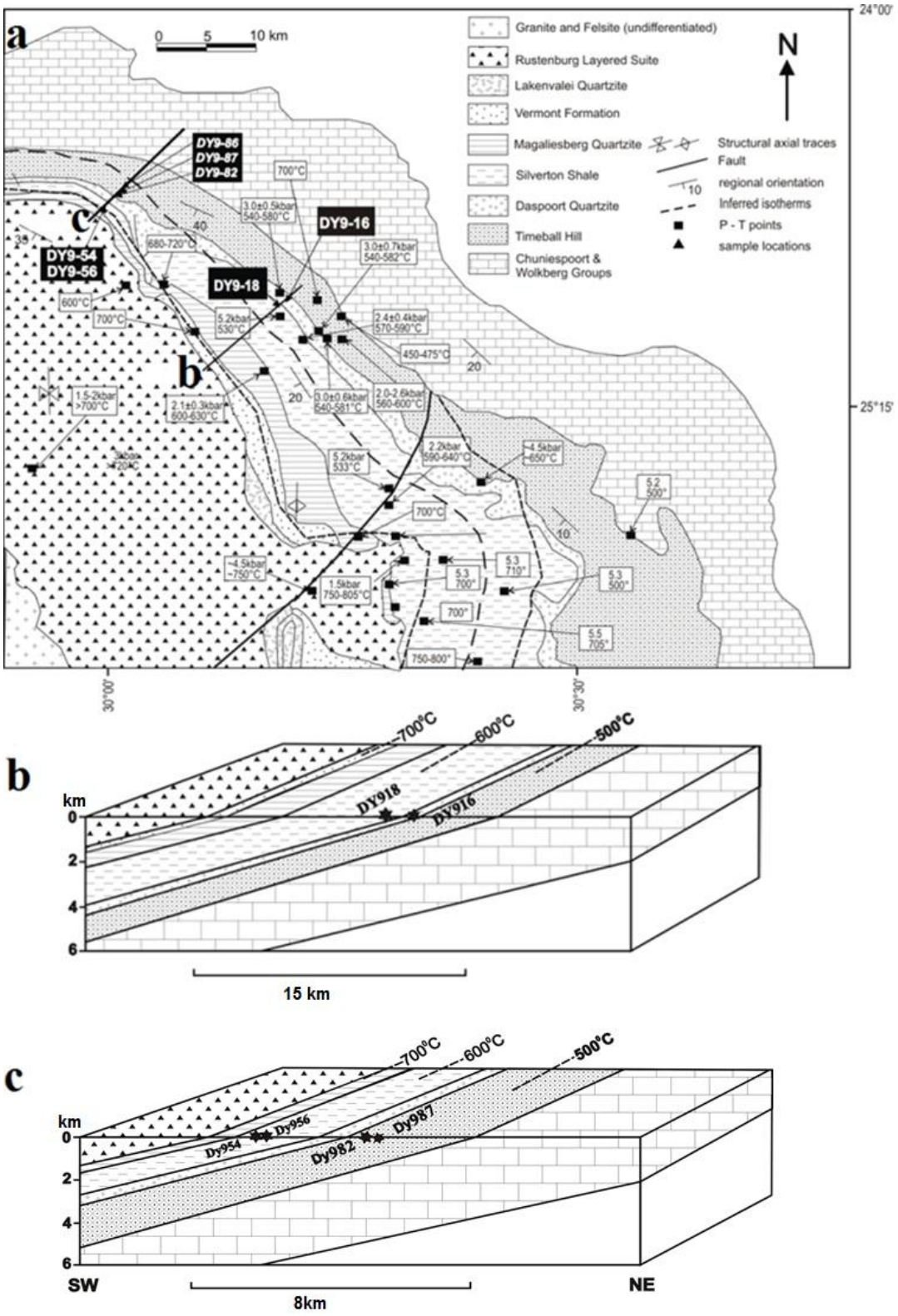

Figure 3-1. (a) Geological map of the north eastern Bushveld and its contact aureole, with 500, 600 and 700^{0}C isotherms taken from Harris et al. (2003) and Sharp and Chadwick (1982), including several published P-T estimates (see Table 1-2); The (b) and (c) represent cross sections of the aureole and locations of the studied samples, the mafic rocks in these section denotes the LZ -CZ.

3.2 Sample locations and petrographic descriptions

Three garnet-bearing hornfelses collected from the Silverton and Daspoort formation of the Pretoria Group were chosen for the purpose of this exercise. DY954 and DY956 are closely spaced occurring within the Silverton formation at about 500 and 800 m from the intrusion. DY918 was sampled in the Daspoort formation at about 4.5 km from the intrusion (Figure 3-1 a and b).

3.2.1 Sample DY918

The sample is fine-grained characterised by interlayering of lighter and darker domains on a scale ranging from millimetres to centimetres. Within the darker domains, chlorite and biotite flakes forms in the fine-grained matrix, (15.5% and 7.8%). Subidioblastic to idioblastic garnet porphyroblasts (6%) varying in size from 0.2-1.4 mm occurs within the darker and in isolated instances garnet aggregates can be noted (Figure 3-2 a). The majority of the garnet porphyroblasts are fractured with no visible zonation and are mostly inclusion free (Figure 3-2 a). The garnet-free lighter domains are dominated by coarse-grained quartz and plagioclase domain with less than 0.5% Chl+Bt (Figure 3-2 a and c). Accessory ilmenite is present within the matrix of both domains and as inclusions in some garnet poikiloblasts.

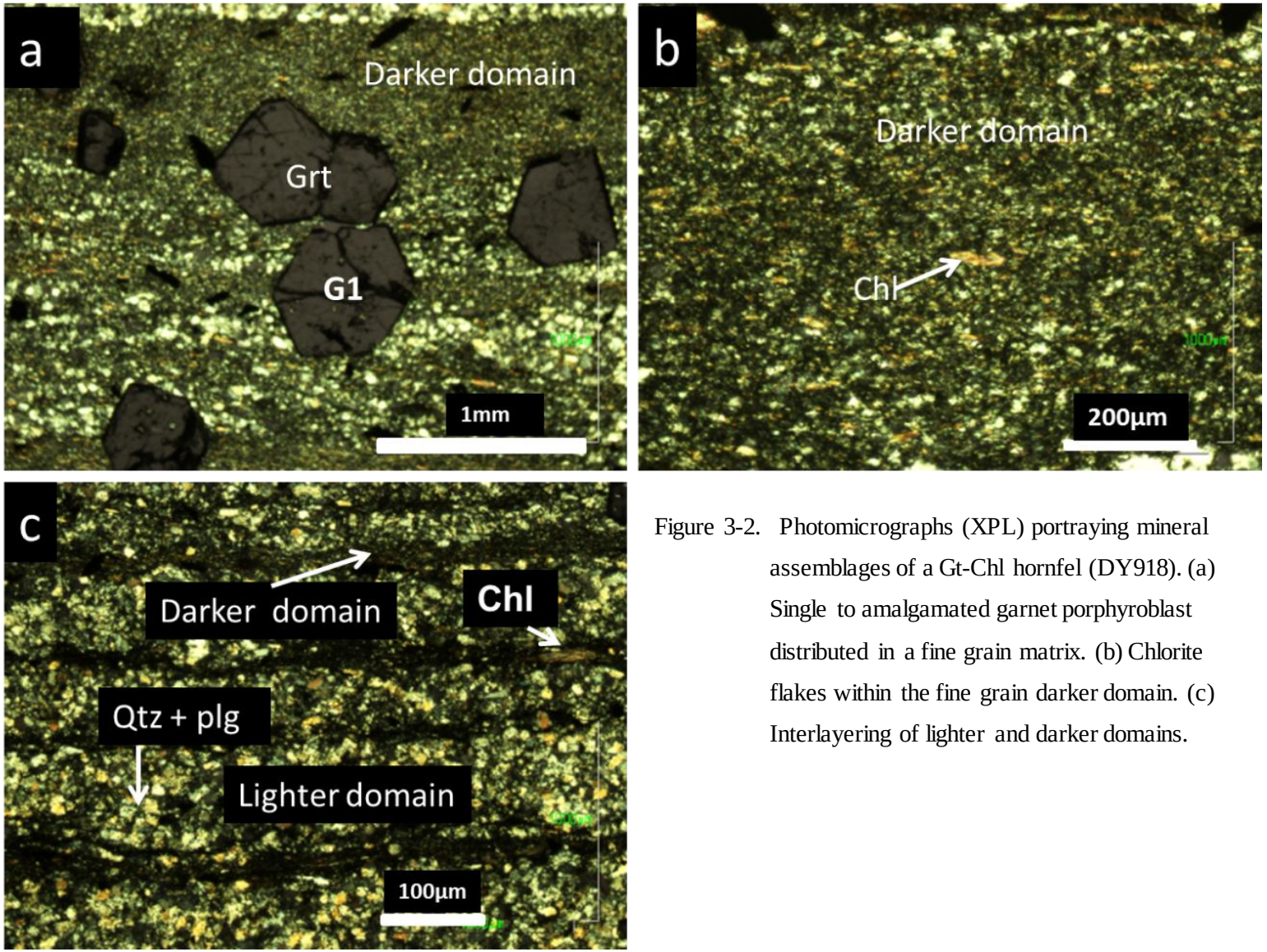

Figure 3-2. Photomicrographs (XPL) portraying mineral assemblages of a Gt-Chl hornfel (DY918). (a) Single to amalgamated garnet porphyroblast distributed in a fine grain matrix. (b) Chlorite flakes within the fine grain darker domain. (c) Interlayering of lighter and darker domains.

3.2.2 Sample DY954

The sample has a matrix assemblage of garnet (3%), biotite (32%), staurolite (0.9%), muscovite (1%), And (2%), ilmenite (0.3%), plagioclase (54%), chlorite (0.2%) and quartz (6.6%) (Table 3-1). The garnet porphyroblasts and poikiloblasts range in size from 0.3-1 mm in diameter and they range in crystal shapes from subidioblastic to idioblastic. Based on microstructural features, the garnet grains can be subdivided into five types; (i) grains isolated in the matrix, (ii) included within biotite, (iii) adjacent to biotite forming a reaction rim, (iv) aggregates and (v) resorbed garnet porphyroblasts (Figure 3-3 a-f). In general all garnets are fractured, mostly inclusion-free with no visible zonation at thin-section scale. Biotite porphyroblasts and poikiloblasts vary from tabular to anhedral and are typified by brownish to greenish pleochroic colours (Figure 3-3 e & f). Biotite also occur as inclusions within andalusite and adjacent to both andalusite and garnet. Biotite poikiloblasts contain common inclusions of quartz and ilmenite. Andalusite poikiloblasts range in size from 1.5-4 mm and are typified by chiastolite crossing with some grains altering to fine-grained clay minerals (Figure 3-3 f); its contains inclusions of quartz, muscovite, ilmenite and chlorite. Formation of muscovite and biotite along its rim regions is common (Figure 3-3 f). Staurolite porphyroblasts and ilmenite occur as accessory phases (Figure 3-3 e). Lenticular muscovite is abundant in the matrix and cross-cuts biotites grains flakes in rare cases (Figure 3-3 e). Plagioclase, quartz and chlorite also form part of the fine-grained matrix.

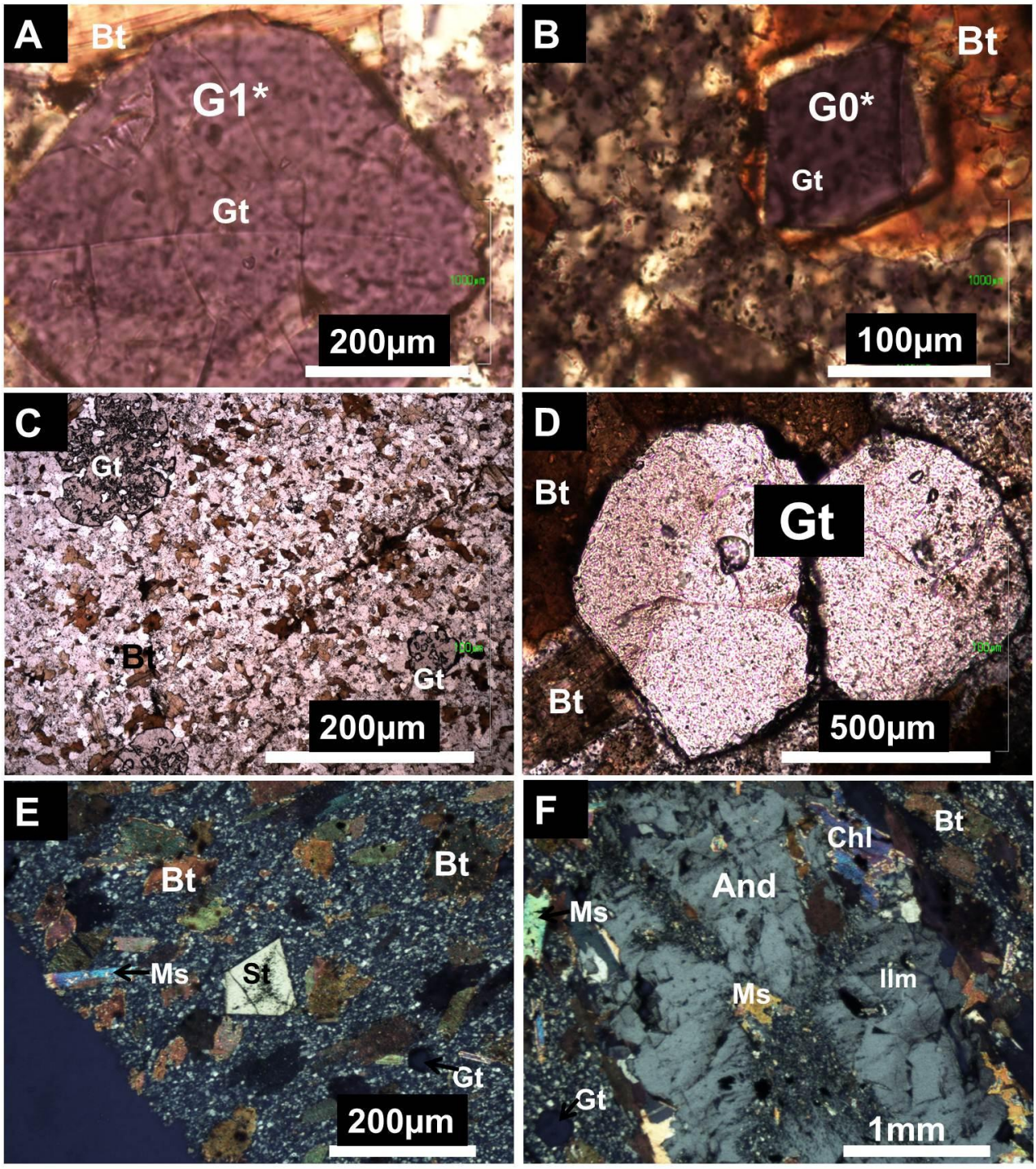

Figure 4-3 Photomicrographs showing representative mineral microstructures of DY954 hornfels. (a) Garnet porphyroblast (G2) adjacent to biotite. (b) Garnet (G0) included within biotite. (c) Resorbed garnet occurring around biotites in the fine grained matrix. (d) Aggregate garnet porphyroblast overgrowing biotite. (e) Epitaxial chlorite and muscovite cross cutting biotite, with isolated staurolite porphyroblast in the fine grained matrix. (f) Andalusite poikiloblast containing muscovite and ilmenite inclusions typified by chiastolite crossing and formation of biotite, muscovite and chlorite on the rim region.

3.2.3 Sample DY956

The hornfels comprises of biotite (35%), muscovite (0.5%), chlorite (0.4%), plagioclase (16%), staurolite (1), andalusite (2%), garnet (2%), quartz (43%) and ilmenite (0.1%) mineral paragenesis of different proportions (Table 3-1). Garnet proportion is less compared to the above mentioned hornfels. They can be subdivided into three microstructural settings; isolated porphyroblasts in the matrix, porphyroblasts overgrowing or adjacent to biotite and garnet aggregate (Figure 3-4 a, b and d). The biotite exhibits greenish to brownish pleochroic colours and range in shape from tabular to subhedral flakes (Figure 3-4 a - i). Andalusite poikiloblasts containing common inclusions of biotite, muscovite, ilmenite, staurolite and chlorite (Figure 4-3 e, g and h). They are also typified by chiastolite crosses (Figure 3-4 e, g and h).

Staurolite poikiloblasts ranging from idioblastic to subidioblastic are commonly characterised by inclusion free rims (Figure 3-4 c, f & i). In some cases staurolite appears to have been partial resorbed into quartz and also invades andalusite poikiloblasts (Figure 3-4 f-g). Tabular muscovite flakes are present within the fine-grained matrix and in rare cases together with biotite they exhibit an epitaxial texture with chlorite (Figure 3-4). In a rare case, recrystallized quartz with acicular inclusions of muscovite and chlorite (plus plagioclase and ilmenite) have been noted (Figure 3-4). Ilmenite occurring as platy and elongated acicular grains can be found as parallel inclusions in biotite and garnet.

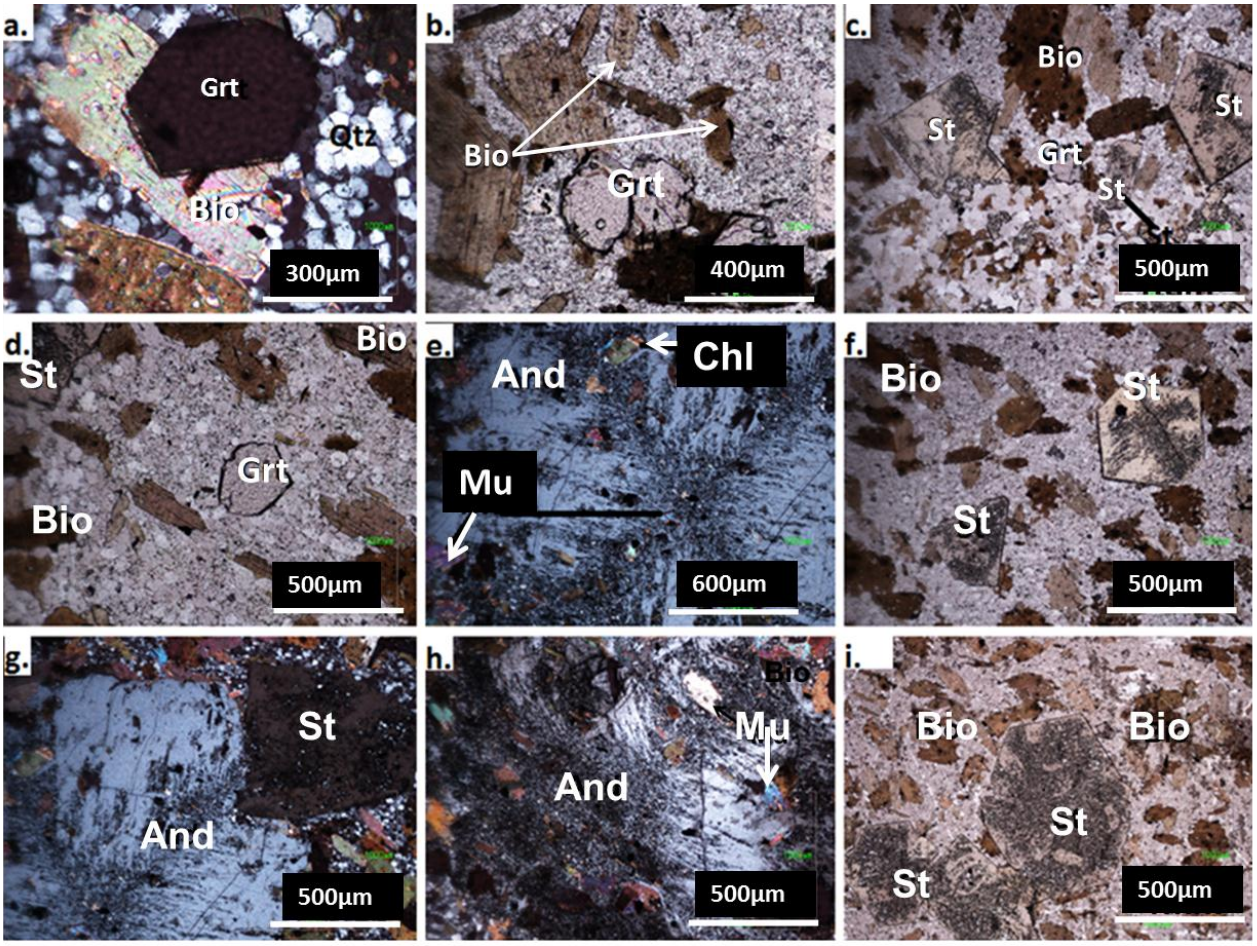

Figure 3-4. Photomicrographs showing mineral micro-textures of Bt-And-St-Gt hornfels (DY 956). (a.) Garnet porphyroblast overgrowing biotite and is surrounded by quartz rich matrix. (b) garnet aggregate overgrowing biotite. (c) Staurolite poikiloblast occurring around biotite and garnet porphyroblast. (d) Garnet isolated in the matrix surrounded by biotite and staurolite. (e) Andalusite poikiloblast typified by chiastolite crossing and containing inclusions of biotite, muscovite and ilmenite.(f) Euhedral staurolite with inclusion free rims surrounded by biotite.(g) Andalusite poikiloblast surrounded by biotite on the rims and staurolite poikiloblast appear to be invading the former.(h) Intensely altered andalusite poikiloblast with inclusions of biotite and muscovite. (i) Weathered euhedral staurolite surrounded by biotite.

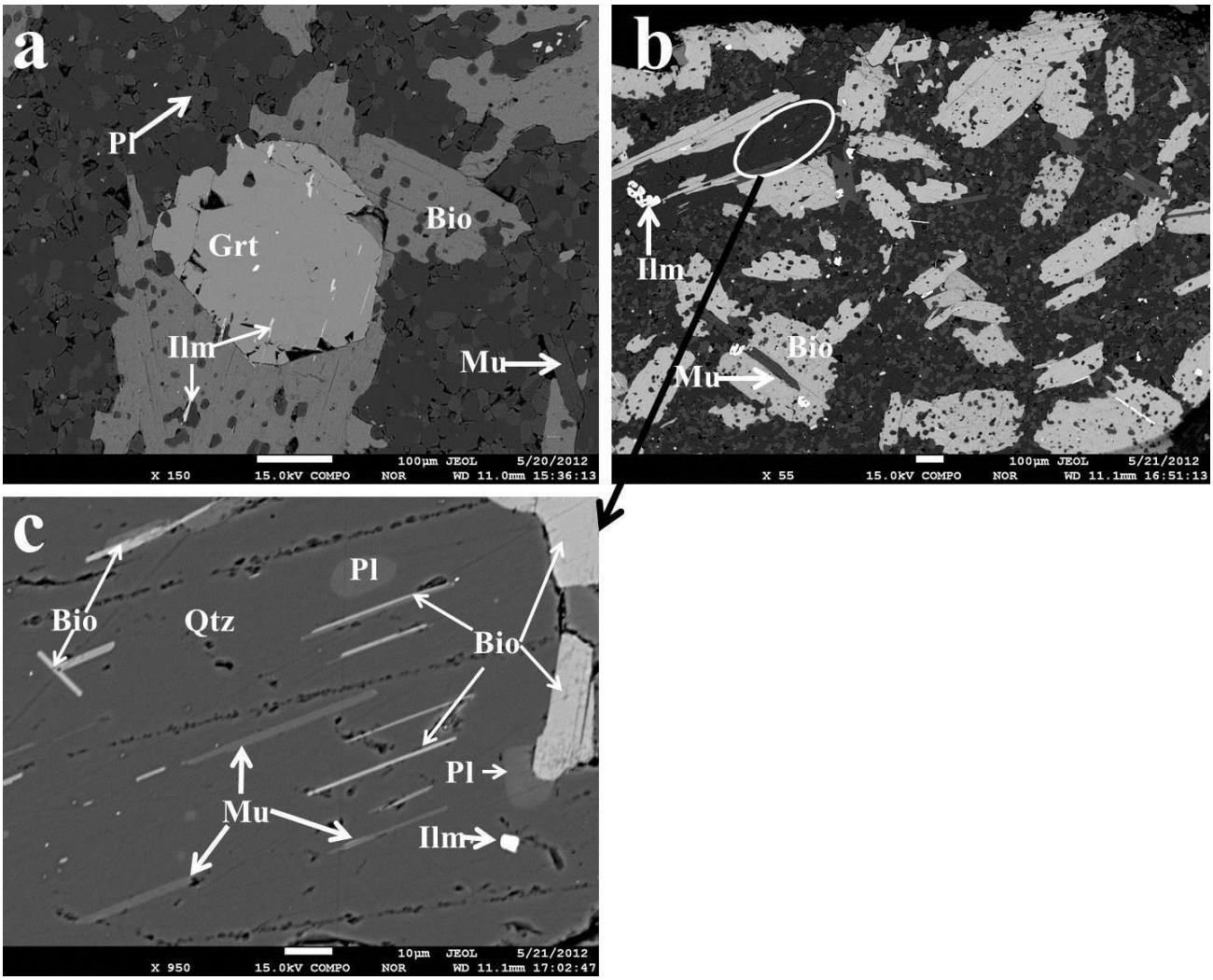

Figure 3-5. Back scattered images of Bt-And-St-Gt hornfels. (a) Garnet porphyroblast (G1) overgrowing biotite, surrounded by a plagioclase feldspar-quartz rich matrix (b) Epitaxial biotite and muscovite, recrystallized quartz which appears to be epitaxial to both biotite and muscovite; muscovite cross cutting biotite. (c) Recrystallized quartz with acicular and elongated inclusions of biotite, muscovite, plagioclase and ilmenite.

Table 3-1. Mineral modes (%) of gt bearing hornfels.

Mineral	Grt	Mu	Plg	Qtz	ilm	Bio	Chl	St	And
Sample									
DY918	6	-	56.5	12.7	1.48	7.8	15.5	-	-
DY954	3	1	54	6.6	0.32	32	0.18	0.9	2
DY956	2	0.5	16	43	0.1	35	0.4	1	2

3.3 Whole rock chemistry

The bulk rock major element compositions of garnet bearing hornfelses and average pelite compositions from literature (Symmes and Ferry, 1992; Bucher and Grapes, 2011) are listed in table 3-2 and plotted in figure 4-6 for comparison purposes. Sample DY918 is different from average pelitic compositions due to its higher CaO and Na_2O content but low K_2O which is due to high concentration of plagioclase. Furthermore, the recalculated bulk rock composition (DY918 #) follows a similar trend but with higher MgO and slightly higher K_2O due to the presence of garnet in the darker domain and an increase in chlorite and biotite content. DY954 composition is similar to the average pelitic composition but has a slightly higher Fe_{total} and Al_2O_3 with slightly lower MgO content. DY956 follows a similar trend but has a slightly lower CaO and MgO content. The bulk rock compositions of DY956 and DY956 hornfelses correlate to that of average pelitic composition whereas DY918 can be considered semipelitic.

Table 3-2. Representative bulk rock geochemical data of the studied hornfelses and average pelitic compositions

Wt%	DY918	DY918#	DY954	DY956	Av-SF	Av-BG	Avt-BG
SiO_2	60.31	51.04	53.52	60.66	59.77	54.90	61.52
TiO_2	0.83	1.04	0.89	0.77	-	0.78	0.73
Al_2O_3	17.79	20.80	20.77	18.32	16.57	16.60	16.48
$Fe_2O_3^*$	6.43	11.772**	12.60	11.76	6.53	9.70	8.40
MnO	0.09	0.16	0.07	0.08	0.07	-	-
MgO	0.76	3.88	1.89	1.34	2.62	3.40	2.80
CaO	6.22	5.59	2.94	1.12	2.17	0.78	5.42
Na_2O	2.86	2.99	1.61	0.80	1.73	1.30	3.63
K_2O	0.09	0.24	3.62	3.18	3.53	2.70	2.10
H_2O	2.10	2.49	0.77	0.79	7.65	9.20	1.30
Total	97.46	100.00	98.70	98.83	100.64	99.36	102.38

* Total Fe as Fe_2O_3 Av-SF: average pelite of Symmes & Ferry (1991)
** Total Fe as FeO Av-BG:average pelite of Bucher & Grapes (2011)
# Recalculated Av-BG:average tonalite of Bucher & Grapes (2011)

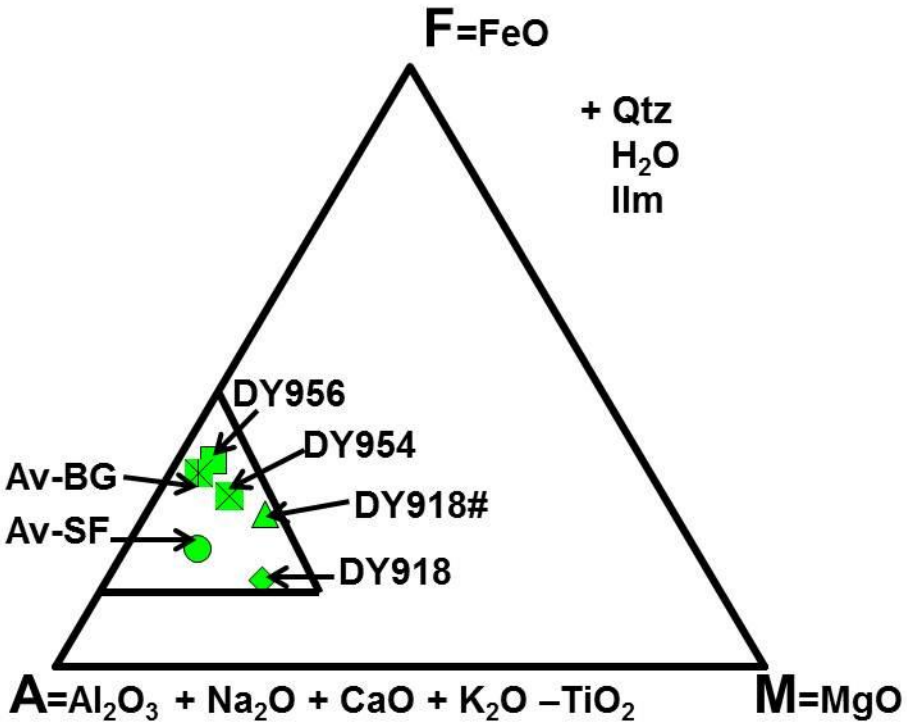

Figure 3-6. Bulk rock geochemical data for all garnet bearing hornfelses and average pelite compositions (Av-SF: Symmes & Ferry, 1992; Bucher & Grapes, 2011) plotted in an AFM projection. DY918#: Recalculated.

3.4 Mineral chemistry

The representative mineral chemistry of plagioclase, biotite, chlorite, chloritoid, ilmenite, white mica and staurolite, from the studied garnet-bearing samples are given in table 4-5 and appendix B.

Table 3-5. Representative mineral chemical data of various mineral phases of garnet bearing hornfelses, obtained from Cameca (c) and JEOL (J)

Sample	DY918							DY954												DY956								
Mineral	Chl^{1J}	Chl^{2J}	Bt^{*J}	$Gt1^{core*+J}$	$Gt1^{rim*+J}$	Pl^{*J}	ilm^{J}	Bt^{0*C}	Bt^{1*J}	Chl^{C}	$G0^{core*+C}$	$G0rim^{*+C}$	$G1^{core*+j}$	$G1^{rim*+j}$	And^{C}	St^{C}	Mu^{*C}	Pl^{0*C}	Pl^{1*J}	ilm^{J}	Bt^{*C}	Chl^{C}	Mu^{*C}	$Gt^{core*+j}$	Gt^{rim*+j}	Pl^{*C}	And^{C}	St^{C}	ilm^{J}
SiO_2	26.43	33.43	38.40	36.78	36.58	53.00		33.96	34.62	26.05	36.41	36.44	36.09	36.08	36.77	27.60	44.69	57.74	58.54	0.00	34.13	23.55	44.60	37.19	37.37	58.98	35.77	26.91	0.00
TiO_2	0.10	0.07	1.48	0.16	0.62	0.00	55.61	1.89	1.75	0.11	0.04	0.03	0.04	0.03	0.25	0.50	0.45	0.00	0.00	54.16	1.64	0.07	0.35	0.00	0.17	0.00	0.04	0.44	52.90
Al_2O_3	23.75	26.30	22.77	21.10	20.49	26.50	0.00	19.89	20.16	22.07	21.44	21.41	21.32	21.40	61.39	50.55	36.65	25.79	27.01	0.02	20.28	23.18	36.50	21.09	21.21	26.40	63.61	54.81	0.00
FeO	18.10	18.10	17.07	35.46	34.89	0.00	42.48	23.97	21.87	29.14	37.47	36.28	37.44	36.93	0.14	16.90	0.93	0.15	0.00	43.81	22.92	31.68	0.01	34.28	34.83	0.00	0.26	15.01	47.14
MnO	0.02	0.02	0.01	1.30	2.00	0.00	0.78	0.05	0.06	0.03	2.54	3.12	2.46	1.96	0.00	0.09	0.00	0.00	0.00	0.51	0.05	0.14	0.29	4.19	4.15	0.00	0.01	0.21	0.81
MgO	12.06	7.59	7.55	2.12	1.78	0.00	0.01	6.84	7.10	7.10	1.58	0.98	1.25	1.68	0.04	1.36	0.35	0.00	0.00	0.01	6.52	9.24	0.02	1.85	1.57	0.00	0.03	1.09	0.06
CaO	0.04	0.05	0.03	2.47	2.06	11.42	0.00	0.00	0.00	0.00	1.59	1.90	2.12	2.24	0.02	0.22	0.00	7.57	9.85	0.00	0.01	0.02	1.31	1.46	1.24	7.73	0.01	0.01	0.00
Na_2O	0.00	0.00	0.07	0.00	0.00	5.30	0.00	0.23	0.30	0.11	0.00	0.00	0.00	0.00		0.12	0.02	7.64	6.50	0.00	0.31	0.07	0.00	0.00	0.00	5.79	0.01	0.01	0.00
BaO	0.00	0.00		0.00	0.00	0.00	0.00	0.00	0.00	0.00	0.00	0.00	0.00	0.00	0.00	0.00	0.00	0.00	0.00	0.00	0.00	0.00	0.00	0.00	0.00	0.83	0.00	0.00	0.00
K_2O	0.00	0.00	7.50	0.00	0.00	0.92	0.00	8.84	7.14	0.08	0.00	0.00	0.00	0.00	0.00	0.16	9.54	0.09	0.04	0.00	9.21	0.04	8.47	0.00	0.00	0.05	0.01	0.00	0.00
Total (excl. H_2O)	80.50	85.56	94.87	99.39	98.41		98.88	95.67	93.00	84.69	101.07	100.16	100.72	100.32	98.62	97.50	92.63	98.98	101.93	98.50	95.06	87.99	91.55	100.05	100.54	99.79	99.74	98.50	100.92
Oxygen	14	14	11	12	12	8	3	11	11	14	12	12	12	12	5	23	11	8	8	3	11	14	11	12	12	8	5	23	3
Si	2.88	3.34	2.82	2.98	3.00	2.49	0.00	2.67	2.73	2.88	2.94	2.93	2.97	2.98	1.01	3.92	3.03	2.61	2.58	0.00	2.65	2.56	3.02	3.01	3.00	2.64	0.97	3.73	0.00
Ti	0.01	0.01	0.08	0.01	0.04	0.00	1.05	0.11	0.10	0.01	0.00	0.00	0.00	0.03	1.98	0.05	0.02	0.00	0.00	1.03	0.10	0.01	0.02	0.00	0.01	0.00	0.00	0.05	1.00
Al	3.05	3.09	1.97	2.00	1.98	1.44	0.00	1.84	1.87	2.88	2.04	2.05	2.05	2.04	0.01	8.46	2.93	1.38	1.40	0.00	1.85	2.97	2.92	2.01	2.02	1.39	2.03	8.95	0.00
Fe^{3+}	0.00	0.00	0.00	0.00	0.00	0.01	0.00	0.00	0.00	0.00	0.00	0.02	0.00	0.00	0.00	0.00	0.00	0.00	0.00	0.00	0.00	0.00	0.00	0.00	0.00	0.00	0.01	0.00	0.00
Fe^{2+}	1.65	1.51	1.05	2.43	2.42	0.00	0.89	1.58	1.44	2.70	2.53	2.53	2.40	2.46	0.00	2.01	0.05	0.01	0.00	0.93	1.49	2.88	0.00	2.34	2.38	0.00	0.00	1.74	0.99
Mn	0.00	0.00	0.00	0.09	0.14	0.00	0.02	0.00	0.00	0.00	0.17	0.17	0.23	0.18	0.00	0.01	0.00	0.00	0.00	0.01	0.00	0.01	0.02	0.29	0.28	0.00	0.00	0.02	0.02
Mg	1.96	1.13	0.83	0.26	0.22	0.00	0.00	0.80	0.83	1.17	0.19	0.15	0.24	0.18	0.00	0.29	0.04	0.00	0.00	0.00	0.75	1.50	0.00	0.22	0.19	0.00	0.00	0.23	0.00
Ca	0.00	0.01	0.00	0.21	0.18	0.57	0.00	0.00	0.00	0.00	0.14	0.19	0.13	0.11	0.00	0.03	0.00	0.37	0.46	0.00	0.00	0.00	0.10	0.13	0.11	0.37	0.00	0.00	0.00
Na	0.00	0.00	0.01	0.00	0.00	0.48	0.00	0.03	0.05	0.02	0.00	0.00	0.00	0.00	0.00	0.03	0.00	0.67	0.56	0.00	0.05	0.01	0.00	0.00	0.00	0.50	0.00	0.00	0.00
Ba	0.00	0.00	0.00	0.00	0.00	0.00		0.00	0.00	0.00	0.00	0.00	0.00	0.00	0.00	0.00	0.00	0.00	0.00		0.00	0.00	0.00	0.00	0.00	0.02	0.00	0.00	0.00
K	0.00	0.00	0.70	0.00	0.00	0.05	0.00	0.87	0.71	0.01	0.00	0.00	0.00	0.00	0.00	0.03	0.82	0.01	0.00	0.00	0.91	0.01	0.73	0.00	0.00	0.00	0.00	0.00	0.00
Total	9.56	9.09	7.45	7.98	7.98	5.04	1.96	7.91	7.74	9.68	8.02	8.04	8.03	7.98	3.00	14.82	6.89	5.04	5.00	1.97	7.81	9.96	6.80	7.99	7.99	4.92	3.01	14.72	2.00
X_{Fe}	0.46	0.57	0.56	0.90	0.92	0.00	1.00	0.66	0.63	0.70	0.93	0.94	0.91	0.93		0.87	0.60			1.00	0.66	0.66	0.22	0.91	0.93			0.89	1.00
X_{an}						0.54												0.35	0.45							0.42			
X_{ab}						0.46												0.64	0.54							0.57			
X_{or}						1.00												0.00	0.00							0.00			
X_{alm}				0.81	0.82						0.82	0.81	0.79	0.82										0.79	0.78				
X_{sps}				0.03	0.05						0.06	0.06	0.05	0.06										0.09	0.10				
X_{prp}				0.09	0.07						0.05	0.05	0.08	0.06										0.07	0.06				
X_{grs}				0.07	0.06						0.04	0.05	0.04	0.04										0.04	0.04				

*: analysis used for garnet isopleth thermobarometry 0 included garnet and local equilibrium assemblage

+: analysis used for Classical geothermobaromerty 1 garnet isolated in the matrix and local equilibrium assemblage

3.4.1 Gt-Chl Hornfels (DY918)

The plagioclase within the fine grained matrix has a composition that is dominated by andesine with minor traces of labrodorite; with an X_{ab} and X_{an} content of 0.46 and 0.54 respectively (Figure 3-6). Biotite has an Al^{IV} content that ranges from 1.74-1.79 and $X_{Fe\ (Fe/\ (Fe+Mg)}$ = 0.56, whereas Ti content ranges from 0.074-0.089 wt. %. Chlorite can be subdivided into chamosite (Chl^1) with an Fe/Fe+Mg 0.46 and an intermediate composition of chamosite and clinochlore (Chl^2) with an Fe/Fe+Mg of 0.57 (Table 3-4).

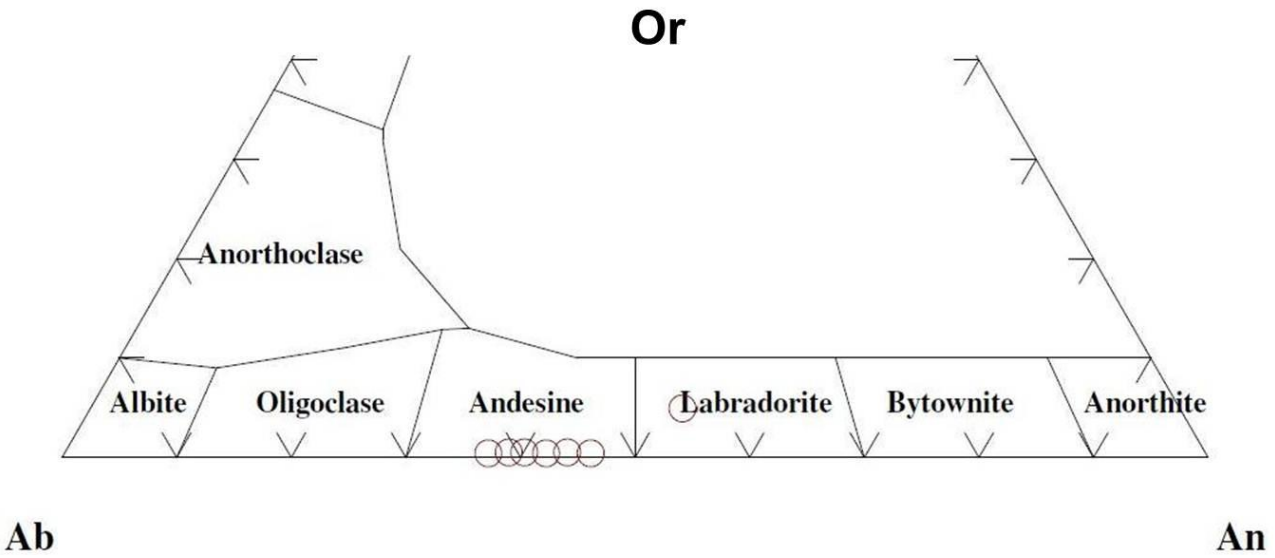

Figure 3-7. Classification of plagioclase, circles represent the analysed feldspars of sample DY9-18.

Both G0 and G1 garnets visually shows no distinct core and rim regions but base on the end member composition profiles the core and rim can be separated (figure 3-7 a and b). The G0 garnet is characterised by zoning profiles of two garnet grains with each similar to G1, but the former has slightly higher X_{sps} content of 0.07 compared to 0.05 at the core for G1 (Figure 3-7 a). These grains are zoned, particularly with respect to X_{alm} and X_{sps}, which reaches a low and high of about 0.82 and 0.05 at the core and a rise and fall of 0.86 and 0.01 towards the rim region. On contrast, pyrope and grossular are fairly homogenous from rim to core region at ~0.07 and 0.05 respectively.

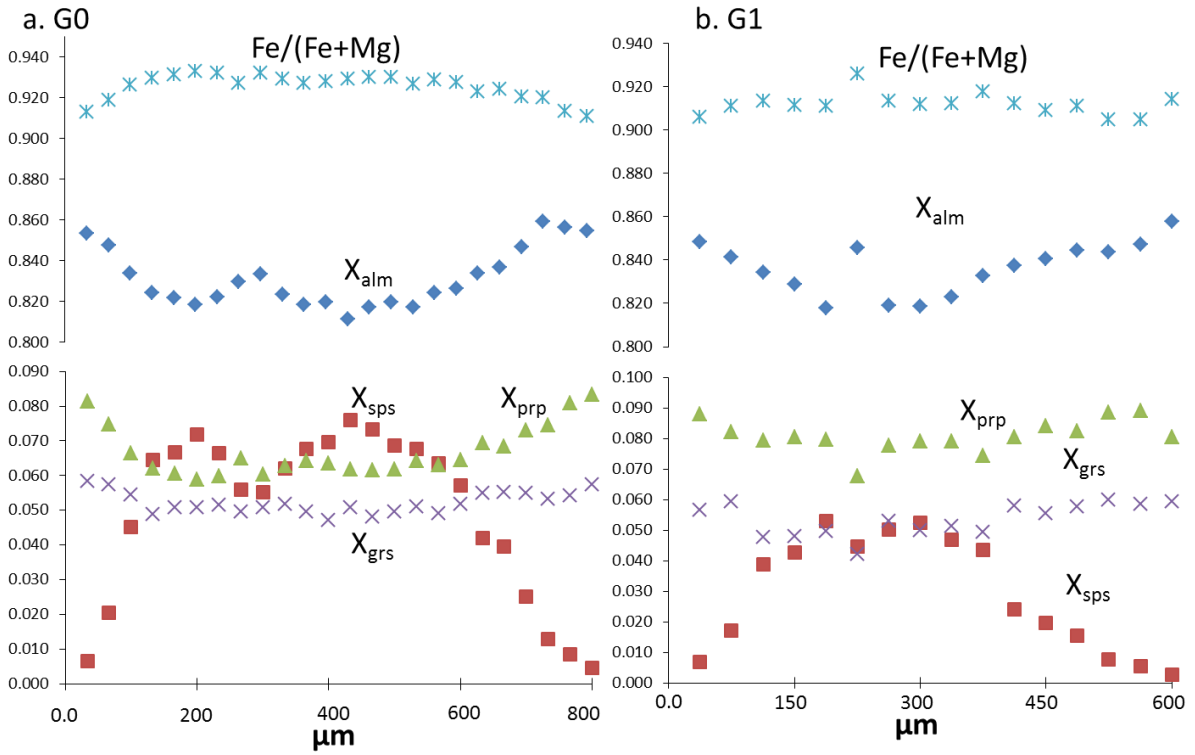

Figure 3-8. Compositional profiles across (a) G0 garnet aggregates and (b) G1 garnet porphyroblast.

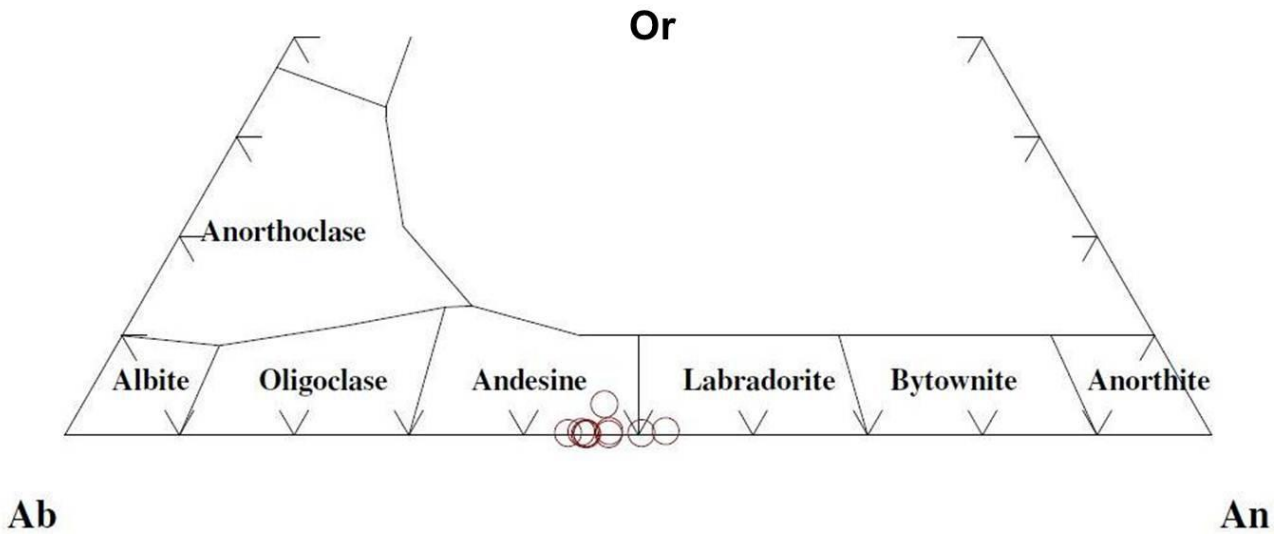

Figure 4-9. Composition of plagioclase (circles) from DY954 in terms of An-Ab-Or.

3.4.2 Bt - Gt – And – St - Pl hornfels (DY954)

Biotites Mg/Mg+Fe ranges of 0.34 - 0.37 and Ti = 0.09 – 0.12 (Bt^0 - Bt^1) plotting well within eastonite and siderophyllite field of Fe/ (Fe+Mg) vs. Al (VI), with (Table 4-4). Staurolite composition is fairly homogenous from core to rim region, with Mg/Mg+Fe 0.24 – 0.27, whereas chlorite Fe/Mg+Fe is 0.7.

White mica exhibit a slight variation in composition, with Si = 3.01 -3.12. Plagioclase has an albite content that ranges from 0.56 - 0.67 plotting between andesine and labrodorite fields of Ab-An-Or (Figure 4-8).The garnet composition is divisible into end-members of almandine (~79%), spessartine (~8%), pyrope (~8) and grossular (~4).

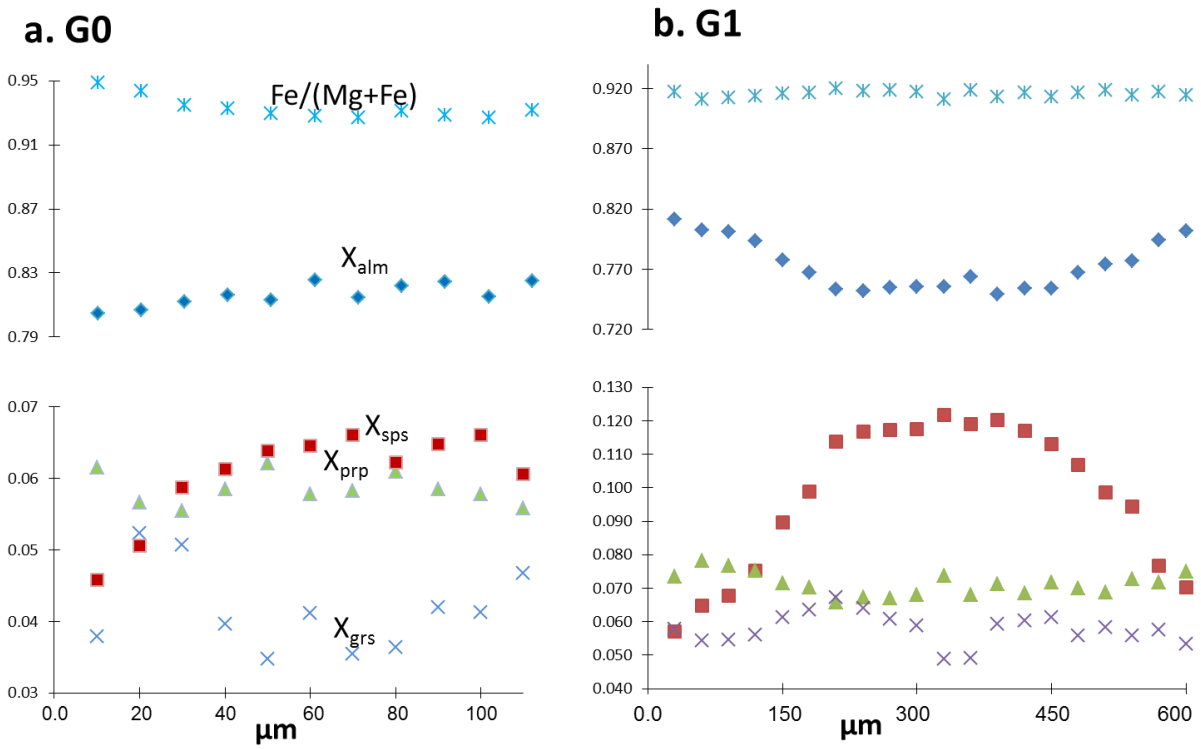

Figure 3-10. Compositional garnet zoning profiles across (a) G0 and (b) G1 of sample DY954

G0 garnet displays a fairly homogenous compositional profiles particularly with respect to Fe/ (Fe+Mg), X_{sps}, X_{alm} and $X_{prp.}$ In contrast, X_{sps} is subtle zoned with ~0.065 at the core and ~0.045 at the rim region (Figure 3-10 a). G1 garnet displays zoning which is marked by a high of ~0.12 X_{spss} at the core and a fall to 0.055 at the rim region. Furthermore, almandine zoning is characterised by a low of ~0.74 at the core and 0.82 at the rim region. On the other hand, Fe/ (Fe+Mg), X_{grs}, and $X_{prp\ displays}$ a fairly homogenous behaviour across the grain. G1 garnet is more enriched in spessartine as compared to G0 (Figure 3- 10b).

3.4.3 Bt - And – Pl - Gt - St- hornfels (DY956)

All Staurolite porphyroblasts displays a fairly homogenous composition with an Fe/Fe+Mg of 0.86 - 0.87. Biotite composition falls within annite and siderophyllite in a field of Fe/ (Fe+Mg) vs. Al (VI) and has an Mg/Mg+Fe of 0.44. Chlorite has a Fe/Fe+Mg content of 0.7 whereas, plagioclase has an anorthite content of 0.5% plotting within andesine field of Ab-An-Or (Figure 4-10).

The garnet porphyroblast in DY9-56 (Figure 3-12) exhibit a more homogenous compositional behaviour when compared to those in samples DY918 and DY9-54, particularly Fe/(Fe+Mg), X_{grs} X_{alm} and X_{sps}. In contrast a subtly zoning is displayed by X_{prp} with a high of ~0.06 at the core and then falls to ~0.05 at the rim region (Figure 3-12).

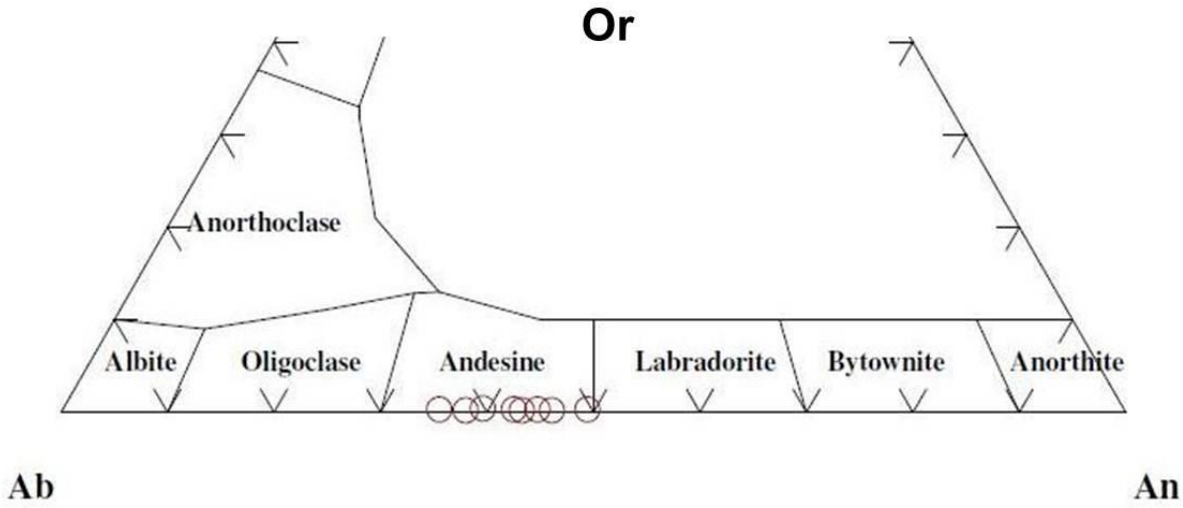

Figure 3-11. Composition of plagioclase (circles) from DY954 in terms of An-Ab -Or.

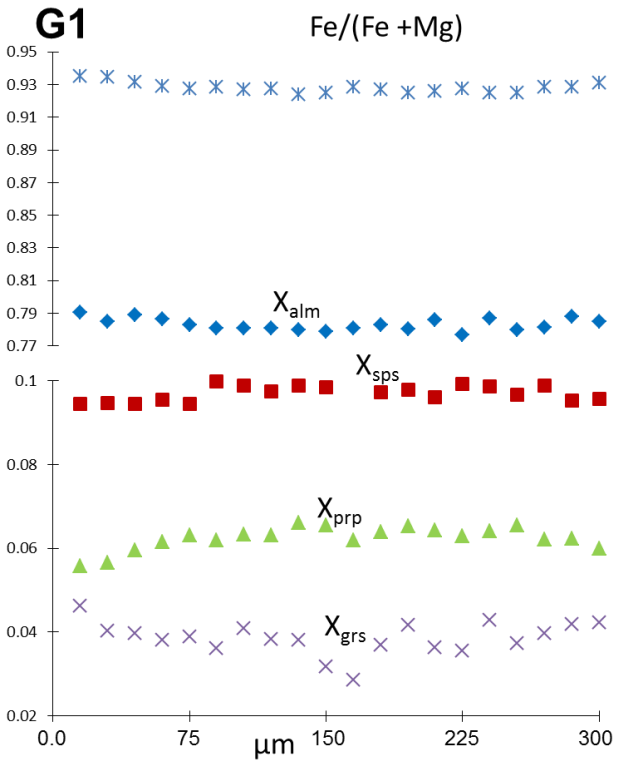

Figure 3-12. Compositional profile across a garnet porphyroblast in sample DY956

3.5 Relationship between mineral chemical and whole rock geochemical data

All the AFM diagrams were calculated from a six component K_2O-FeO-MgO-Al_2O_3-SiO_2-H_2O system which was further reduced to a 3 component diagram for simplification by assuming that they are saturated in H_2O, SiO_2, ilmenite, muscovite and plagioclase (only for sample DY954 and DY956).

The AFM diagram of DY918 in figure 3-13 predicts that both bulk1 and bulk2 are compatible with Gt –Pl – Chl and Gt-Bt- Pl assemblages. Both bulk rock composition plots above the Gt-Chl tie-line with bulk1 exhibiting a higher Alkaline content compared to bulk2 hence explaining the overall higher abundance of plagioclase within the rock. In addition, Bulk2 has a higher MgO and FeO content because the darker domain is enriched in ferromagnesian minerals (Figure 4-13).

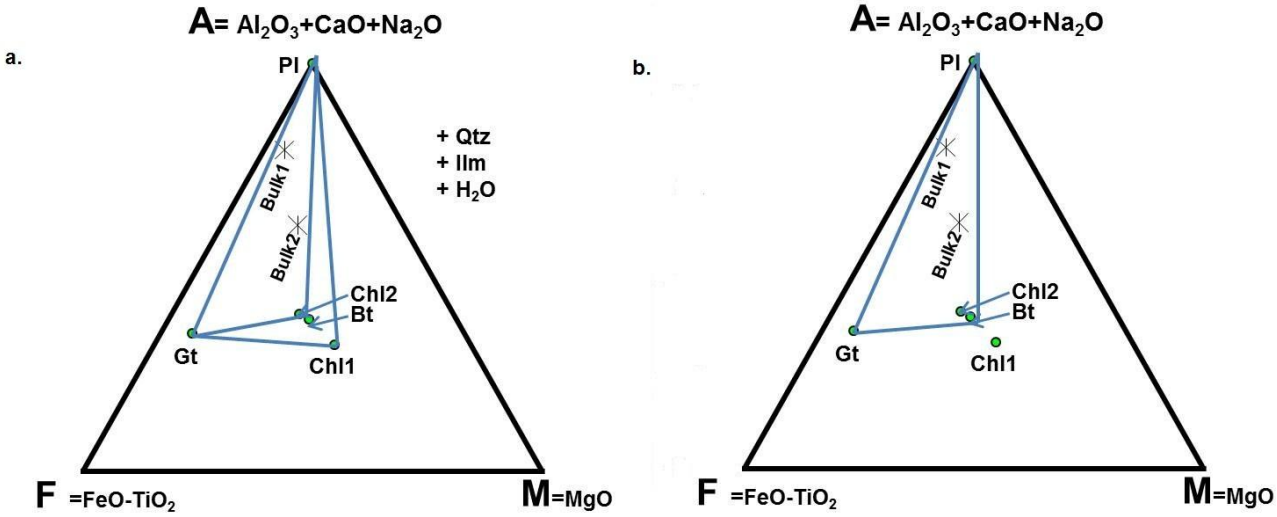

Figure 4-13. Schematic AFM diagram representing the bulk rock composition of DY918 hornfels divisible into bulk1 (measured) and bulk2 (recalculated) and observed mineral rock assemblages. Chl1 and Chl2 represent chamosite rich and an intermediate composition of chamosite and clinochlore.

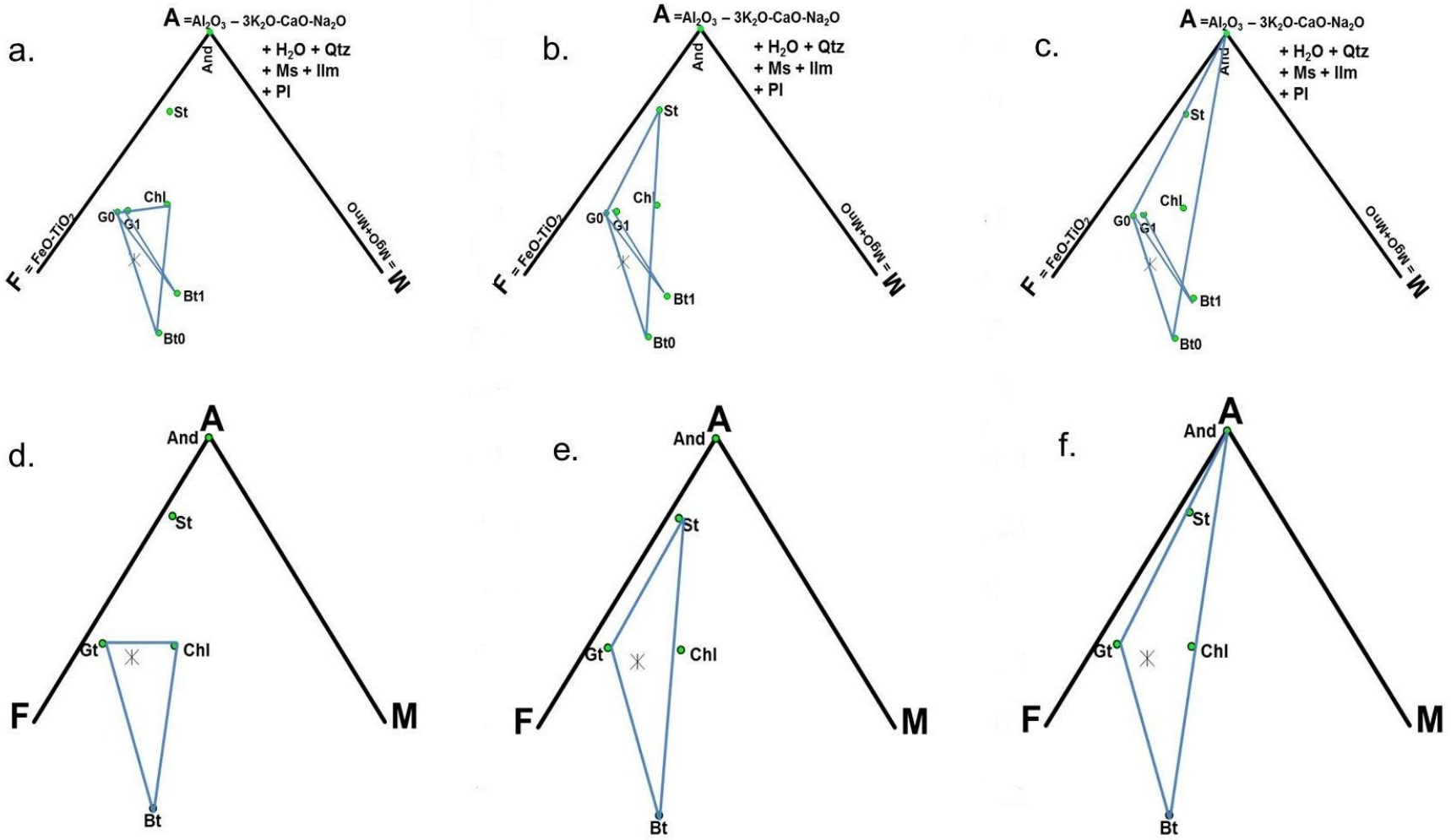

Figure 3-14. Schematic AFM diagrams representing observed mineral assemblages in DY954 (a – c) and DY956 (d-f) hornfelses. Bulk rock and mineral compositions indicated by stars and dots respectively.

AFM diagrams in figure 3-14 of both DY954 and DY956 hornfelses are compatible with Bt-Gt-Chl, Bt-Gt-St and Bt-Gt-And mineral assemblages. The chemographic relations of G0 and G1 garnet is G1>G0 (Mg+Mn) and their counterpart Bt^0 and Bt^1 have distinct compositions, Bt1>Bt0 (FeO – TiO_2). The bulk rock compositions of both hornfelses plots below the Gt-Chl tie-line and all G1-Bt1 bearing assemblages are not compatible with respective bulk rock compositions. Hornfels DY954 further predicts a garnet forming reaction indicated by the intersections of Gt-Bt with St-Bt0 and And-Bt0 tie-lines.

The AKF diagrams of DY954 (a.) and DY 956 (b.) hornfelses in figure 3-15 predict andalusite, staurolite and garnet forming reactions; Ms + Chl = St + Bt, Ms + Chl = And + Bt, Ms + Gt + Chl = St + Bt and Ms + Gt + Chl = And + Bt. Furthermore, assemblages of Ms-St-Chl, Ms-St-Gt and Ms-And-St are not compatible with the bulk rock compositions.

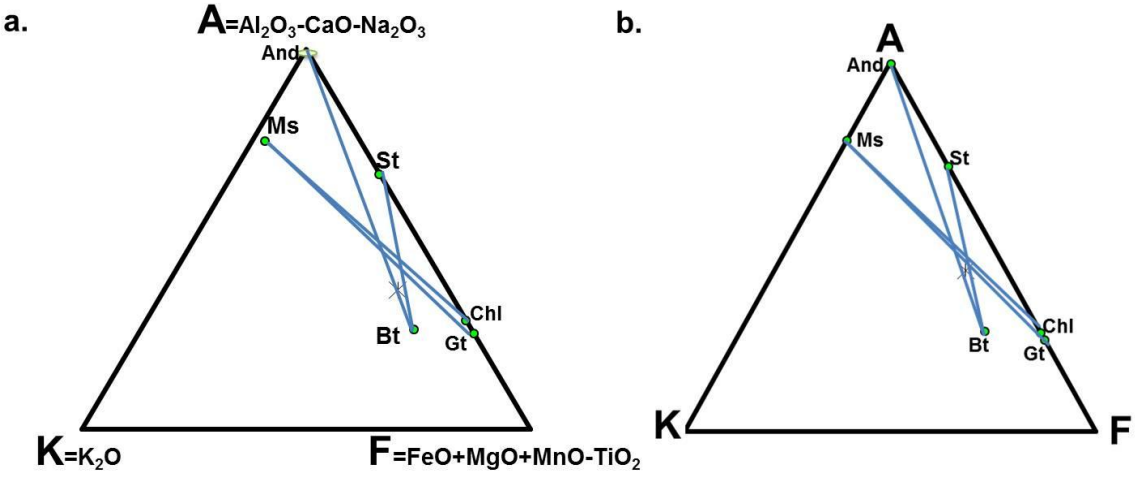

Figure 3-15. AKF diagram showing bulk rock (star) and mineral (dots) composition of DY954 (a) and DY956 (b) hornfelses. Tie-lines joining Ms-Chl, St-Bt, And-Bt and Ms-Gt are indicated by solid lines.

3.6 Pseudosection and garnet isopleth thermo-barometry

The H_2O content for all pseudosection was estimated from a T-X diagram as the amount that best represented all the observed minerals. When H_2O was assumed to be saturated, low grade phases such as Ms and Chl were found to be stable throughout the given P-T window as a result of the excess H_2O.

3.6.1 Gt-Chl hornfels (DY918)

At 2.5 kbar, the observed peak mineral assemblage is indicated by field (i) which is stable less than 550 ^{0}C at X_{H2O} between 0.35 and 0.75, whereas the low T assemblage represented by field (ii) is stable between 445 and 505 ^{0}C at $X_{H2O} > 0.75$ (Figure 3-16). At higher T and H_2O, garnet – opx-spin assemblage is stable, whereas at lower temperature and H_2O deficient conditions talc, garnet and orthopyroxene are stable. Therefore, the observed mineral assemblages of the Gt-Chl hornfel (DY918) are stable under water saturated and low temperature conditions.

The measured bulk rock composition of DY918 represents both the lighter and darker chemical domains, with the former dominated by plagioclase and quartz, whilst the latter is dominated biotite, chlorite, garnet, plagioclase, quartz and ilmenite with garnet formation only restricted to the darker domain. The bulk rock of the darker chemical domain was recalculated (Table 3-2) and used for pseudosection calculations since its represent local equilibrium with the phases of interests. A $MnO-Na_2O-CaO-K_2O-FeO-MgO-Al_2O_3-SiO_2-H_2O$ + Ilm system was used to calculate the pseudosection, chosen based on major oxides that best represent all the observed phases. The observed mineral paragenetic sequence from modelled pseudosection, is best represented by a broader fields of Bt - Chl - Pl - Qtz - Ilm and Bt - Chl - Pl - Qtz - Gt - Ilm occurring within 500 ^{0}C < T <550 ^{0}C temperature window (Figure 3-17).

The G1 garnet rim records P-T condition of 505 ± 13 ^{0}C at 3.05 ± 0.2 kbar and 525 ±13 ^{0}C at 0.6 ±0.2 kbar, whilst the core records 548 ±13 ^{0}C at 1.4 ±0.2 kbar (Figure 3-17). These conditions predict a field of Bt - Chl - Pl - Grt - Opx - Ilm - H_2O which does not describe the observed mineral assemblage. However, field of plg + chl + bio + grt + qtz + ilm + H_2O which best describes the observed mineral assemblage is within error of the predicted field.

The estimated P-T condition shows that the core formed at slightly higher P-T conditions than the rim for all garnet grains. The combination of the observed mineral phases and the garnet isopleth suggest that the rock underwent a prograde clockwise path, with field (i) and (ii) indicating low temperature and a peak metamorphic grade assemblage respectively (Figure 3-17)

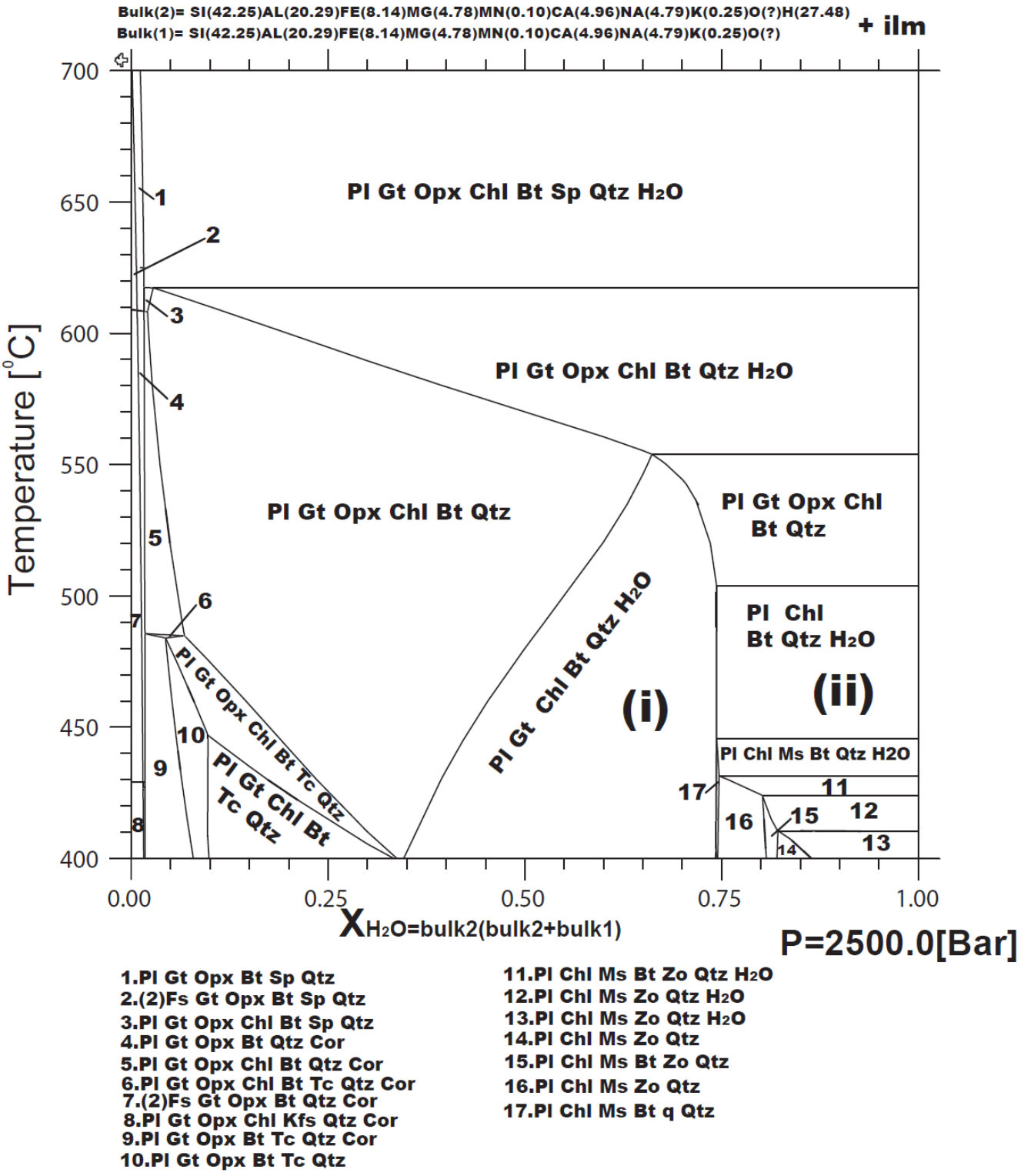

Figure 3-16. T-X binary section for the recalculated bulk rock composition (darker domain) of DY918 hornfels, showing the influence of access H_2O on the stability of observed mineral phases. Fields (i) and (ii) indicate the observed and predicted assemblages

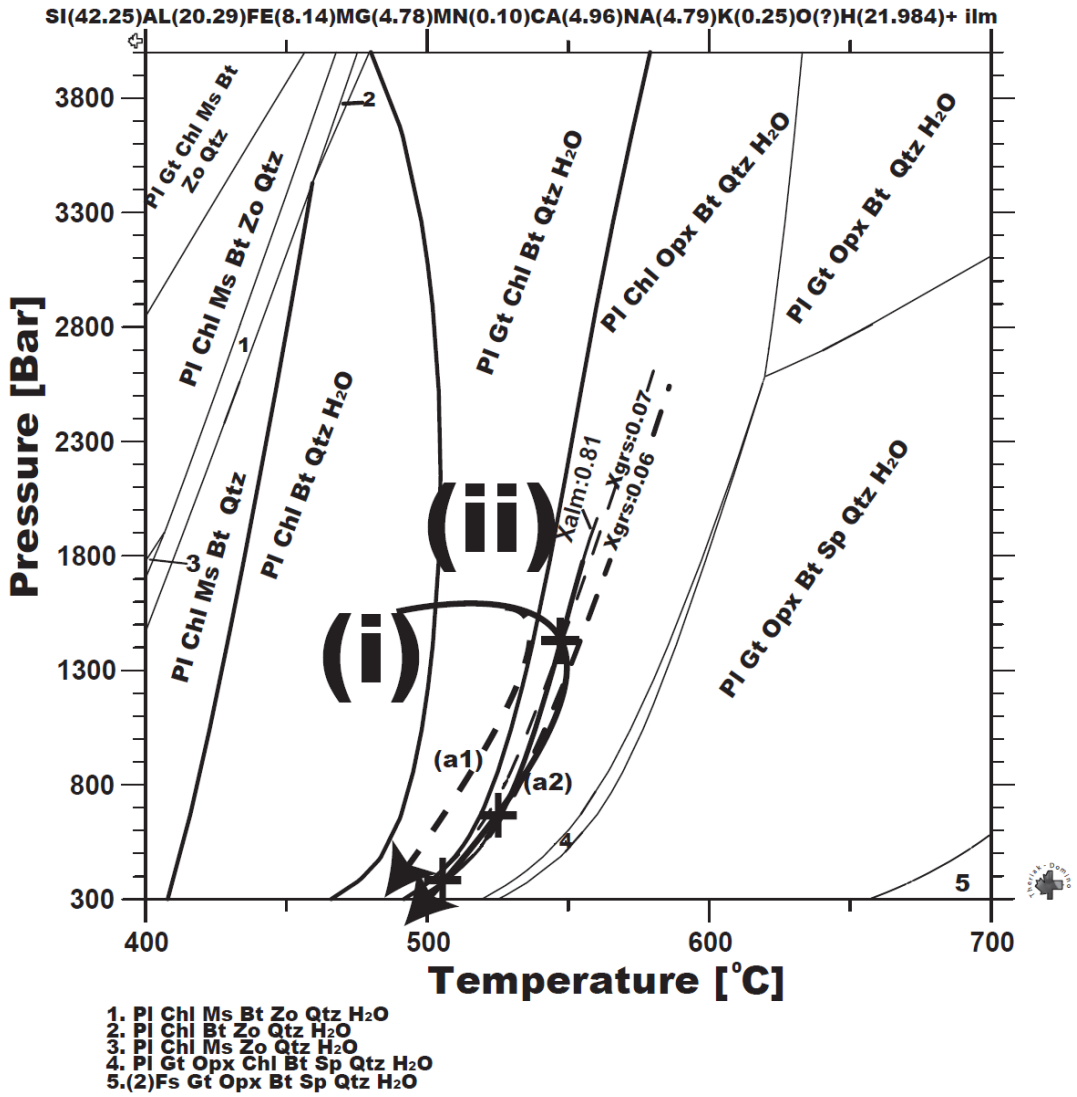

Figure 3-17. MnNCKFMAST pseudosection calculated for the recalculated bulk rock composition of sample DY918. Fields (i) and (ii) represent the fields that best locates the observed mineral paragenesis, while the crosses indicate the intersections of almandine and grossular garnet end members. Path a2 is the predicted path, whilst a1 represent a parallel alternative path within the field of interest.

3.6.2. Bt - Gt-And-St-Pl hornfel (DY954)

The pressure was fixed at 3kbar, the observed mineral assemblages are indicated by fields (i) to (iv) and are stable between 430 and 645 ^{0}C at X_{H2O}> 0.4 (Figure 3-18). At higher T and H_2O (> 650 ^{0}C at X_{H2O} 0.75), Gt + Sill are stable, whereas between 580 and 650 ^{0}C under H_2O saturated conditions the peak metamorphic condition are defined by field (i) where Gt + And are stable; while St is only stable between 540 and 580 ^{0}C under the same H_2O conditions but below 580 ^{0}C at just above 0.45 but below 0.5 X_{H2O} content (Figure 3-18). Lower temperatures and water saturated conditions are defined by stabilisation of Ms- Chl -Ctd. Therefore, the mineral paragenesis defining the hornfels (DY954) are stable at X_{H2O} > 0.4 below 650 ^{0}C.

The pseudosection was calculated using a MnO-Na_2O-CaO-K_2O-FeO-MgO- Al_2O3-SiO_2 – H_2O + Ilm system under water saturated (assuming no H_2O loss) conditions and was chosen based on the observed minerals. The successive growth stages of the observed mineral assemblages in this hornfels are best described by field (i) to (vi) which are stable: 450 ^{0}C < T < 680 ^{0}C at P < 3.8 kbar P-T window (Figure 3-19). The lower temperature mineral assemblages are represented by fields of Bt - Chl - Pl – Ms - And - Qtz and Bt – Chl – Pl – And – Qtz. At about 500 ^{0}C, the lower stability limit of garnet is marked by a thinner field of Bt – Chl – And – Pl – Gt – Qtz – H_2O which grades up to a broader field of Bt - Pl - And - Gt - Qtz - H_2O that is defined by the complete consumption of chlorite at peak metamorphic conditions. The formation of staurolite which is associated with an increase in pressure and a drop in temperature which is marked by garnet instability is indicated by the field of Bt – St - Pl - Qtz - And. As cooling continues, retrograde muscovite is formed at the expense of andalusite resulting in a stable assemblage of Bt - St - Ms - Pl - Qtz. These successive growth stages of the rock are controlled by prograde heating and retrograde cooling, the consumption of chlorite and formation of garnet from field (i) to (ii) does support this notion, whereas the production of staurolite and muscovite as a result of a drop in temperature and increase in pressure in field (iii) to (iv) supports a retrograde process.

The estimated rim and core P-T conditions for G0 garnet are 590 ± 30 ^{0}C at 2.65± 0.35 kbar and 625± 30^0 C at ~1.6 ± 0.35 kbar respectively. On the other hand, G1 suggest metamorphic conditions of 625± 30 ^{0}C 2.2 ± 0.35 kbar and 520 ± 30 ^{0}C at 0.5±0.35 kbar (Figure 3-17). The P-T estimates of G0 garnet suggest that the formation of the core and rim occurred over a temperature interval of ~35 ^{0}C.

In contrast, G1 garnet exhibit much longer interval of ~105 ^{0}C which might suggest that it has experienced an elongated period of heating and therefore, it is possible to assume that the two garnets experienced different metamorphic conditions which also influenced their micro-textural settings. The obtained P-T estimates and all the predicted fields that defines the rock prograde evolution assumes an anticlockwise P-T path (Figure 3-19)

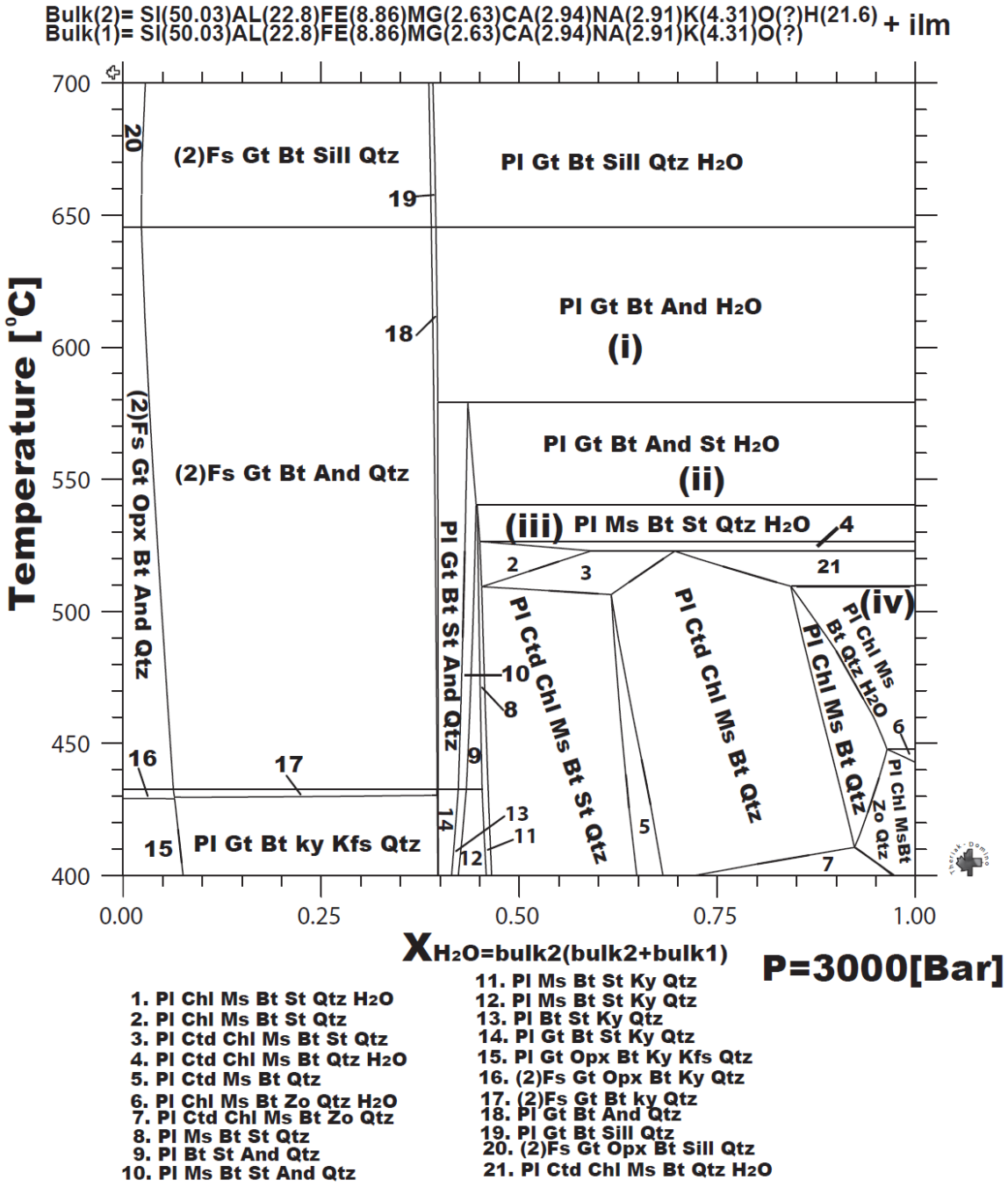

Figure 3-18. T-X binary section of sample DY954 showing the influence of H_2O variation on the stability of the observed mineral phases. Fields (i) and (iv) indicate observed and predicted assemblages

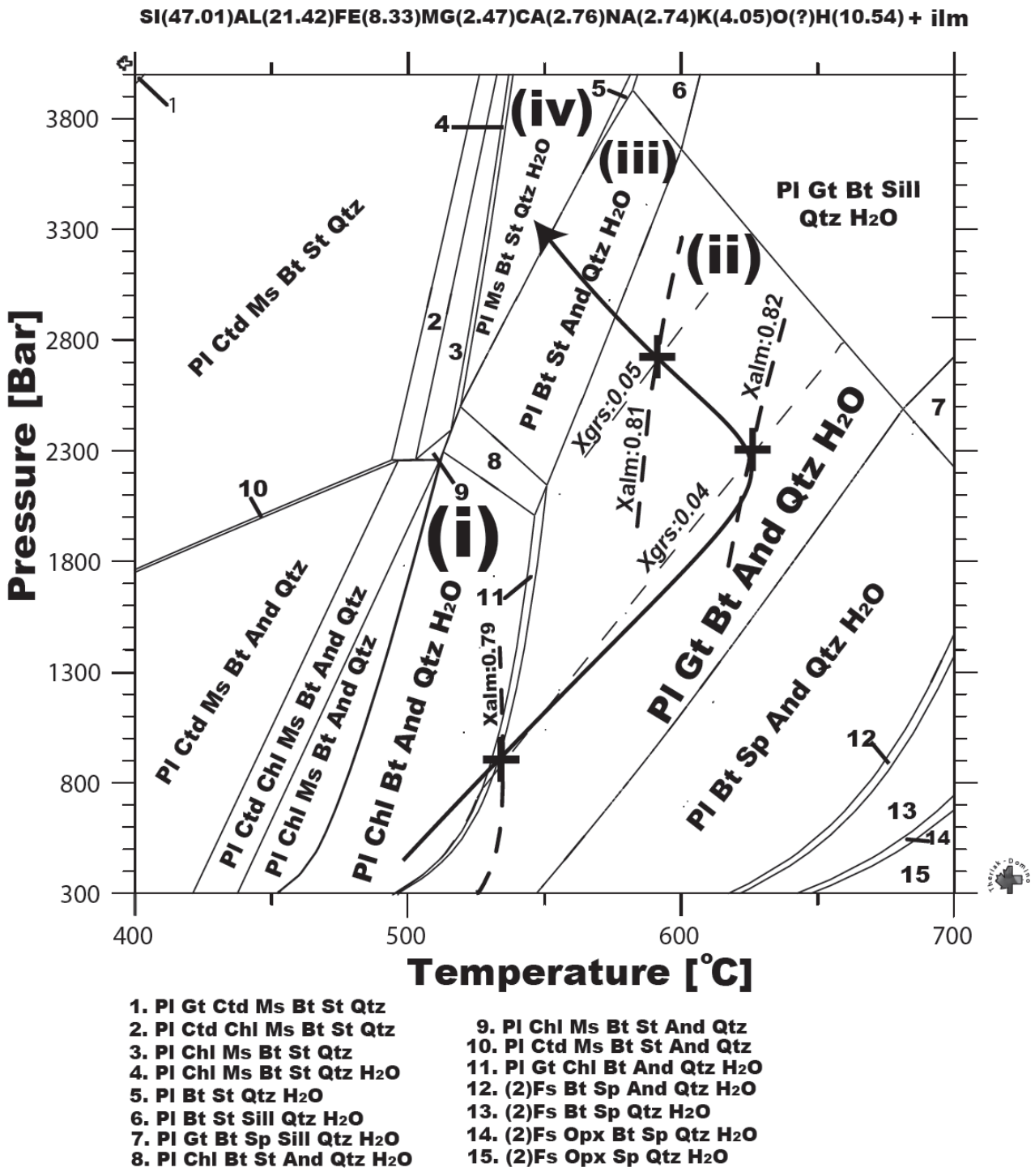

1. Pl Gt Ctd Ms Bt St Qtz
2. Pl Ctd Chl Ms Bt St Qtz
3. Pl Chl Ms Bt St Qtz
4. Pl Chl Ms Bt St Qtz H_2O
5. Pl Bt St Qtz H_2O
6. Pl Bt St Sill Qtz H_2O
7. Pl Gt Bt Sp Sill Qtz H_2O
8. Pl Chl Bt St And Qtz H_2O
9. Pl Chl Ms Bt St And Qtz
10. Pl Ctd Ms Bt St And Qtz
11. Pl Gt Chl Bt And Qtz H_2O
12. (2)Fs Bt Sp And Qtz H_2O
13. (2)Fs Bt Sp Qtz H_2O
14. (2)Fs Opx Bt Sp Qtz H_2O
15. (2)Fs Opx Sp Qtz H_2O

Figure 3-19. MnNCKFMAST pseudosection calculated for a measured bulk rock composition of sample DY954. Dash lines shows the garnet end members of X_{alm} and X_{grs}, the intersections of these end members are depicted by crosses which are joined by an inferred anticlockwise P-T path. Fields (i) to (iv) represents the paragenetic sequence followed by the rock.

3.6.3 Bt - And – Pl - Gt - St- hornfels (DY956)

The pressure was fixed at 3kbar because of the presence of andalusite. The observed mineral assemblages are indicated by field (i) to (v) and are stable between 400 and 645 ^{0}C at X_{H2O} > 0.35 (Figure 3-21). At higher T and H_2O (> 650 ^{0}C at X_{H2O} 0.75), Gt + Sill are stable, whereas between 560 and 650 ^{0}C under H_2O saturated conditions the observed peak metamorphic assemblage is defined by field (i). Furthermore, under H_2O saturated conditions and temperature interval of 530 to 550 ^{0}C, St + Ms become stable. Under lower temperatures St is only stable at X_{H2O} between 0.35 and 0.75 whereas, Chl-Ctd-Ms are more stable at X_{H2O} > 0.45 (Figure 3-21). Therefore, the mineral assemblages of DY956 hornfels are stable at X_{H2O} > 0.35 and 400 to 650 ^{0}C temperature conditions.

The observed prograde mineral assemblages depicting the growth stages of DY956 hornfels, are best represented by field (i) to (iv), constrained within 460 ^{0}C < T < 700 ^{0}C and 0.3 kbar <P < 4 kbar (Figure 3-22). The early growth stage is indicated by the field of Bt - Chl - Pl - Gt - Qtz - Ilm, which is followed by a field of Bt - St - Pl - Chl - Gt - Qtz - Ilm defined by staurolite formation as pressure increases. The successive field of Bt - St - Pl - Gt - And - Qtz - Ilm - H_2O is defined by consumption of Chl which marks the peak pressure conditions experienced by the rock. A further increase in temperature and a drop in pressure shifts the rock to a broader field of Pl - Bt - Gt - And - Ilm - Qtz - H_2O, which marks the upper stability limit of staurolite and peak equilibrium conditions experienced by the rock

The two isopleths of X_{alm} and X_{grs} garnet compositions for the core and rim records P-T condition of 495 ± 20 ^{0}C at 0.5 ± 0.3.kbar and 510 ± 20 ^{0}C at 1.4 ± 0.3.kbar (Figure 3-20). These estimates predicts field (i) which marks the onset of garnet growth, the absent of staurolite which occurs at high pressure to this field does suggest that this field is not representing the peak metamorphic conditions. Therefore, field (iv) represent the peak equilibrium conditions experienced by the rock.

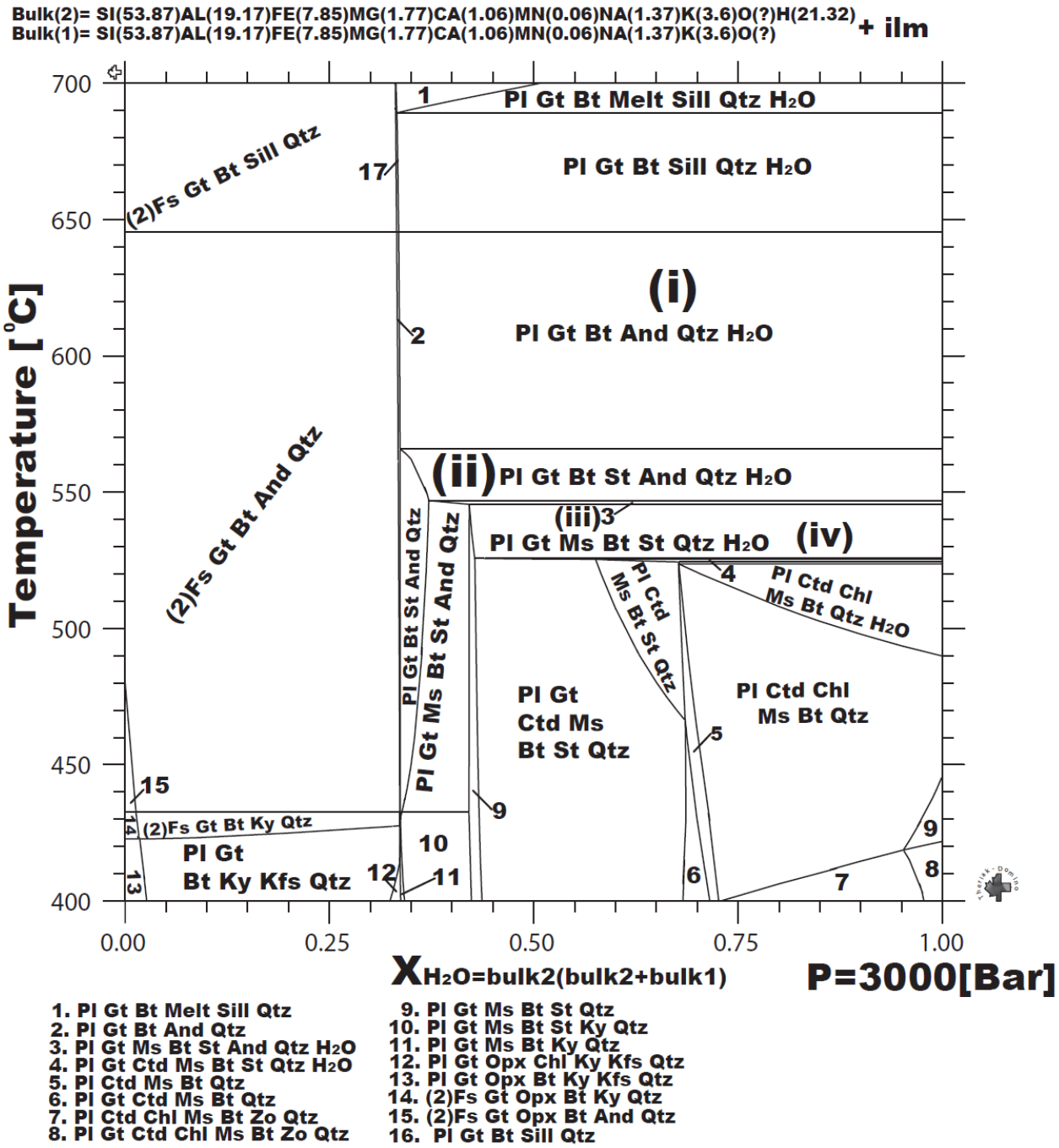

1. Pl Gt Bt Melt Sill Qtz
2. Pl Gt Bt And Qtz
3. Pl Gt Ms Bt St And Qtz H_2O
4. Pl Gt Ctd Ms Bt St Qtz H_2O
5. Pl Ctd Ms Bt Qtz
6. Pl Gt Ctd Ms Bt Qtz
7. Pl Ctd Chl Ms Bt Zo Qtz
8. Pl Gt Ctd Chl Ms Bt Zo Qtz
9. Pl Gt Ms Bt St Qtz
10. Pl Gt Ms Bt St Ky Qtz
11. Pl Gt Ms Bt Ky Qtz
12. Pl Gt Opx Chl Ky Kfs Qtz
13. Pl Gt Opx Bt Ky Kfs Qtz
14. (2)Fs Gt Opx Bt Ky Qtz
15. (2)Fs Gt Opx Bt And Qtz
16. Pl Gt Bt Sill Qtz

Figure 3-20. T-X binary section calculated for DY956 shows the influence of H_2O variation on the stability of the observed mineral phases. Fields (i) to (iv) represent the observed mineral paragenesis.

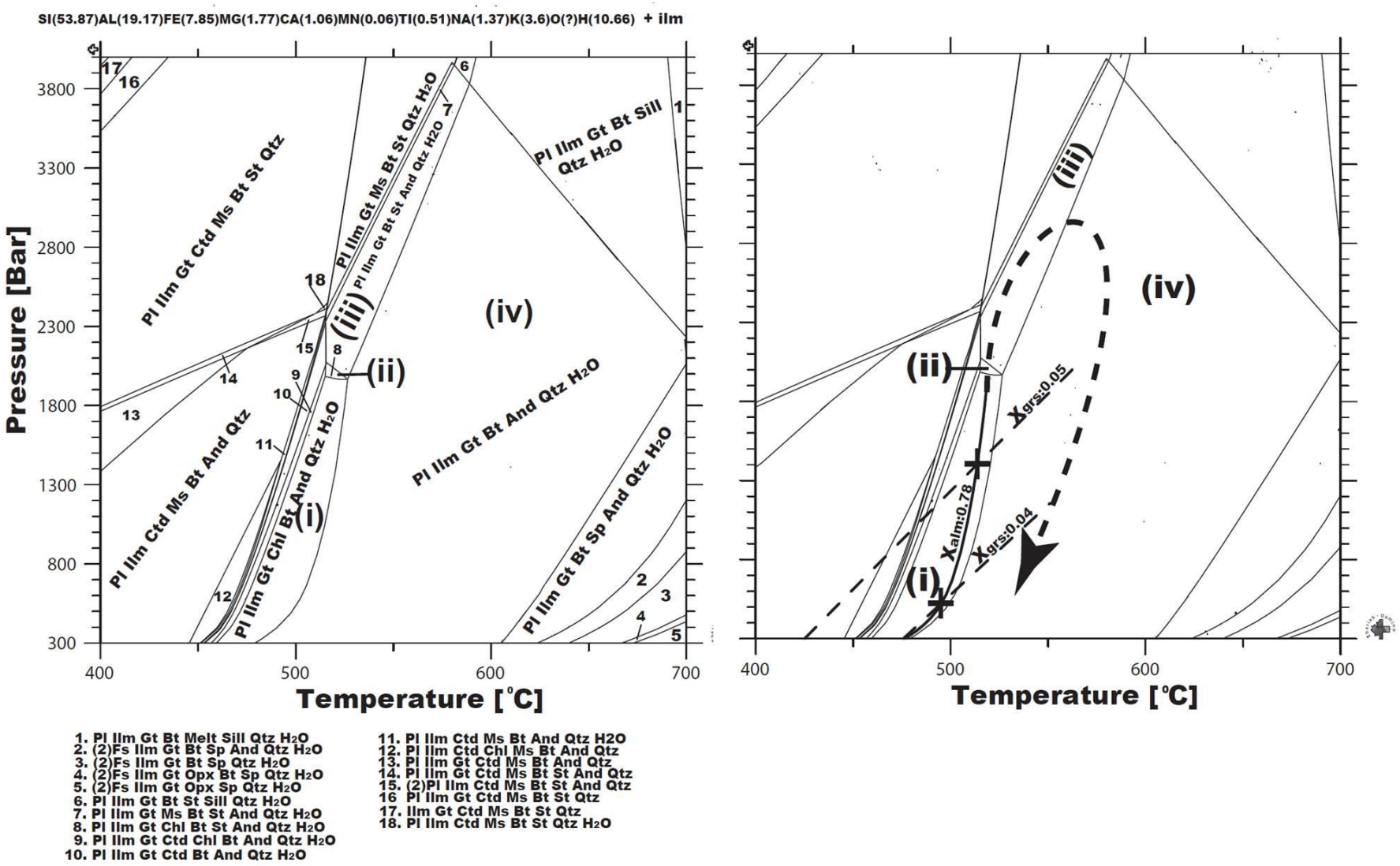

Figure 3-21. MnNCKFMAST pseudosection calculated for a measured bulk rock composition of DY956. (a) Fields (i) to (iv) represent the observed mineral paragenesis and (b) shows estimated P-T conditions (crosses) and an inferred path (dotted arrow).

3.7 Conventional geo-thermobarometry

Two geo-thermobarometry models were chosen for these rocks namely, Garnet-Biotite-Plagioclase-Quartz (GBPQ) and Garnet-Muscovite-Plagioclase-Quartz (GMPQ) from Wu et al. (2004) and Wu and Zhao (2006) respectively. The same garnet compositions used in garnet isopleth thermobarometry were also used for these calculations with the addition of mineral assemblages that are presumably in local equilibrium with them.

3.7.1 Pl-Gt-Chl-Bt Hornfel (DY918)

Only GBPQ classical geo-thermobarometry was used to calculate the P-T condition for this rock. G1 garnet records temperature and pressure of 577.5 ^{0}C at 2.42 kbar and 560 ^{0}C at 1.15 kbar for the core and rim respectively (Figure 3-22 a and b). These estimates suggest a small temperature interval (~17.5 ^{0}C) during growth of the core and rim regions in the garnet.

3.7.2 Bt-Pl-Gt-And-St hornfel (DY954)

Both GMPQ and GBPQ were used to calculate the P-T conditions. Two different estimates were obtained from G0 and G1 garnets; the former records 577.5 ^{0}C at 1.905 kbar and 578.5 ^{0}C at 1.51kbar while the latter records 597 ^{0}C at 1.45 kbar and 566.5 ^{0}C at 0.05 kbar for both core and rim respectively (Figure 3-23 a-d).

The GMPQ of G1 garnet records 515 ^{0}C at 1.3 kbar and 476 ^{0}C at 0.20 kbar on the core and rim regions (Figure 4-24 a-d). The GBPQ of G0 and G1 garnets predict a very short and an elongated temperature interval (1 and 30 ^{0}C) for these garnet growths. In contrast, GMPQ estimates of G1 garnet predicts lower P-T conditions than GBPQ but the temperature intervals with respect to the garnet growth rate exhibit a similar pattern.

3.7.3 Bt-Pl-And-Gt-St hornfel (DY956)

The GMPQ recorded P-T conditions of 306.5 ^{0}C at 1.84 and 295.5 ^{0}C at 2.05 kbar (Figure 4-25); whereas the GBPQ records 572 ^{0}C at 1.1 kbar and 585 ^{0}C at 0.85 kbar on the core and rim regions (Figure 4-26).

The P-T conditions recorded by both geothermobarometers in DY954 and DY956 are different and do not appear to be exhibiting similar patterns in both core and rim regions. Furthermore, GMPQ records much lower P-T than GBPQ.

The low temperatures recorded by the GM thermometer indicate the maximum stability of muscovite which precedes the formation of garnet, whereas the GB thermometer is recording peak equilibrium condition of garnet growth and the rock as a whole.

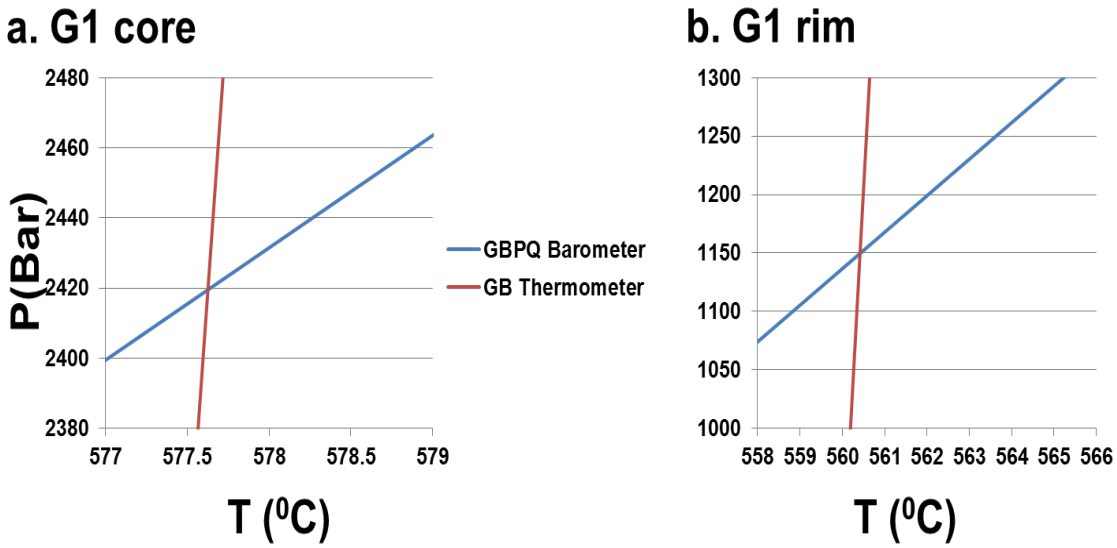

Figure 3-22. Garnet-Biotite-Plagioclase-Quartz thermobarometry of DY918

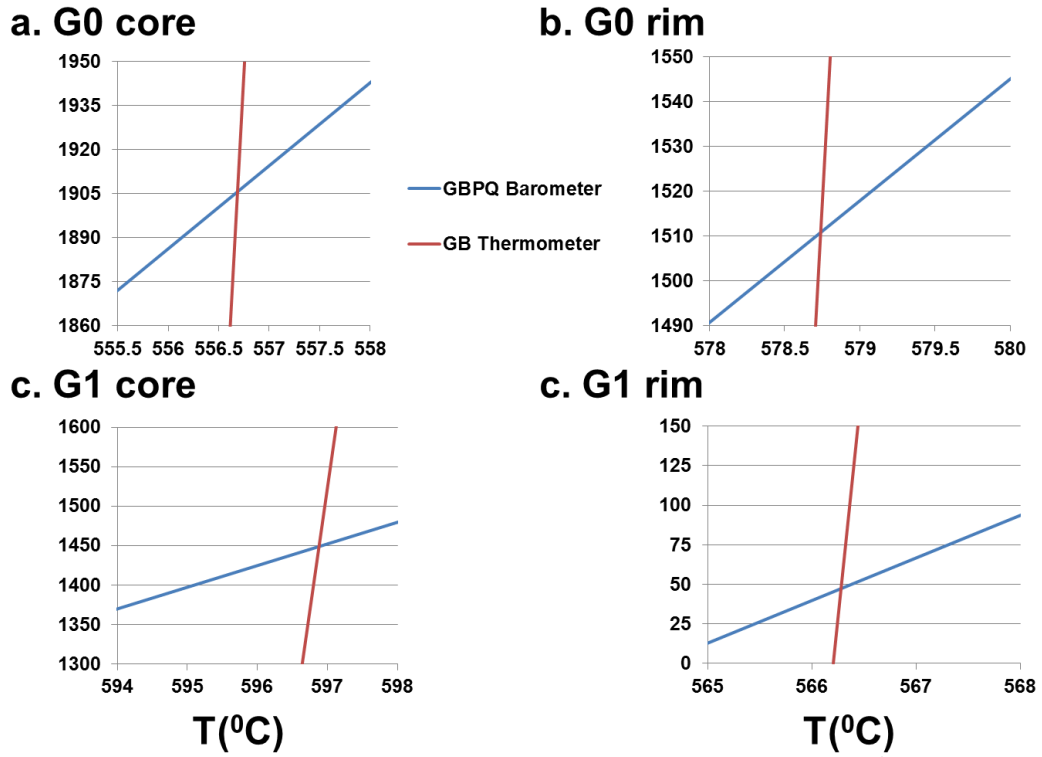

Figure 3-23. Garnet-Biotite-Plagioclase-Quartz thermobarometry of DY954

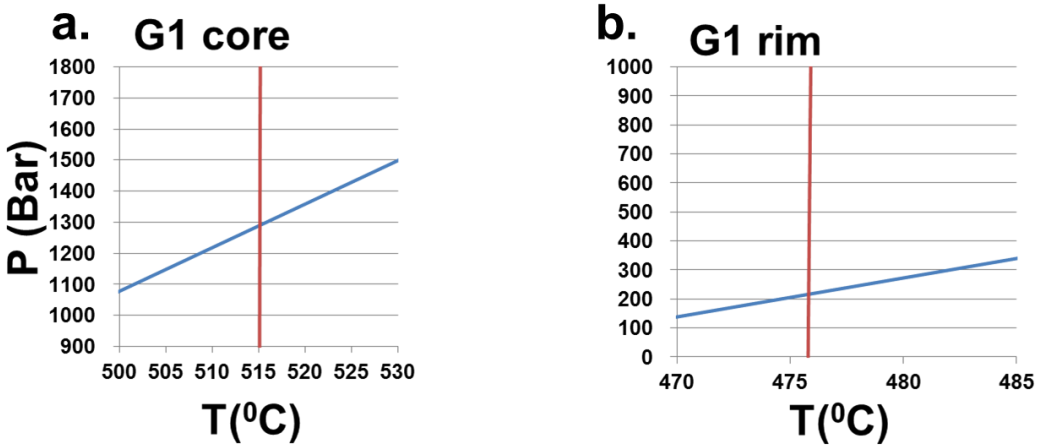

Figure 3-24. Garnet-Muscovite-Plagioclase-Quartz thermobarometry of DY954

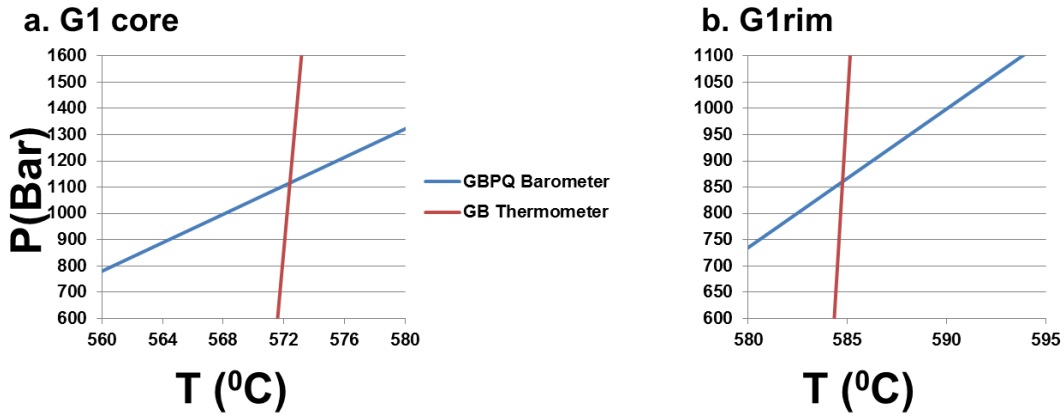

Figure 3-25. Garnet-Biotite-Plagioclase-Quartz thermobarometry of DY956

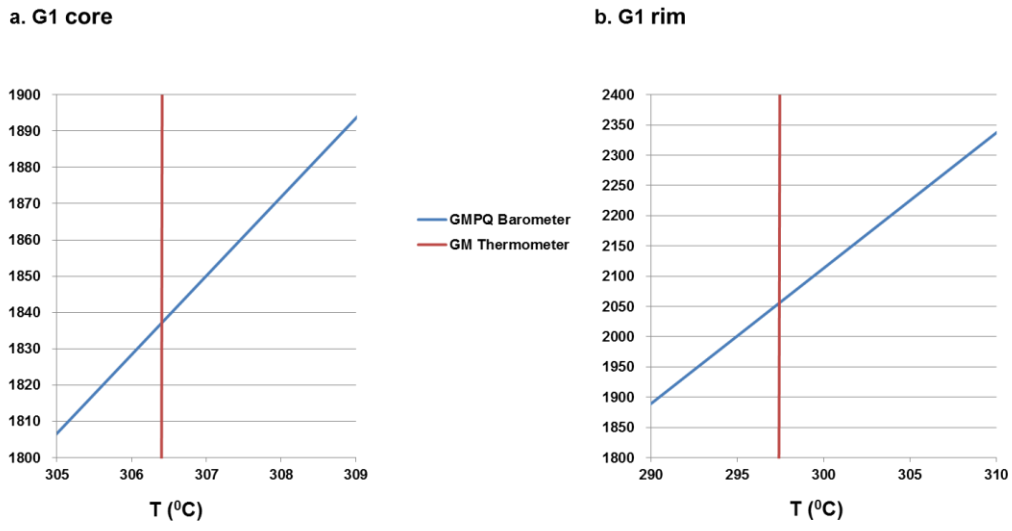

Figure 3-26. Garnet-Muscovite -Plagioclase-Quartz thermobarometry of DY956

3.8 Depth of burial

The depth of burial can be useful to elucidate how far the rock has been exhumed over time. Using the estimated equilibrium P-T conditions, the densities of the phases were obtained from theriak in Theriako Domino. The following formula was used to calculate depth of burial;

$$P = pgh \text{ or } h=P/pg$$

P = pressure (Pascal)

h = depth of burial (km)

ρ = density (kg/m^3)

g = gravity ($9.8\ m/s^2$)

3.8.1 Pl-Gt-Chl-Bt Hornfels (DY918)

G1 garnet; P~1.3kb, ρ ~2772kg/m^3, h=4.6km

The depths estimate of DY918, suggests that the rock was metamorphosed at a depth of about 4.6 km, predicting that the emplacement of the magma responsible for the heating of this rock intruded at shallower levels.

3.8.2 Bt-Pl-Gt-And-St hornfels (DY954)

G0 garnet; P 2.2 kbar, p 2850 kg/m^3 h= 7.6 km

G1 garnet; P 0.8 kbar, p 2834 kg/m^3 h= 2.9 km

The calculated depths of burial for G0 and G1 in DY954, predict that the two garnets equilibrated at a stratigraphic levels of about 7.6 and 2.9 km which might imply that the rock experience different loading regimes (weight of the overlying strata) hence affecting the pressure conditions.

3.8.3 Bt-Pl-And-Gt-St hornfel (DY956)

G1 garnet; P~1.8kb, p~2830kg/m^3, h=6.2km

DY956 calculated depths of burial suggests the rock was metamorphosed at depth of about 6.2 km and that the emplacement of the magma responsible for the heating of this rock occurred at the same depth

Based on the obtained depths estimates from the three rocks, it is evident that they experienced different loading regimes which affected their equilibration pressures.

3.9 Discussion

3.9.1 Pl-Gt-Chl-Bt Hornfels (DY918)

The hornfels is typified by the occurrence of garnet porphyroblasts in a fine grain matrix of quartz, plagioclase, chlorite and biotite. In addition, the sample is made up of light and darker chemical domains which control the crystallization of these mineral phases in different proportions; for example garnet porphyroblasts are constrained within the darker fine-grained chemical domain. The lighter domain consists of coarse-grained plagioclase and quartz with accessory phases of ilmenite and low percentage of interstitial chlorite and biotite. The separation of these chemical domains is not due to metamorphic differentiation but is inherited from the rhythmic layering of the parent pelites/mudrock.

The mineral paragenetic sequence in the modelled pseudosection is successfully described by two successive fields of Bt - Chl - Pl - Qtz - H_2O and Bt - Chl - Gt - Pl - Qtz - H_2O. The latter, represent the peak metamorphic assemblage experienced by the rock occurring between 430 and 560 ^{0}C. Considering the garnet end member isopleths and chemical zoning profiles of G1, it is plausible that garnet growth was influenced by changes in P-T conditions, with the core and rim of G1 recording ~ 548 ^{0}C at ~ 1.4 kbar and ~505 ^{0}C at 0.3 kb respectively. The GB-GBPQ thermobarometers records ~577.5 ^{0}C at 2.42 kbar and 560.5 ^{0}C at 1.15 kbar for rim and core respectively.

Even though the two techniques records different conditions, with the garnet isopleth recording lower P-T conditions, they are both exhibiting similar growth patterns from the core to rim regions. The lower temperature estimates from pseudosection might be due to errors associated with the recalculated bulk rock composition. Classical geothermobarometry estimates suggest that the rock equilibrated under hornblende hornfels facies. Furthermore, the P-T conditions obtained from the core and the rim suggest that that the rock followed a prograde clockwise P-T path during its growth stages.

3.9.2 Bt-Pl-Gt-And-St hornfel (DY954)

Biotites chemistry suggests one generation that ranges from siderophyllite to eastonite. Garnets exhibit different microstructural settings and chemical zoning profiles as shown by G0 and G1 garnets. The different chemical behaviour of the garnets may be attributed to resetting of the garnet chemistry due to the Fe-Mg exchange between biotite and garnet or retrograde diffusion during cooling.

The predicted mineral assemblages from the pseudosection (Figure 3-19), mineral reactions from AKF diagram (Figure 3-15) and observed mineral assemblages suggest that andalusite formed from the breakdown of chlorite and muscovite as the rock graded up and the univariant equilibria accounting for andalusite formation is;

$$Ms + Chl + Qtz = And + Bt + H_2O \quad (14)$$

With further increase in metamorphic grade (just above 530 ^{0}C) the modal abundances and size of andalusite and garnet generally increases co-exist for an elongated temperature interval (over 100 ^{0}C) by consuming chlorite and muscovite (Reaction 15).

$$Ms + Chl = Bt + Gt + And + Qtz + H_2O \quad (15)$$

Once the rock has reached ~ 630 ^{0}C at 2.3 kbar, cooling and pressure increase (from ~3.3 kbar) commences resulting in the formation of staurolite in a stable assemblage of St – Bt – And at the expense of garnet and this is texturally supported by occurrence of resorbed garnets. Furthermore, the textural replacement of andalusite by formation of the secondary muscovite along the rim regions (Figure 3-3f) can be accounted for by the reverse reaction of univariant equilibria 16. This indicates a retrograde cooling path which forms a stable assemblage of Bt-Ms - St under peak pressure conditions.

$$St + Ms + Qtz = And + Bt + Gt + H_2O \quad (16)$$

The estimated P-T conditions from isopleth thermobarometry for the cores and rims of G0 and G1 are 625 ^{0}C at 2.2 kbar and, ~590 0C at ~2.65 kb and 520 ^{0}C at 0.5 kbar and a are 625 ^{0}C at 2.2 kbar, respectively. On the other hand, the P-T conditions estimated from the GB-GBPQ thermo barometer records 577.5 ^{0}C at 1.905 kbar and 578.5 ^{0}C at 1.51kbar; 597 ^{0}C at 1.45 kbar and 566.5 ^{0}C at 0.05 kbar for both the core and rim regions of G0 and G1 garnets. Both methods records different P-T estimates but all plots within the peak metamorphic assemblage field and exhibit similar growth patterns from core to rim regions.

Furthermore, it is apparent from both techniques that the G1 garnet was subjected to prograde heating (~ 100 ^{0}C from core to the rim region) whereas G0 formed during a retrograde cooling within the garnet stability field. The modal proportions of biotite decreases with increasing temperature within the garnet stability field and their Fe and Mg are transported to garnet crystallisation sites to produce more garnet. The increase in pressure during cooling is probably as the result of another magma pulse emplacement which was less hot but denser and resulting in an incomplete formation of G0. When considering the mineral micro-textures and estimated P-T conditions, it is possible that the rock was subjected to an isothermal expansion and an isobaric cooling assuming an anti-clockwise P-T path.

3.9.3 Bt-Pl-And-Gt-St hornfel (DY956)

The garnet zoning profiles for this rock exhibit a homogenous variation for all the end members with a subtly zoning defined by Xprp. The recorded P-T conditions on the core and rim from isopleth thermobarometry are ~510 ^{0}C at 0.8 kbar and 525 ^{0}C at 1.9 kbar. The GB-GBPQ thermobarometers records 572 ^{0}C at 1.1 kbar and 585 ^{0}C at 0.85 kbar on the core and rim regions. Both estimates indicates increasing P-T conditions from core to rim regions with the isopleth thermobarometry predicting field (i) which represent the early growth stage of garnet whereas classical geo-thermobarometry predict a later growth stage shown in field (v) (Figure 3-20). Therefore, the Gt-Chl-Bt-And assemblage is stable under low P-T conditions and grades upward to Bt-Gt-Chl-St-And during a slight increase in T and P; a further increase in P-T conditions allows more St + And to form at the expense of Chl and is represented by an assemblage of Gt – Bt – St - And. These continuous reactions are controlled by solid solution of Fe and Mg between chlorite, garnet and staurolite and are accounted by the following equilibria

$$Ms + Gt + Chl + Qtz = St + Bt + H_2O \quad (18)$$

$$Ms + Chl + Qtz = And + Bt + H_2O \quad (19)$$

The staurolite inclusion in andalusite could also suggest that both reactions occurred together at some point during an increase in P-T condition. Once the maximum depth of burial is reached, temperature continues to increase causing the assemblage to grades upward forming a peak assemblage of Gt-Bt-And at the expense of St (Figure 3-21 b) and isobaric cooling at around 580 ^{0}C and ~3 kbar begins and complete the clock wise P-T path. Therefore, the idealised reaction forming the peak assemblage is;

$$Ms + St + Qtz = And + Gt + Bt + H_2O \quad (20)$$

The inferred P-T paths form these garnets bearing hornfelses describes the observed prograde and retrograde paragenesis and calculated pseudosections for each hornfels. Chl-Gt hornfels (DY918) mineral assemblages and garnet isopleth thermobarometry suggest the rock belongs to upper albite hornfels facies whereas the Gt-Bt geothermobarometry records hornblend hornfels facies. In contrast, DY954 and DY956 hornfels records hornblend hornfels facies for both techniques.

The garnet isopleth temperature results obtained from DY918 and DY956 (510 – 525 and 505 – 548 0C) are within errors to those obtained by Uken (1998) (e.g. 535-563 0 C at 2.8-3.2 kb) who worked with the similar rock of the north-eastern BC aureole and. However, DY954 hornfels recorded higher temperature estimates for the core and rims of G0 and G1 garnets (e.g. 625 0C) which are within error to the result obtained by Kaneko et al. (1990b) and Waters and Lovegrove (2002), their estimates ranged from 560-570 and 570 – 580 ^{0}C respectively.

The differences in P-T conditions by G0 and G1 garnets of DY954 hornfels could be attributed to two stages of metamorphism as suggested by Nell (1985) and Walmach (1984), the growth of G1 garnet reflect the intrusion of the LZ + CZ magmas and the incomplete growth of G0 garnet reflect the intrusion of the MZ and UZ magmas which caused an increase in pressure due to loading. The other two hornfelses do not show any evidence of this two stage evolution and also the garnet and staurolite forming reactions in these rocks were different.

Chapter 4

Metamorphic evolution of St bearing Gt-And absent Fe-and Al-rich metapelitic rocks, Timeball Hill Formation, NE Bushveld contact aureole

4.1 Introduction

Fe- and Al- rich metapelites containing mineral assemblages of Ctd-Bt, Ctd-bt-And, Crd-Gt-Ms and Ms-Crd-St-Bt, have been described, and are considered to represent rare mineral assemblages in contact aureoles (Pattison et al., 1999; Likhanov et al., 2001 and references herein). Waters and Lovegrove (2002) reported the occurrence of an assemblage of Ctd-Ms-Chl-Qtz in the lower Timeball Hill formation near Penge and suggested that the formation of Bt-St-And in the upper Timeball Hill was directly related to chloritoid breakdown. Low to medium grade metapelitic phase relations and influence of additional/absent component have been studied by numerous workers (Pattison et al., 1999; Likhanov et al., 2001 and references herein; Waters and Lovegrove (2002); Pattison and Tinkham, 2009).

In this chapter three Fe-and Al-rich staurolite bearing, garnet and andalusite free metapelites (DY916, DY982 and DY987) from the Timeball Hill formation of the north-eastern BC contact aureole will be discussed. DY916 is located on the lower Timeball Hill (LTH) about 20 km south of DY982 and DY987, which are located in the upper Timeball Hill (UTH) formation (Figure 3-1). This study will attempt to elucidate the staurolite forming reactions and the absent of And-Gt phases in these rocks. This will be done through a combination of petrology, whole rock geochemistry and thermodynamic stabilities of the observed minerals.

4.2 Petrography

4.2.1 DY916

The mineral assemblage consists of chlorite, biotite, staurolite, ilmenite and quartz, characterised by weak alignment of biotite and chlorite along bedding (Figure 4-1 e and f). In general the rock is dominated by three microstructural settings of biotite porphyroblasts and poikiloblasts, namely: biotite flakes exhibiting pressure shadows and aligned in the direction of bedding, tabular biotite exhibititing epitaxial growth with chlorite, and along staurolite rim regions (Figure 4-1 a-f)

Chlorite occurs as isolated flakes in the matrix and as a replacement product along staurolite rim regions (Figure 4-1c and d). Idioblastic staurolite pokiloblasts are altered to fine-grained clay minerals on the core regions (replaced by epoxy during thin-section making) and chlorite and biotite alonng the rim regions (Figure 4-1 b). The fine grain matrix consist of chlorite, quartz and accessory ilmenite.

4.2.2 DY982

The rock is characterised by poikiloblasts of biotite, staurolite and chloritoid in a fine-grained matrix of chlorite, plagioclase, muscovite, ilmenite and quartz (Figure 4-2 a -e). Weak sigmoidal foliation is defined by elongated muscovite and ± chlorite which cuts across biotite (Figure 4-2 e). Biotite poikiloblasts are widely distributed in the rock, occuring mainly as subhedral grains showing brownish and greenish pleochroism.

Biotite poikiloblasts with inclusions of quartz, plagioclase, chloritoid, ilmenite, and staurolite are common (Figure 4-2 a-f). They also form as alteration products of staurolite (Figure 4-2 f). Staurolite poikiloblasts within the rock range in shape from euhedral to subhedral (Figure 4-2 a-f), with some exhibiting inclusion free rims (Figure 4-2 c). The observed inclusions are quartz, biotite and chloritoid (Figure 4-2 f). In rare cases, formation of chloritoid and biotite after staurolite can be noted (Figure 4-2 b). Tabular chloritoid is common in the matrix and also occurs as needle like inclusions within biotite and staurolite. Accicular to tabular muscovite and chlorite, together with quartz, ilmenite and plagioclase dominates the fine grained matrix.

4.3.3 DY987

This metapelite has the same mineral composition as DY982 but it is characterised by a darker chemical domain containing porphyroblasts of staurolite, biotite, plagioclase and chloritoid occuring within the fine-grained matrix of muscovite, chlorite, ilmenite, quartz and small-sized plagioclase grains. The biotite poikiloblasts contain inclusions of chlorite, plagioclase, ilmenite and quartz. The weak foliation which cuts across biotite is defined by acicular to tabular Ms-Ctd-Chl (Figure 4-3 d-f). Idioblastic to sub-idoblastic staurolite poikiloblasts occurs as fresh to altered grains, alteration to biotite is common along it rim regions (Figure 4-5 c, e, g-i). Chlorite and chloritoid ranges from tabular to accicular, occuring either in the fine-grained matrix or as inclusions in biotite (Figure 4- 5a). Plagioclase occurs as porphyroblasts, inclusions in biotite and interstial to quartz in the fine grained matrix (Figure 4-5d, g and i).

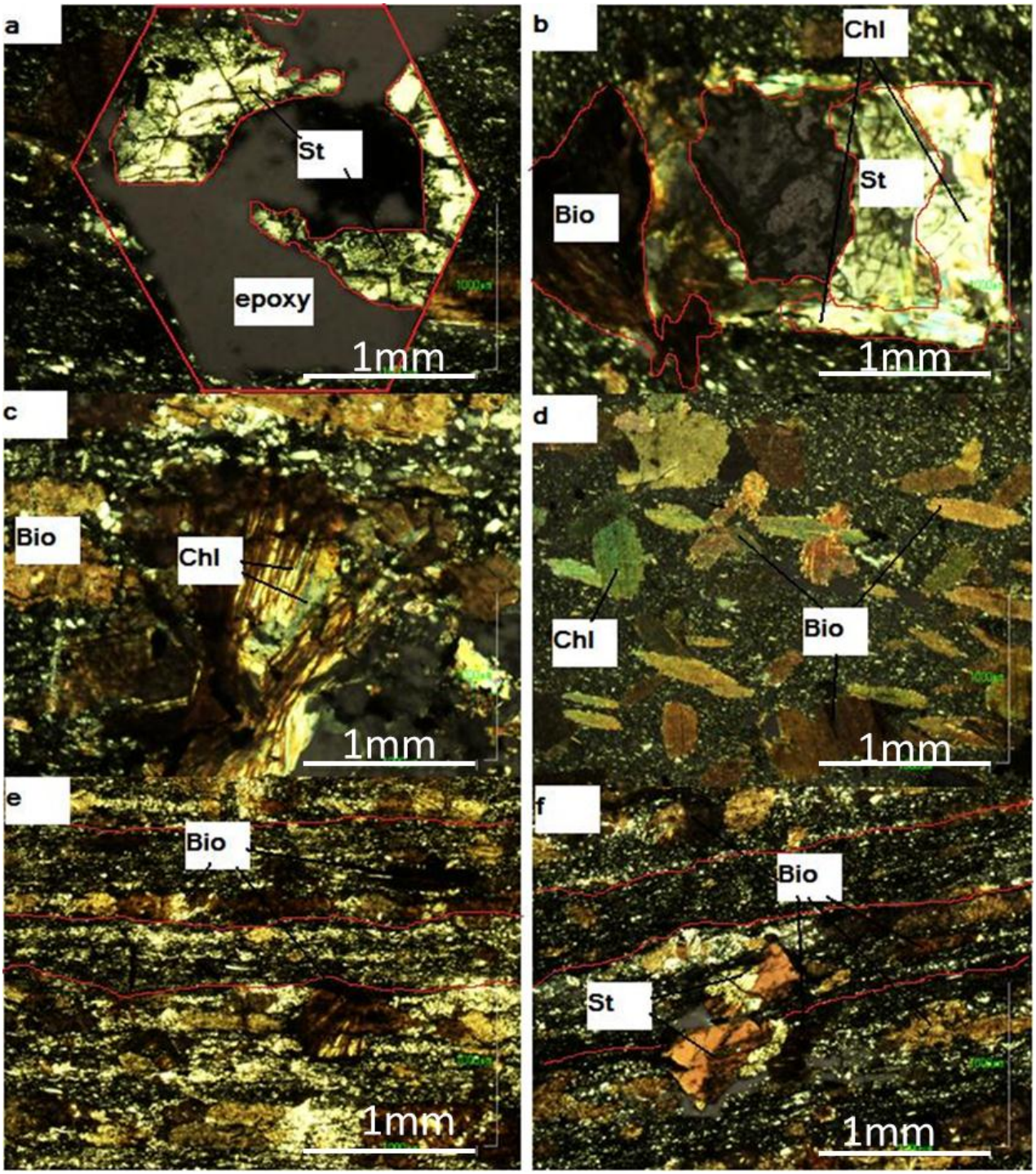

Figure 4-1. XPl photomicrographs showing mineral assemblages of DY916. (a.) Resorbed idioblastic staurolite (b.) Staurolite altering to biotite and chlorite along it rim regions (c) epitaxial biotite and chlorite growth. (d.) Randomly oriented biotite and chlorite flakes. (e) Biotite flakes forming along the bedding and (f) Staurolite growth aligned to the bedding.

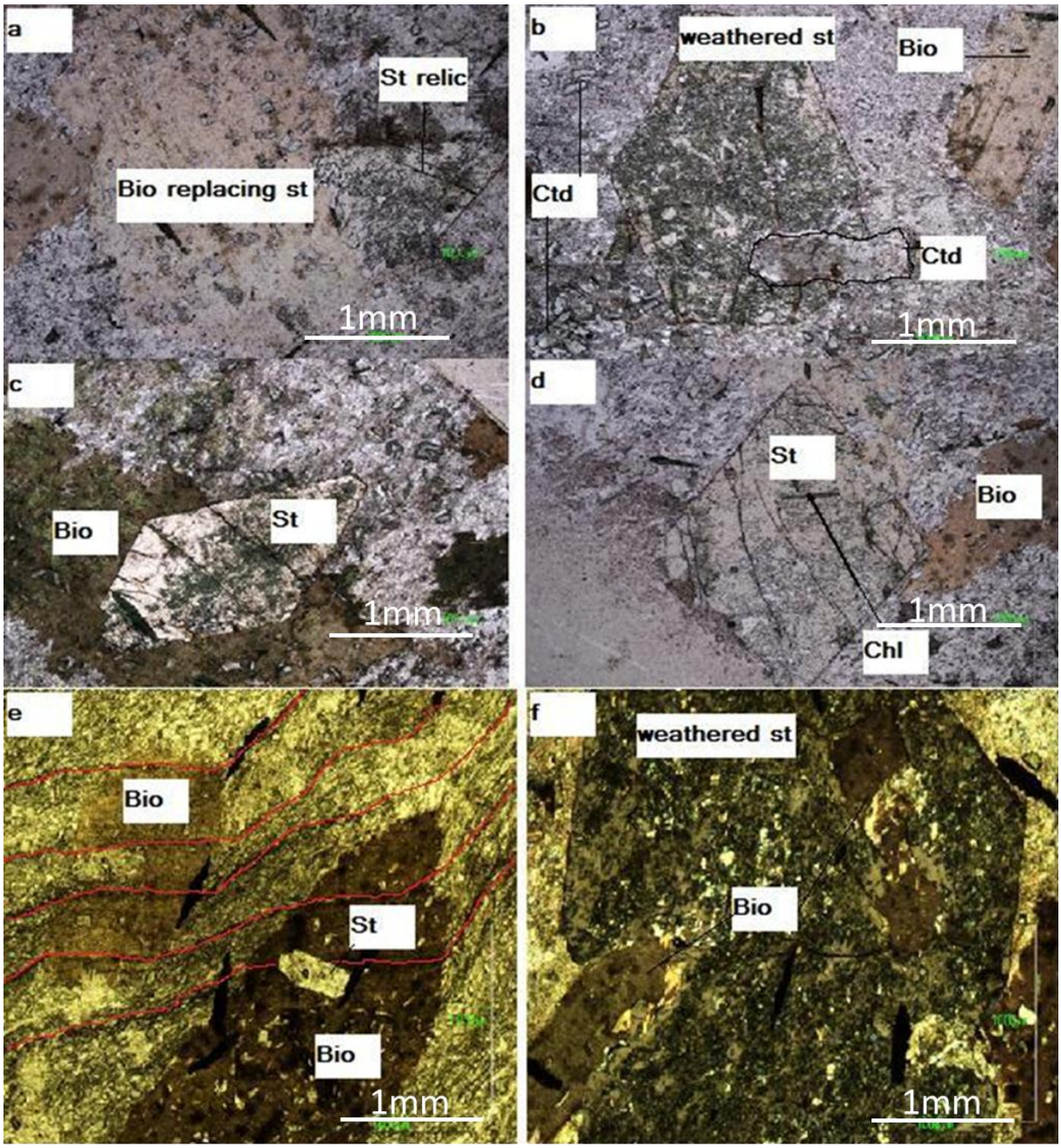

Figure 4-2. Photomicrographs showing representative micro-textures of mineral assemblages in DY982. (a) Biotite poikiloblast replacing staurolite (b) Altered staurolite replaced by chloritoid and surrounded by tabular biotite and chloritoid. (c) Idioblastic staurolite overgrowing biotite. (d) Staurolite poikiloblast containing lenticular chlorite inclusions. (e) Biotite poikiloblast with staurolite inclusions (f) Staurolite altering to biotite.

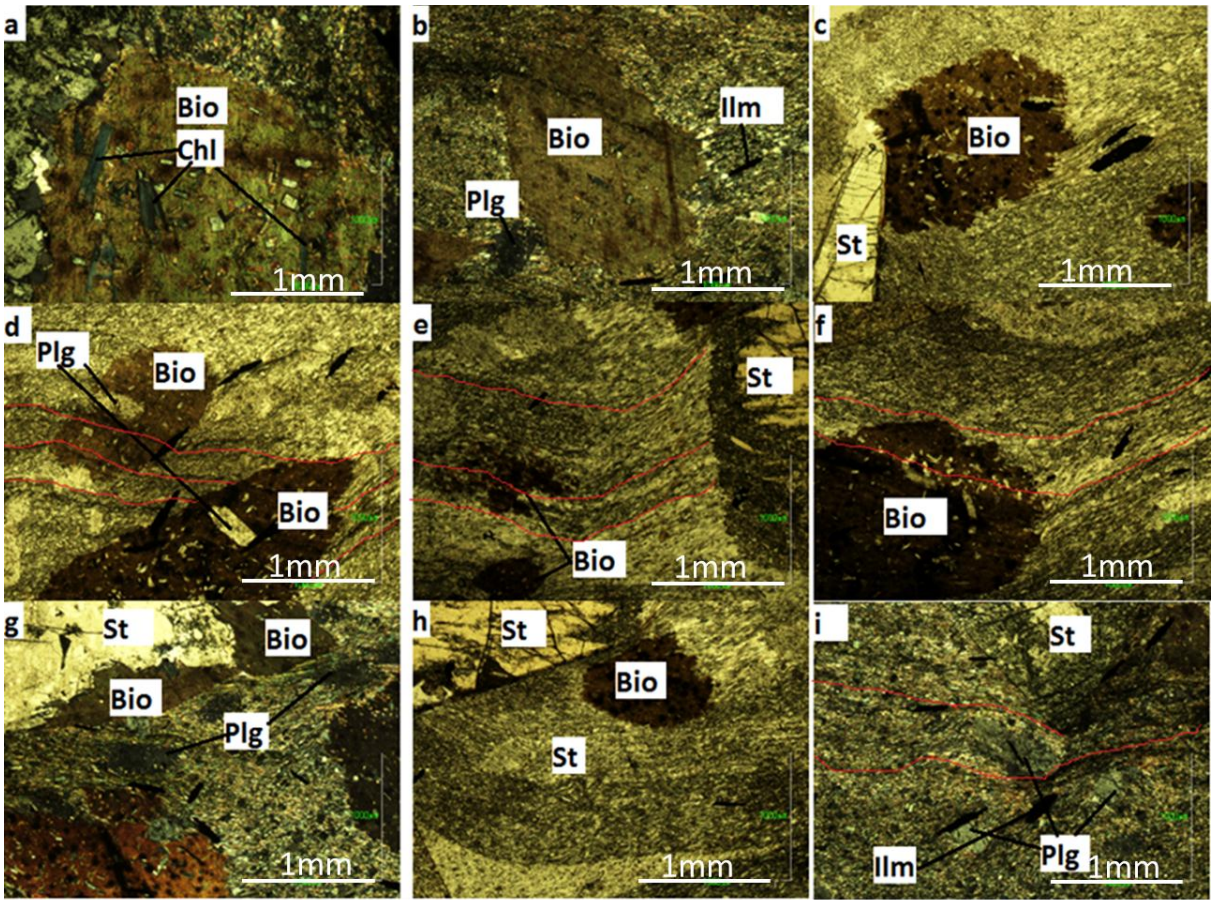

Figure 4-3. Photomicrographs (XPL) displaying representative micro-textures of mineral assemblages in DY987 (a) Biotite poikiloblast with chlorite inclusions. (b) Biotite poikiloblast surrounded by plagioclase in a fine grain matrix.(c) Euhedral staurolite invading a biotite poikiloblast (d) Syn tectonic biotite poikiloblasts with plagioclase inclusions oriented parallel to the foliation. (e) Staurolite with intense alteration in the rim regions and weak crenulated foliation running through the biotite. (f) Syn tectonic biotite poikiloblast. (g) Biotite rim replacement product along staurolite rim region surrounded by plagioclase and biotite. (h) Altered staurolite partially replaced by biotite. (i) Weak crenulated foliation, with staurolite and plagioclase in the fined grained matrix

4.3 Whole rock data

DY916 has a higher total FeO when compared to the other two metapelites (DY982 and DY987) and average pelite compositions (Symmes and Ferry, 1992; Bucher and Grapes, 2011), but has lesser CaO and and Na_2O content (Table 4-1). The depletion of CaO and Na_2O in this hornfels accounts for the absent of plagioclase which is present on the other metapelites. On the other hand, DY982 exhibit a higher Al_2O_3 content of 26.08 wt% compared to 16.72 and 23.66 wt% for DY916 and DY987. The Fe/(Fe+Mg+Mn) content in these hornfelses is 0.91 (DY916 and DY982) and 0.93 (DY987), whereas the Mn/(Fe+Mg+Mn) content is 0.05 and 0.03 repsectively. Concerning the AFM diagram in figure 5-4, the three metapelites plots on the lower MgO side when compared to average pelitic compositions but DY982 and DY987 have a similar Alkaline (A) content to the average pelite composition. Even though, the whole rock geochemical data of these staurolite-bearing metapelites does exbhit a spread in the AFM diagram but on average their compositions plots on the average pelitic composition field.

Table 4-1. Representative whole rock composition of DY916, DY982 and DY987 metapelites.

Wt%	DY916	DY982	DY987	Av-SF	Av-BG
SiO_2	59.28	54.81	55.95	59.77	54.90
TiO_2	1.11	0.85	0.77	-	0.78
Al_2O_3	16.72	26.08	23.66	16.57	16.60
Fe_2O_3*	16.02	10.51	10.08	6.53	9.70
MnO	0.08	0.05	0.03	0.07	-
MgO	1.50	0.78	0.99	2.62	3.40
CaO	0.38	0.54	0.56	2.17	0.78
Na_2O	0.00	0.70	0.87	1.73	1.30
K_2O	3.09	3.40	3.86	3.53	2.70
H_2O	1.07	1.81	2.92	7.65	9.20
Total	99.25	100.00	99.72	100.64	99.36

* Total Fe as Fe_2O_3

Av-SF: average pelite of Symmes & Ferry (1991)
Av-BG:average pelite of Bucher & Grapes (2011)

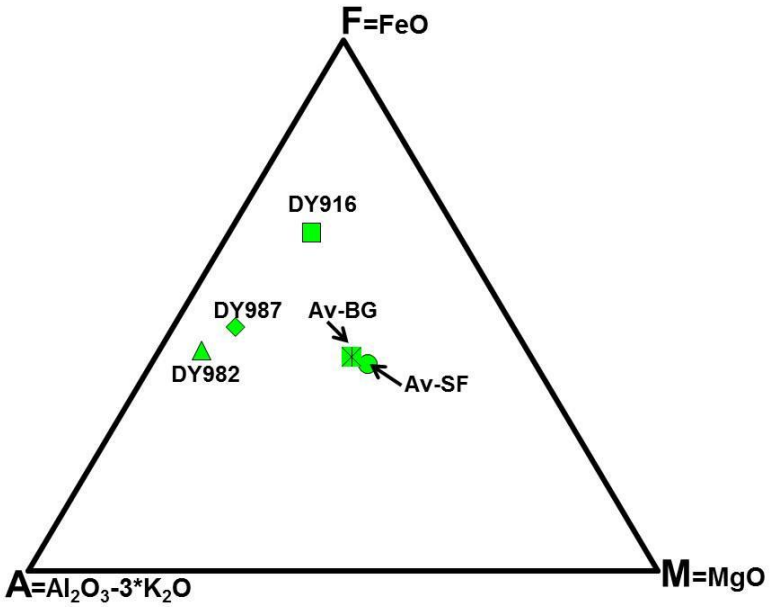

Figure 4-4. Bulk rock geochemical data of staurolite bearing hornfelses and average pelite compositions (Av-SF: Symmes & Ferry, 1992; Bucher & Grapes, 2011) plotted in an AFM projection (After Thompson, 1956)

4.4 Mineral chemistry

Three Fe-and Al- rich metapelitic chemical analyses of all observed phases are reported as point analysis in each mineral. As a check for chemical variation, all the minerals were analysed on the core and rim regions. Mineral stochiometric values were determined for plagioclase, biotite, chlorite, chloritoid, ilmenite, muscovite and staurolite normalising to 14 (Ctd & Chl), 11 (Bt), 3 (Ilm), 11 (Mu), 23 (St), and 8 O_2 (Plg).

Staurolite occurs as one of the common phases in the three studied metapelites and has a homogenous $X_{Fe/(Fe+Mg)}$ content of ~ 0.89 in all metapelites regardless of their micro-textural settings and sample locations (Table 4-3). All analysed staurolites from all metapelites exhibit no chemical zoning in terms of both X_{Fe} and X_{Mg}. Staurolites plots distinctly on the higher Alkaline (A) side on the AFM diagrams (Figure 4-5 a-c) compared to the bulk and other other ferromagnesian phases.

Biotite is ubiquitous in all metapelites occuring in different micro-textural settings. Chemical behavioural patterns were compared in terms of $X_{Al}(T2)$, $X_{Fe\ =Fe/(Fe+Mg)}$ and $X_{Ti\ =Ti/(Fe+Mg)}$ in order to understand their chemical signatures and investigate whether they represent more than one generation of biotites.

In Bt-Chl-St metapelite DY916, biotites could be divided into three micro-textural settings namely, biotite showing epitaxial growth with chlorite (Bt1), biotites flakes which are aligned in the direction of bedding (Bt2) and biotite forming as a rim reaction product along staurolite rim region (Bt3). The tetrahedral Al variation of these biotites is ~0.68, 0.63 – 0.69, and 0.51 – 0.63 with a Ti content of ~ 0.1 (all biotites) and Fe/(Fe+Mg) ratio of 0.66 - 0.68, ~0.66 and 0.64 – 0.7. On the other hand, the Mn content is 0.004 – 0.008, 0.005 – 0.008 and 0.002 – 0.007 respectively.

In the upper Timeball Hill, Bt-St-Pl-Ctd metapelites (DY982 and DY987) have a tetrahedral Al variation 0.63- 0.72 with a Ti content ~0.1 and Fe/(Fe+Mg) ratio of 0.62 to 0.66. In contrast, the Mn content of DY982 is 0.001 – 0.005 and 0 for DY987. The biotite composition from the lower to the upper Timeball Hill is fairly homogenous and the dominant component in these biotites is siderophyllite with minor traces of eastonite.

Prograde chlorite is ubiquitous in the lower Timeball Hill (DY916) but decreases in quantity grading up to the upper Timeball Hill (DY982 and DY987). The Si content and Fe/(Fe +Mg) ratio of chlorite decreases from 3.47 to 2.53 and 0.67 to 0.63 going from LTH to UTH. On the other hand, the UTH chlorite are relatively aluminous (~3.05), iron (~2.76) and magnesium rich (~1.6) as compared to LTH (DY916) with Al , Fe and Mg conten of 2.6-2.8, 2.08-2.69 and 1.03-1.32 respectively.

Chloritoid in this study is only restricted to metapelites of the UTH occuring in DY982 and DY987 studied metapelites. It has a fairly homogenous composition in both metapelites with an Fe/(Fe + Mg) ratio that ranges from 0.87 to 0.88 and relatively high Mg content varying from 1.87 to 1.93.

Plagioclase is also widely distributed within the metapelites of the UTH (DY982 and DY987) ranges from oligioclase to andesine, with an X_{ab} content of ~ 0.58 and ~ 0.66 for both metapelites.

Prograde muscovite is mainly found within the fine-grained matrix of the UTH metapelite (DY982 and DY987) but not in large quantities. It has a paragonite (Na/(Na+K) component that ranges from 0.24 to 0.29 and ~0.23 and Fe and Mg content that varies from 0.05 to 0.06 and ~0.04.

Table 4-2. Representative point analysis of mineral chemistry of the metapelitic rocks from the Timeball Hill formation. Letter J represent analysis obtained from JEOL and all unmarked analysis were obtained from CAMECA

Sample	DY916					DY982							DY987						
Mineral	Chl[1]	Chl[2]	Bt	St	ilm	Chl[J]	Ms	Ctd	Bt	St	Pl	Ilm[J]	Chl	Ms	Ctd	Bt	St	Pl	Ilm
SiO_2	33.50	26.06	34.21	26.71	0.57	23.183	47.52	24.15	34.41	27.05	60.54	0.00	22.31	45.84	24.24	34.96	26.89	58.81	0.21
TiO_2	0.04	0.12	1.60	0.45	51.27	0.074	0.27	0.00	1.65	0.46	0.00	53.61	0.07	0.23	0.02	1.62	0.48	0.01	52.19
Al_2O_3	21.25	21.58	20.11	54.72	0.18	23.676	36.34	41.06	20.24	54.66	26.74	0.13	22.32	36.48	41.26	20.57	54.65	25.74	0.01
Cr_2O_3	0.05	0.04	0.05	0.07	0.01	0.00	0.06	0.04	0.00	0.04	0.00	0.04	0.00	0.02	0.04	0.05	0.03	0.01	0.01
FeO	24.02	29.25	24.46	14.78	44.75	30.516	0.98	23.25	22.59	15.27	0.01	46.28	28.39	1.07	25.01	21.86	15.10	0.10	46.73
MnO	0.09	0.14	0.08	0.24	2.07	0.058	0.01	0.19	0.02	0.09	0.00	0.30	0.08	0.00	0.20	0.03	0.09	0.00	0.35
MgO	6.70	8.08	6.19	1.04	0.10	9.798	0.41	1.87	6.97	1.06	0.00	0.01	9.71	0.40	1.93	7.54	1.18	0.00	0.14
CaO	0.23	0.12	0.05	0.00	0.02	0.021	0.02	0.00	0.00	0.01	8.76	0.00	0.03	0.00	0.02	0.02	0.01	6.99	0.02
Na_2O	0.00	0.00	0.43	0.04	0.06	0.069	1.78	0.01	0.41	0.01	6.72	0.00	0.13	1.64	0.00	0.32	0.01	7.71	0.01
K_2O	0.00	0.00	8.53	0.00	0.00	0.011	8.47	0.02	8.61	0.00	0.04	0.00	0.18	8.50	0.03	8.48	0.00	0.06	0.00
Total	85.88	85.39	95.71	98.06	99.03	87.41	95.86	90.58	94.89	98.66	102.82	100.36	83.21	94.18	92.75	95.44	98.44	99.44	99.67
Oxygen	14	14	11	23	3	14	11	12	11	23	8	3	14	11	12	11	23	8	3
Si	3.47	2.87	2.41	3.72	0.01	2.52	3.10	2.02	2.42	3.75	2.63	0.00	1.82	3.05	2.00	2.43	3.73	2.64	0.01
Ti	0	0.01	0.09	0.05	0.98	3.04	0.01	0.00	0.09	0.05	0.00	1.01	0.00	0.01	0.00	0.09	0.05	0.00	0.99
Al	2.60	2.80	1.67	8.98	0.01	0.01	2.80	4.05	1.68	8.93	1.37	0.00	2.14	2.87	4.01	1.68	8.94	1.36	0.00
Cr	0.00	0.00	0.00	0.00	0.00	0.00	0.00	0.00	0.00	0.00	0.00	0.00	0.00	0.00	0.00	0.00	0.00	0.00	0.00
Fe^{3+}	0.00	0.00	0.00	0.00	0.00	0.00	0.00	0.00	0.00	0.00	0.00	0.00	0.00	0.00	0.00	0.00	0.00	0.00	0.00
Fe^{2+}	2.08	2.69	1.44	1.72	0.95	2.78	0.05	1.63	1.33	1.77	0.00	0.97	1.94	0.06	1.72	1.27	1.75	0.00	0.98
Mn	0.01	0.01	0.01	0.03	0.04	0.01	0.00	0.01	0.00	0.01	0.00	0.01	0.01	0.00	0.01	0.00	0.01	0.00	0.01
Mg	1.03	1.32	0.65	0.22	0.00	1.59	0.04	0.23	0.73	0.22	0.00	0.00	1.18	0.04	0.24	0.78	0.24	0.00	0.01
Ca	0.01	0.00	0.00	0.00	0.00	0.00	0.00	0.00	0.00	0.00	0.41	0.00	0.00	0.00	0.00	0.00	0.00	0.34	0.00
Na	0.00	0.01	0.06	0.01	0.00	0.01	0.23	0.00	0.06	0.00	0.57	0.00	0.02	0.21	0.00	0.04	0.00	0.67	0.00
K	0.00	0.00	0.77	0.00	0.00	0.00	0.71	0.00	0.77	0.00	0.00	0.00	0.02	0.72	0.00	0.75	0.00	0.00	0.00
Total	9.20	9.72	7.08	14.73	2.01	9.96	6.94	7.95	7.07	14.73	4.97	1.99	7.12	6.96	7.99	7.04	14.74	5.02	2.00
X_{Fe}	0.67	0.67	0.69	0.89	1.00	0.64		0.87	0.65	0.89		1.00	0.62	0.60	0.88	0.62	0.88	0.93	0.99
X_{an}											0.42							0.33	
X_{ab}											0.58							0.66	
X_{or}											0.00							0.00	

4.6 Relationship between the mineral phases and bulk rock composition

A simple FMASH system was chosen for the Chl-Bt-St metapelite (DY916) and was reduced to a 3 component system in order to calculate an AFM diagram, by assuming that quartz and H_2O were in excess. As for the Bt-St-Chl-Ctd-Ms metapelites (DY982 and DY987) a KFMASH system was chosen and reduced to an AKF system by projecting from plagioclase, quartz, ilmenite and H_2O.

The AFM diagram suggest that the bulk rock composition is compatible with an assemblage of St - Ilm - Chl – Bt (Figure 4-5). On the other hand, the AKF diagram (DY982 and DY987) in figure 4-6 predicts a chloritoid in isograd which is defined by assemblages of Ctd- Bt and Ms-Ctd. It further suggest that stauorolite and chloritoid are produced by reactions of Ms + Chl = St + Bt and Ms + Chl = Ctd + Bt respectively. The bulk rock composition is compatible with assemblages of Ms – Chl- Bt, Ms – St – Chl, Ms – Ctd – Bt.

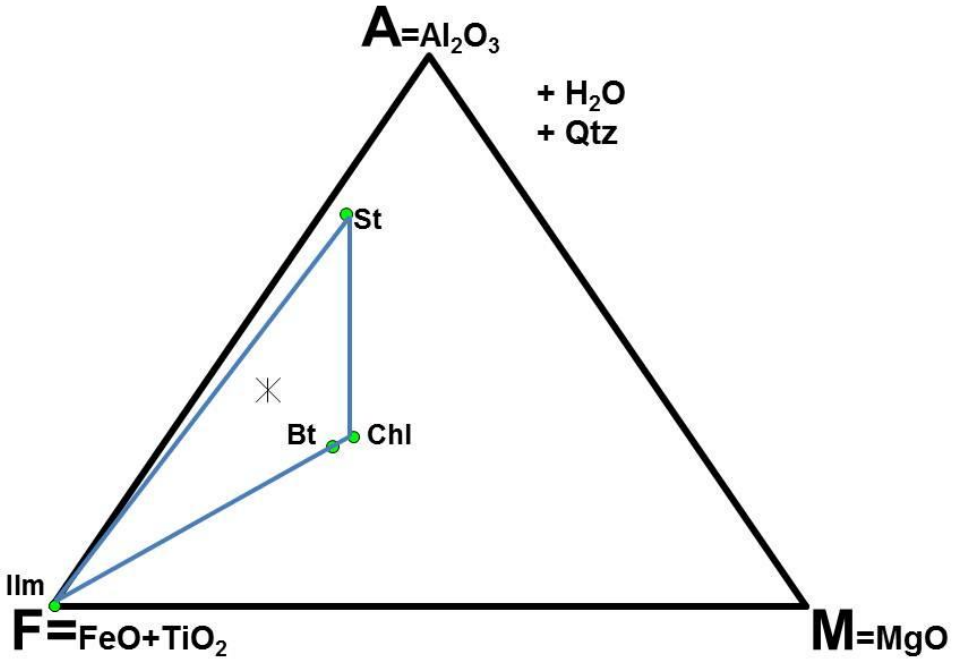

Figure 4-5. AFM diagram showing bulk rock composition (star) and minerals (dots) of DY916. Tie-lines joining St-Chl, Chl-Bt-Ilm, Ilm-St are shown in solid lines.

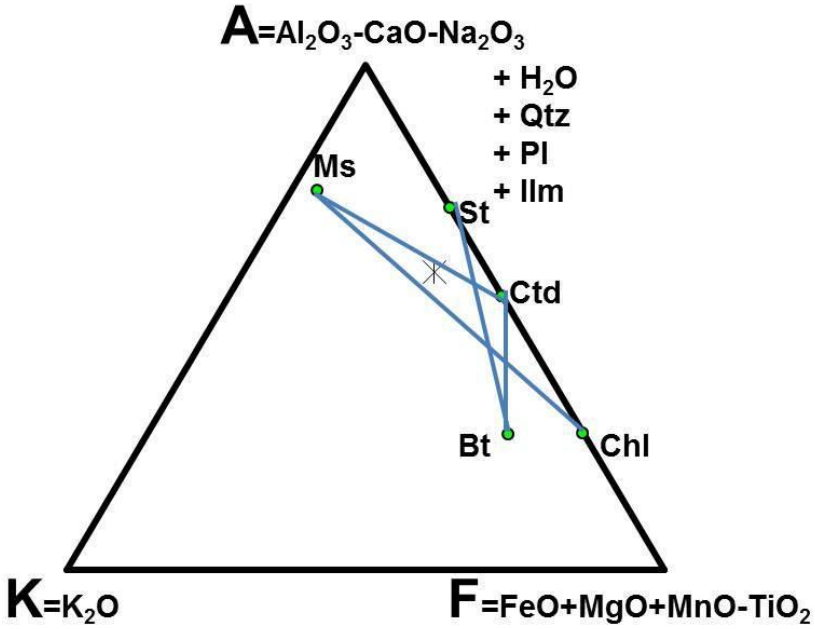

Figure 4-6. AKF diagram showing bulk rock composition (star) and minerals (dots) of DY982 and DY987 at chloritoid in isograd. Tie-lines joining Ms-Ctd, Bt-St, MS-Chl are shown in solid lines.

4.7 Pseudosections

4.7.1 Chl-Bt-St metapelite (DY916)

A K_2O-FeO-MgO-Al_2O_3-SiO_2-H_2O chemical system was chosen for this rock because these components best represent the chemical composition of all observed minerals (e.g. Chl-Bt-St-Qtz-ilm). Ilmenite was chosen as a saturated phase because it is present throughout the P-T window as the only Ti-bearing phase and does not define specific P-T conditions.

The T-X binary section in figure 4-9 was fixed at 2.5 kbar and predicted a mineral assemblage of Chl-Bt-St-Qtz-H_2O, which is stable between 530 and 570 ^{0}C at $X_{H2O} > 0.25$ (corresponding to 8.45 atomic proportions). Therefore, the mineral assemblage of DY916 is stable under water-saturated and intermediate temperature conditions. The H_2O content was recalculated to 2.64 wt. % (equivalent to 16.89 atomic proportions) on the basis of X_{H2O} that best described the observed mineral assemblage.

The observed mineral assemblage in the P-T pseudosection is represented by a single field of Chl - Bt - St - Qtz - H_2O – Ilm, occurring at 480 ^{0}C < T < 575 ^{0}C (Figure 4-10). The pseudosection also suugest two forms of chlorite (e.g. orthochamosite and clinochlore) which are stable under low and intermediate temperature conditions.

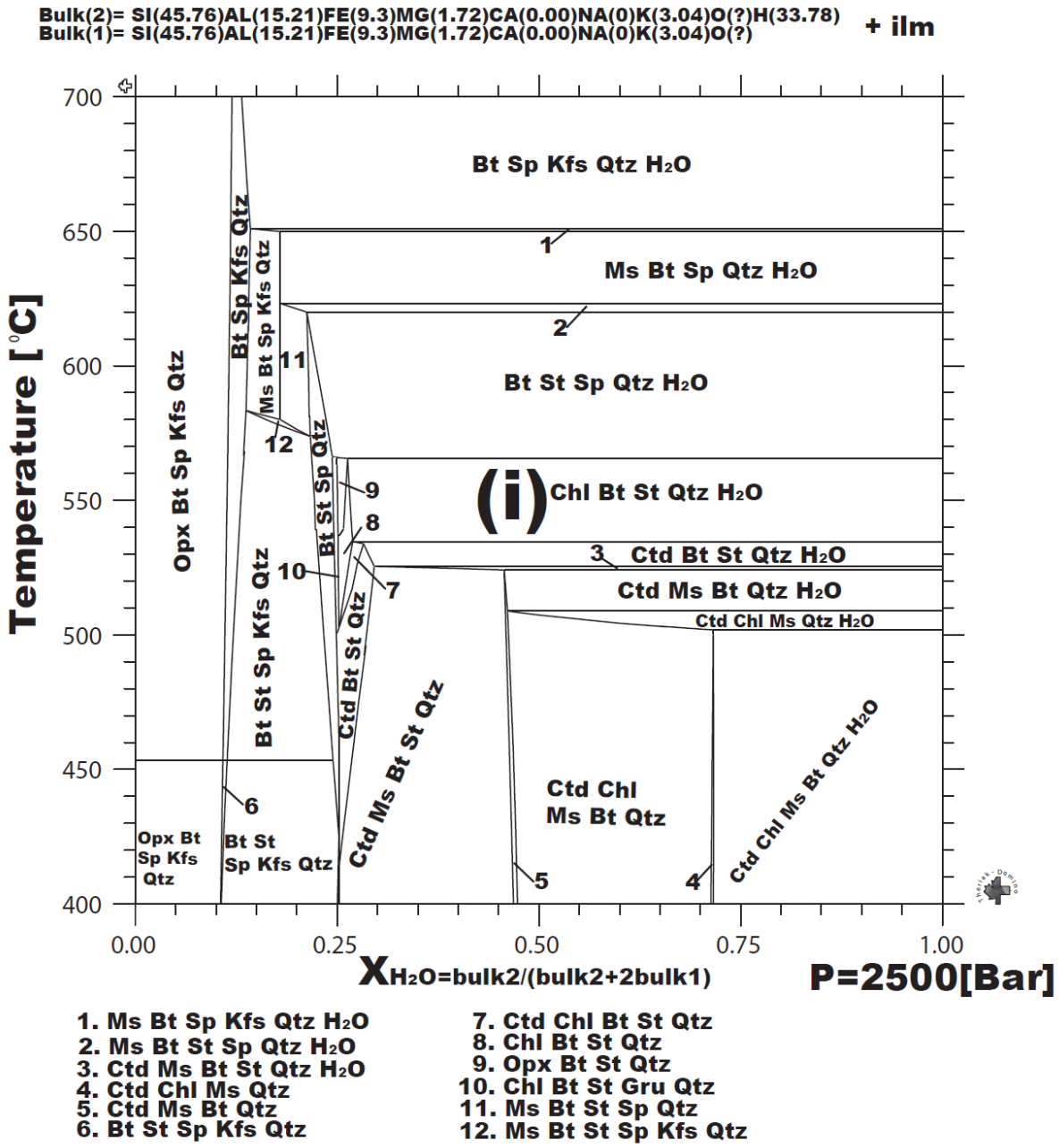

Figure 4-9. T-X binary section for the measured bulk rock composition of sample DY916 showing the influence of variable excess H_2O on the stability of observed mineral phases. Field (i) represents the observed mineral assemblage.

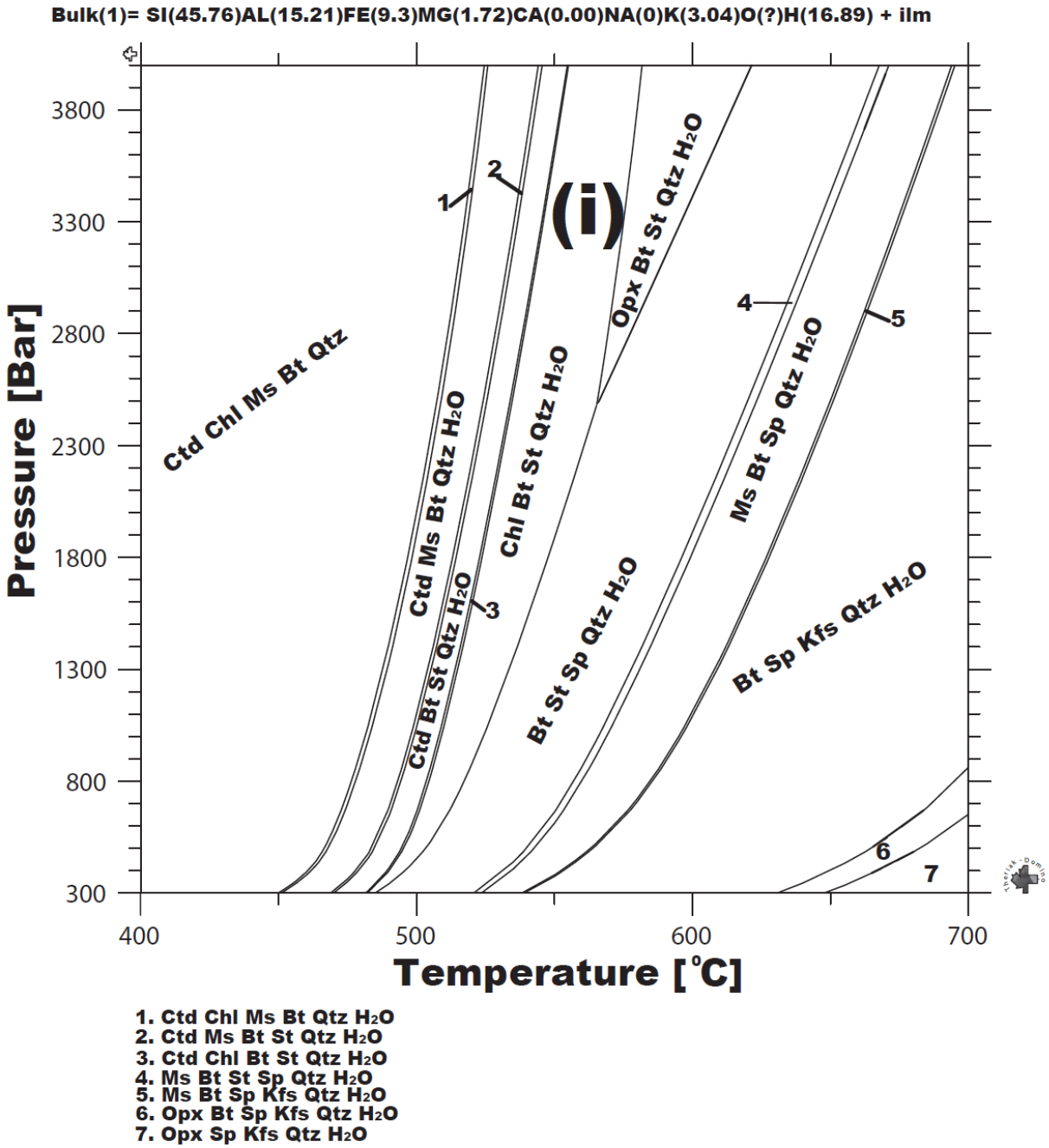

1. Ctd Chl Ms Bt Qtz H_2O
2. Ctd Ms Bt St Qtz H_2O
3. Ctd Chl Bt St Qtz H_2O
4. Ms Bt St Sp Qtz H_2O
5. Ms Bt Sp Kfs Qtz H_2O
6. Opx Bt Sp Kfs Qtz H_2O
7. Opx Sp Kfs Qtz H_2O

Figure 4-10. P-T pseudosection for sample DY916, calculated in KFMASH system. Field (i) represents the observed mineral assemblage.

4.7.2 Bt-St-Pl-Ctd-Ms-Chl metapelite (DY982)

The metapelites was modelled in a Na_2O-CaO-K_2O-FeO-MgO-Al_2O_3-SiO_2-H_2O chemical system and the system was chosen based on the components that represent all observed stable minerals (Bt-Chl-Ctd-Ms-Pl-St). However, TiO_2 was ignored because ilmenite is the only Ti-bearing phase and is ubiquitous in all fields. Furthermore, the titanium content in biotite did not influence the biotite stability field.

In a T-X binary fixed at pressure of 3 kbar, the predicted fields that best describes the metamorphic evolution of the rock are field (i) to (vii) which are stable at a temperature less than 620 ^{0}C and X_{H2O} > 0.5, corresponding to 11.6 atomic proportions (Figure 4-11). Therefore, the mineral assemblages of DY982 are stable under water saturated and low to intermediate temperature conditions (400 - ~615 ^{0}C). In the calculated pseudosection the measured bulk rock composition was used but the H_2O content was recalculated to 4.45 wt.% (equivalent to 22.6 atomic proportions) on the basis of X_{H2O} that best described the observed mineral assemblages (e.g. Figure 4-11).

The onset of metamorphism is defined by a field of Pl - Ctd - Chl - Ms - Qtz, followed by a field of Pl - St – Ctd - Chl - Ms - Qtz which is characterised by the formation of staurolite. Consequntly with increasing temperature chlorite is consumed in a field of Pl - St - Ctd - Ms - Qtz - H_2O. The prograde metamorphism is completed by the consumption of chloritoid (just above 500 ^{0}C) and is defined by a peak assemblage of Pl - St - Ms - Qtz - H_2O (Figure 4-12). The rock evolution depicted from the pseudosection suggest that muscovite and plagioclase were stable throughout the evolution of the rock, whereas chlorite and chloritoid upper stability limit is below the formation of the peak assemblage in field (iv).

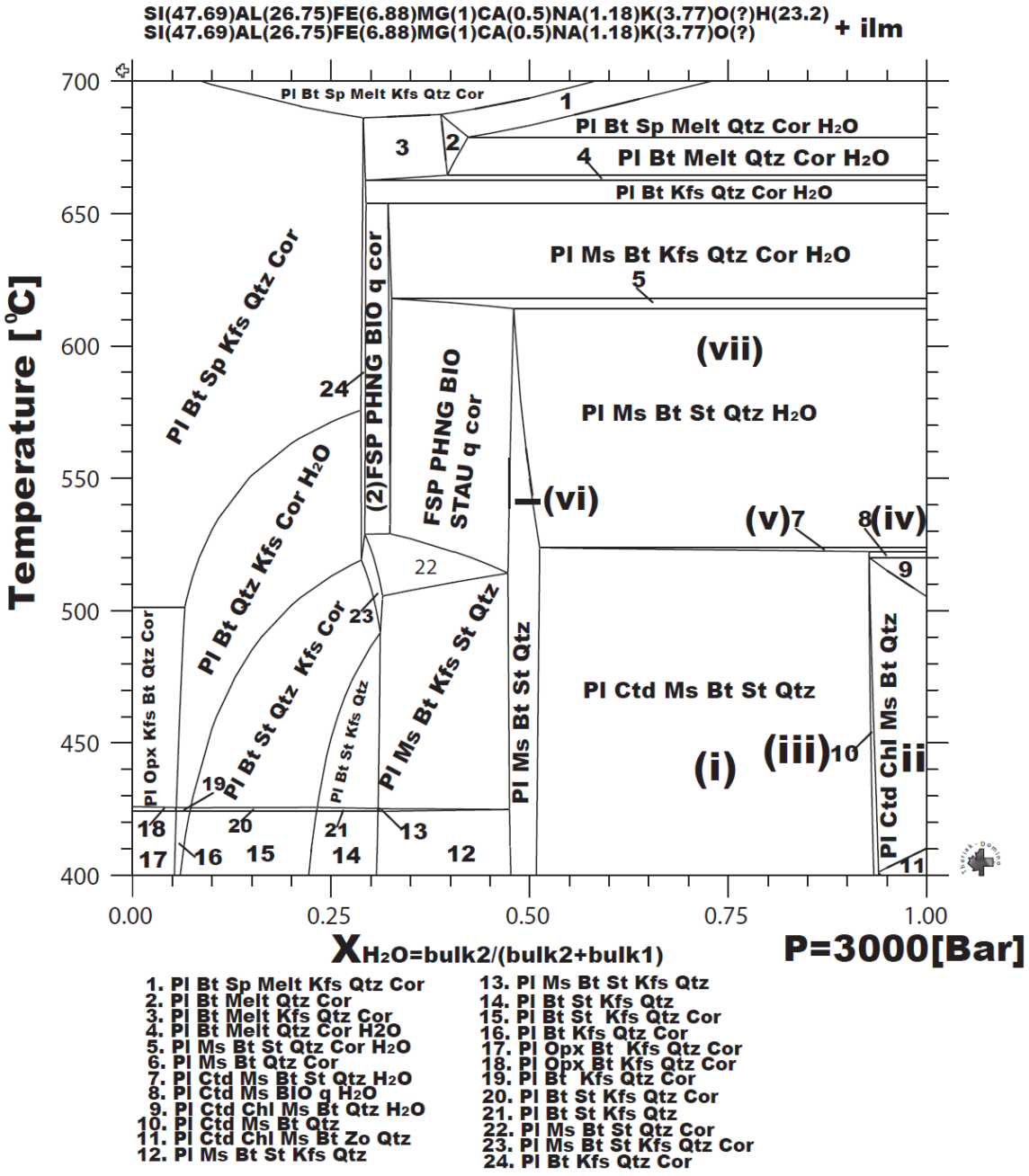

1. Pl Bt Sp Melt Kfs Qtz Cor
2. Pl Bt Melt Qtz Cor
3. Pl Bt Melt Kfs Qtz Cor
4. Pl Bt Melt Qtz Cor H2O
5. Pl Ms Bt St Qtz Cor H2O
6. Pl Ms Bt Qtz Cor
7. Pl Ctd Ms Bt St Qtz H2O
8. Pl Ctd Ms BIO g H2O
9. Pl Ctd Chl Ms Bt Qtz H2O
10. Pl Ctd Ms Bt Qtz
11. Pl Ctd Chl Ms Bt Zo Qtz
12. Pl Ms Bt St Kfs Qtz
13. Pl Ms Bt St Kfs Qtz
14. Pl Bt St Kfs Qtz
15. Pl Bt St Kfs Qtz Cor
16. Pl Bt Kfs Qtz Cor
17. Pl Opx Bt Kfs Qtz Cor
18. Pl Opx Bt Kfs Qtz Cor
19. Pl Bt Kfs Qtz Cor
20. Pl Bt St Kfs Qtz Cor
21. Pl Bt St Kfs Qtz
22. Pl Ms Bt St Qtz Cor
23. Pl Ms Bt St Kfs Qtz Cor
24. Pl Bt Kfs Qtz Cor

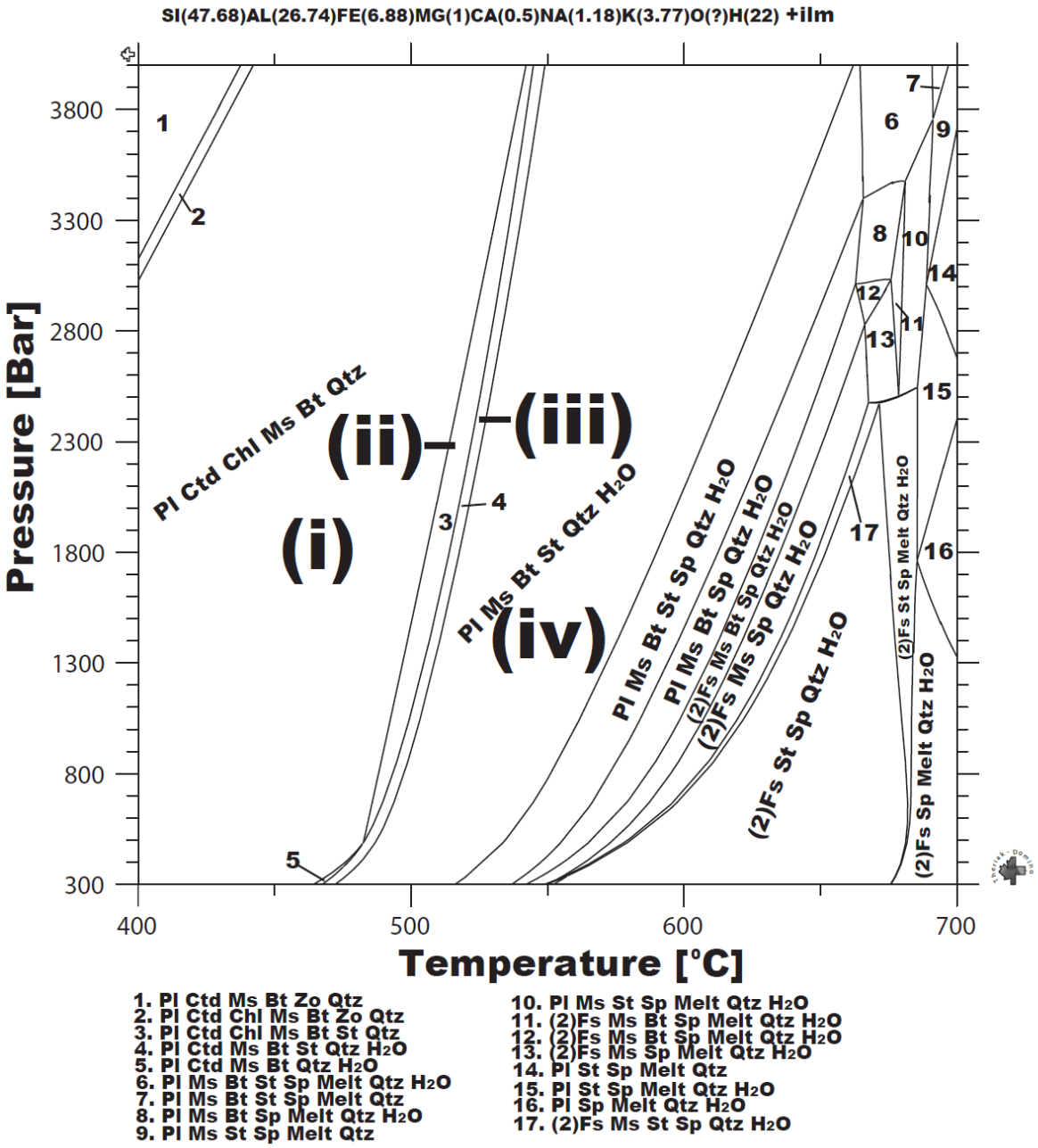

Figure 4-12. NCKFMAST P-T pseudo-section calculated for sample DY982.

Fields (i) to (iv) represent the observed mineral assemblages.

4.7.3 Bt-St-Pl-Ctd-Ms-Chl metapelite (DY987)

A Na_2O-CaO-K_2O-FeO-MgO-Al_2O_3-SiO_2-H_2O chemical system was chosen based on the major oxides that best described the observed mineral assemblages (Bt-Chl-Ctd-Ms-Pl-St) and was projected from ilmenite because ilmenite is the only Ti-bearing phase enters and does not affect the stability of bioitite of this rock. At pressure of 3 kbar the observed and predicted mineral assemblages on the T-X diagram are best represented by fields (i) to (vi). The peak metamorphic assemblage is stable between 525 and 620 ^{0}C at X_{H2O} > 0.33; corresponding to 10.692 atomic proportions (Figure 4-13). Chloritoid stabilises at X_{H2O} > 0.33 and temperature lower than 530 ^{0}C. The lower temperature grade assemblage of this rock is stable below 520 ^{0}C under water saturated conditions (Figure 4-13). Therefore, the mineral assemblages of DY987 are stable under water-saturated and low to intermediate temperature conditions (400 – 600 ^{0}C).

The modelled pseudosection was calculated from the measured bulk rock composition with H_2O content recalculated to 4.45 wt.% (equivalent to 22 atomic proportions) on the basis of X_{H2O} that best described the observed mineral assemblages (Figure 4-13) .

The prograde sequence of this metapelite is best described by four fields that occurrs between 400 and 570 ^{0}C at 300 to 4000 bars (Figure 4-14). The onset of metamorphism is defined by a broader field of Pl - Ctd - Chl - Ms - Qtz, followed by a thinner field of Pl - Ctd - Chl - Ms - Qtz - H_2O. Consequently with increasing grade St-Chl-Ctd coexist in a thinner field of Pl -St - Ctd - Chl - Ms - Qtz - H_2O, A further increase in grade result in consumption of chloritoid and chlorite which defines the peak assemblage of Pl - St - Ms - Qtz - H_2O (Figure 4-14). The rock evolution depicted from the pseudosection suggest that chlorite and chloritoid are not stable at peak metamorphic conditions, but are low grade mineral phases.

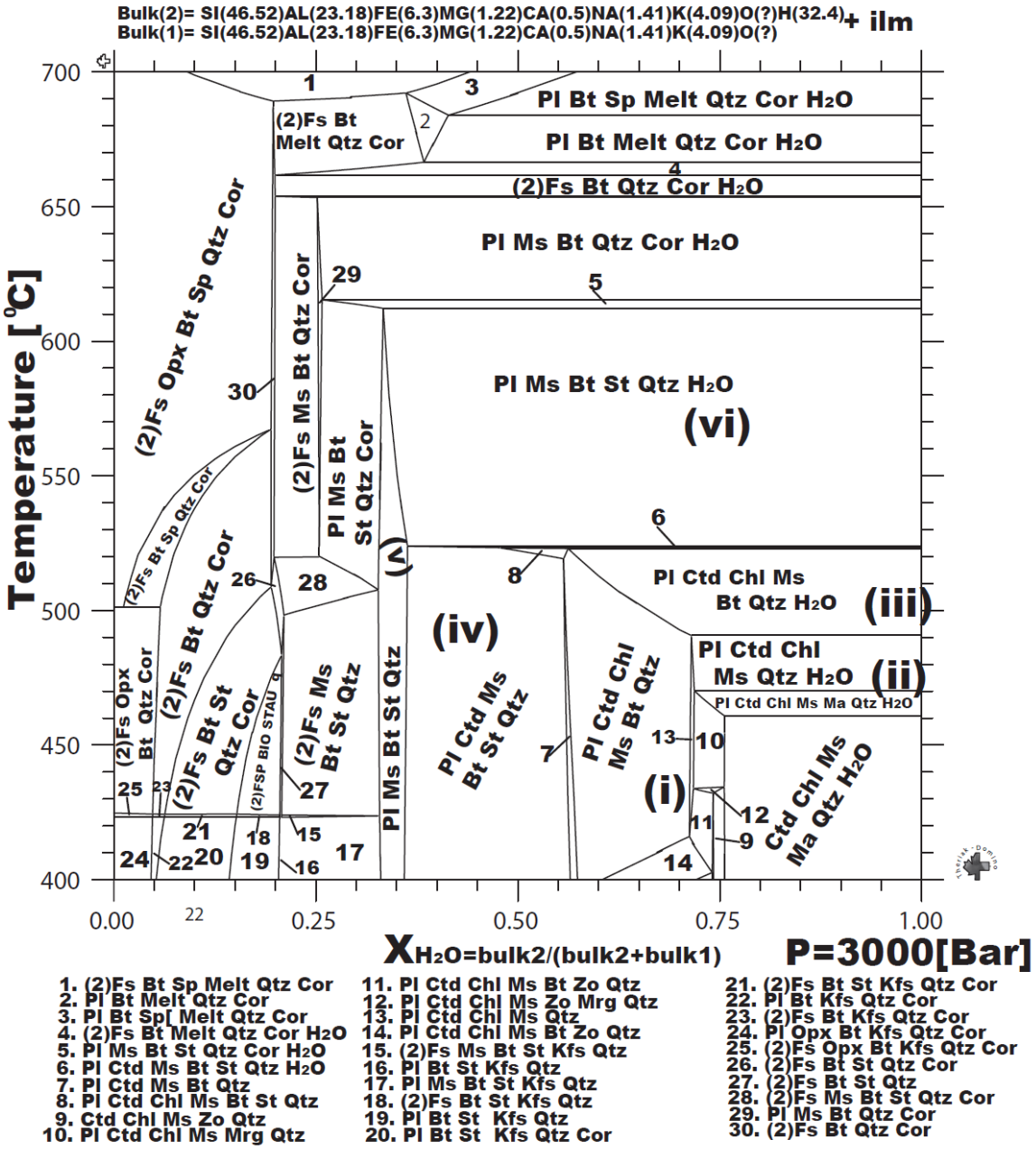

Figure 4-13. T-X binary section for the measured bulk rock composition of sample DY987 showing the influence of variable excess H_2O on the stability of observed mineral phases. Fields (i) to (vi) represent the observed mineral assemblage.

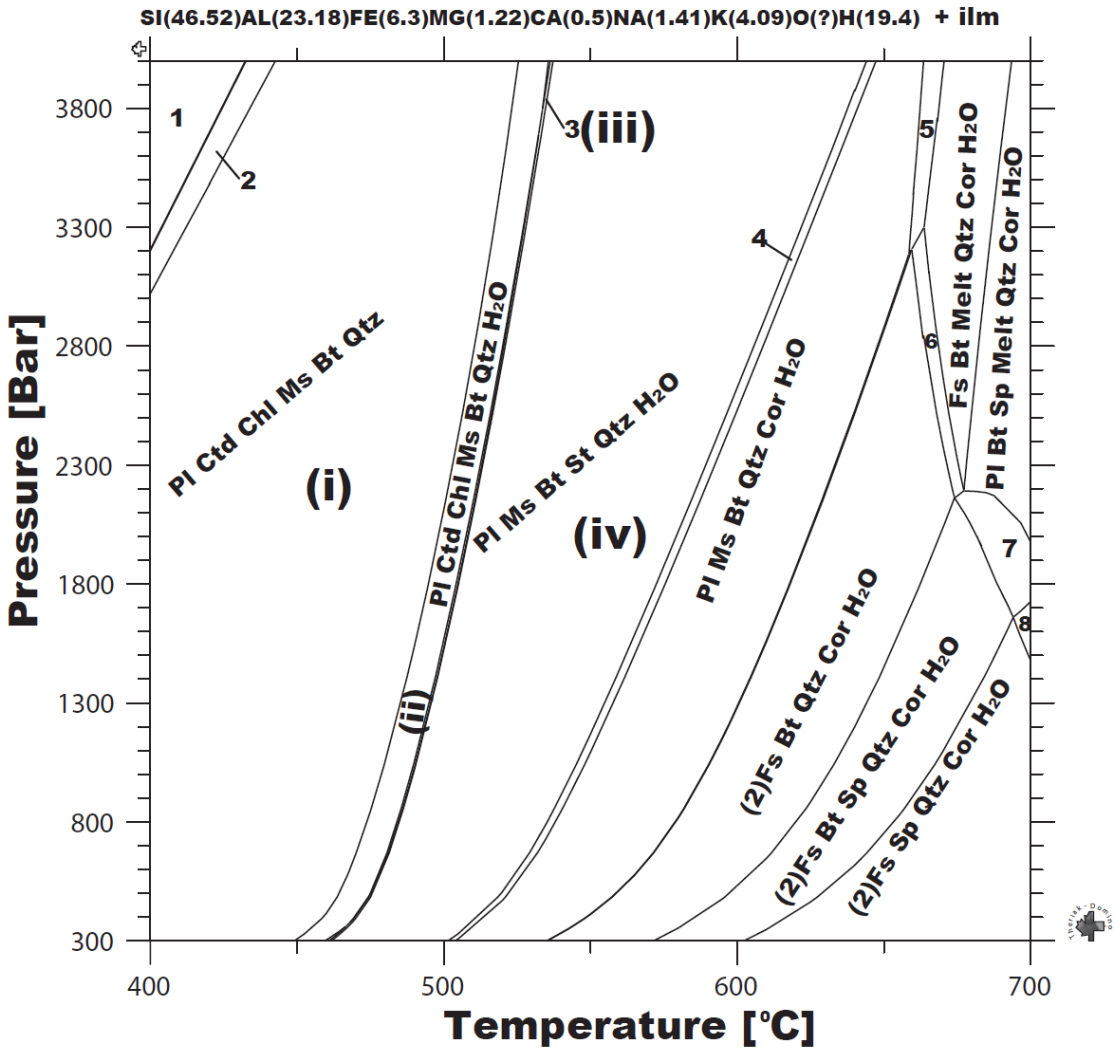

1. Pl Ctd Chl Ms Bt Zo Qtz
2. Pl Ctd Chl Ms Bt Zo Qtz
3. Pl Ctd Chl Ms Bt St Qtz H_2O
4. Pl Ms Bt St Qtz Cor H_2O
5. Pl Ms Bt Melt Qtz Cor H_2O
6. (2)Pl Bt Ms Qtz Cor H_2O
7. (2)Pl Bt Sp Melt Qtz Cor H_2O
8. (2)Pl Sp Melt Qtz Cor H_2O

Figure 4-14. P-T pseudosection for sample DY987, calculated on a NCKFMAST system. Fields (i) to (iv) represent the observed mineral assemblages.

4.8 Geothermobarometry

Further temperature estimates were obtained using two thermometers of Pl-Ms (Green and Usdansky, 1986b) and Ms-Bt (Hoisch, 1989). The Hoisch (1989) calibration is based on the exchange of Mg-Tschermak's components between muscovite and biotite which models the nonideality in the mixing of cations within the octahedral sites of both phases. Green and Usdansky (1986b) utilised a ternary-feldspar subregular solution model and a non-ideal binary white mica solution model to calibrate the Na–K exchange reaction between plagioclase and muscovite. The Pl-Ms and Ms-Bt thermometers recorded ~ 530 ^{0}C at 3 kbar for DY982, whereas DY987 recorded ~541 and 531 ^{0}C at 3 kbar.

4.9 Discussion

The prograde staurolite in Bt-Chl-St metapelite (DY916) is altering to chlorite and biotite along the rim region which implies that it is unstable, probably as a result of a drop in temperature which caused formation of secondary chlorite and biotite. Compositional variations of the different micro-texural settings of the biotite and chlorite flakes in this metapelite are small and this could suggest that they form in an isochemical system. The equilibrium assemblage of Chl-Bt-St is stable between 480 to 540 ^{0}C. The pseudosection predicts that the formation of Chl-Bt assemblage precedes that of staurolite and therefore it possible to conclude that the reaction that best account for formation of staurolite is (assuming that muscovite was totally consumed during the formation of staurolite);

$$Ms + Chl + Qtz = St + Bt + H_2O \qquad (14)$$

The assumed presence of muscovite is supported by the K_2O of 3.09 wt % which is similar to 3.4 wt% measured for the Ms bearing metapelite of DY982. According to Wang and Spear (1991), the assemblage of Bt-Ctd can co-exist in a rock if bulk Fe/(Fe + Mg + Mn) >0.60 and this is consistent with the Chl-Bt-St content of 0.91. Therefore, as predicted by the pseudosection, it possible that the assemblage of Bt-Ctd existed during the earlier stages of the evolution of this metapelite and was effectively consumed during peak metamorphism defined by Chl-Bt-St assemblage.

All described and analysed staurolites in Bt-St-Ctd-Chl metapelites (DY982 and DY987) exhibit no chemical zoning in terms of X_{Fe} and X_{Mg} and have similar compositions. This is also true for biotite flakes; that is, regardless of their micro-textural settings as noted above, they do not exhibit a broader chemical variation but formed in an isochemical system.

Based on the pseudosections of DY982 and DY987, it can be noted that chlorite and chloritoid represent a low temperature assemblages, while staurolite marks the peak metamorphic conditions in the absence of both phases, with plagioclase, biotite, ilmenite and muscovite stable throughout the evolution of these metapelites.

In accordance with the microstructural settings preserved in both metapelites, the rare replacement of staurolite by chloritoid and biotite suggest a retrograde formation of these phases at the expense of staurolite during cooling. The invasion of biotite by staurolite might suggest that the formation of staurolite represent the upper stability limmit of biotite or forming from the same reaction. The AKF diagram in figure 4-6, suggest that an assemblage of St-Bt-Chl-Ctd should not co-exist in the absence of muscovite. In addition, the pseudosections predict that Ctd-Chl-Bt-Ms-St assemblage can co-exist within the rock but only for a short temperature interval as indicated by the thinner fields (Figure 4-10 and 4-13). The intersection of Ctd-Bt with Ms-Chl tielines in the AKF diagram and the occurrence of chloritoid porphyroblasts and biotite poikiloblasts with inclusions of chlorite, ilmenite and muscovite, suggest that the reaction responsible for formation of the former assemblage is;

$$Ms + Chl + Ilm = Cld + Bt + Qtz + H_2O \qquad (15)$$

The formation of staurolite corresponds closely with both reaction 14 and 15 where Chl-Ms-Qtz assemblage grades up to form St-Bt assemblage (e.g. reaction 14) marking the upper stabilty limit of Chl-Ctd assemblage. This reaction can be noted in AKF diagram as the intersection of the Ms-Chl with St-Bt tie-line and further confirmed by mineral abundances in thin section where biotite and staurolite are the dominant phases. Taking Pl-Ms and Bt-Ms thermometry estimates into consideration, the peak metamorphic assemblage of Bt-St-Ms-Pl-Qtz equlibriated between 530 to 541 ^{0}C at a fixed pressure of 3 kbar. Based upon the textural evidence, pseudosection result and classical geothermobarometry, it can be concluded that these metapelites followed a prograde clockwise P-T path which is characterised by retrograde cooling effects during uplift.

Chapter 5

Summary and concluding remarks

The bulk rock compositions of the garnet-bearing hornfelses and staurolite-bearing garnet free metapelites are similar to average pelitic compositions. The garnet-free metapelites have a lower CaO content of less than 0. 6 wt. % as compared to garnet bearing hornfelses where it is in excess of 1.2 wt.%. The bulk MnO/ (MnO + FeO + Mg) content of the garnet-bearing hornfelses ranges from 0.07 to 0.09 wt. %, whereas the garnet free metapelites content ranges from 0.03 to 0.08. The absence of garnet in these metapelites may be attributed to the low concentration of Mn and Ca which partitions strongly into garnet and expands its stability field to lower P-T conditions (Mahar et al., 1997). In addition, garnet-free metapelites do not form andalusite as part of their assemblages even though they have Al_2O_3 that ranges from 16 to 26 wt. % compared to a range of 17.79 to 20.77 wt. % in garnet bearing hornfelses which contains andalusite as well. The stability of Al_2SiO_5 polymorphs can also be influenced by the increase in Fe and Mn which causes the andalusite field to expand (Gambling and Williams, 1985) and does not only depend on the Al_2O_3 content.

The studied rocks can be divided into two metamorphic zones within the BC contact aureole, namely garnet and staurolite zones. Garnet porphyroblasts are ubiquitous in all the three garnet bearing hornfelses which were sampled in Silverton (DY954 and DY956) and Daspoort formation (DY918), but their garnet forming reactions are different (e.g. reaction 17 and 20). The majority of garnet porphyroblasts in these hornfelses do not show any evidence of alteration which suggest that they are stable phases. Garnets in DY918 are restricted within the phyllosilicate-rich layers (darker domains), whereas in the DY954 and DY956 hornfelses they are widely distributed. All these garnets, except for G0 garnet in the DY954 hornfels, show a Mn high in the core regions which decreases towards the rim. Andalusite and staurolite porphyroblast observed within DY954 and DY956 hornfelses do show evidence of alteration which implies that they are metastable phases and their formation in these hornfelses is controlled by different reactions. Based on the above, it can be concluded that the idioblastic garnet porphyroblasts in these hornfeles were continuously forming as the temperature increased. Therefore, these garnet-bearing hornfelses represent a garnet zone which records the hornblende hornfels facies within the BC contact aureole. On the other hand, the staurolite porphyroblasts in garnet-free metapelites marks the peak metamorphic conditions experienced by these rocks and hence represent the staurolite zone within the BC contact aureole of the studied area.

The recorded P-T conditions and depths of burials especially in G0 and G1 garnets of DY954 hornfels imply that the two garnets formed under different P-T conditions; hence they were affected by different stages of metamorphism.

G1 garnets reached a maximum P-T condition of ~ 630 ^{0} at 2.2 kbar while G0 garnet core recorded the same conditions but experienced a pressure increase up to 2.7 kbar and a temperature drop towards the rim. Therefore, this can be interpreted to imply that G1 garnets were formed during a prograde process which was influenced by a separate magma pulse, while G0 was formed by non-isobaric retrograde process which was influenced by a less hot but denser magma pulse which caused the garnet growth not run to completion. Based on the garnet core and rim estimates from both techniques, it is apparent that G0 and G1 garnets experienced different heating regimes, with the latter enjoying a much more prolonged heating; as shown by the temperature difference of about 100^{0}C from the core to the rim compared to 10^{0}C for G0.

The Lu-Hf isotope systematics of these garnet records a 2061 Ma age for all garnet porphyroblasts in the DY918 and DY954 hornfelses which support a co-genetic garnet growth regardless of their stratigraphic positions. According to Rajesh et al. (2013), the 2061 Ma age records the 2061-2060 Ma (Walraven, 1997) magma pulse which represent the Rooiberg Group volcanic suite but recent work of Scoates et al. (2012), suggest that 2061-2060 period does not solely represent the extrusion of the Rooiberg Group felsic rocks but also the coeval sub pulse of the ultramafic to mafic LZ and CZ magmas. Therefore, the 2061 Ma garnet age denotes the emplacement age of the LZ and CZ magma which means that all these garnet formed in response to this emplacement. The fact that none of these garnets separates records the 2059 – 2054 intrusion of the MZ and UP magmas probably means that the crystallisation temperatures of the later magma pulse was not significant enough to shift the Lu-Hf isotopic signatures. Based on this it is safe to assume that the DY954 hornfels does provide evidence for a two stage metamorphic evolution of the BC contact aureole in support of earlier studies (e.g. Nell, 1984 and Walmach, 1989).

The sampled metapelites of the lower and upper Timeball Hill formation of the north-eastern BC contact aureole contains staurolite but lack andalusite and garnet. Idioblastic staurolites are widespread within these metapelites with grain sizes of up 4 mm, texturally majority of them have been altered or overgrown by biotite and chloritoid. The alteration of these staurolite porphyroblast is due isobaric cooling during uplift and the St-Bt assemblage represent the peak equilibrium conditions which marks the upper stability limit of Chl-Ctd assemblage. The presence of foliations within these metapelites does not represent a regional metamorphic fabric but it is due to the intrusion of the separate sub-magma pulses of the RLS.

Taking Pl-Ms and Bt-Ms thermometry estimates into consideration, the peak metamorphic assemblage of Bt-St-Ms-Pl-Qtz equilibrated between 530 to 541 ^{0}C at 3 kbar. Based upon textural evidence, pseudosection result and classical geothermobarometry, it can be concluded that these metapelites followed a prograde clockwise P-T path which is characterised by retrograde cooling effects during uplift.

In conclusion, the garnet-bearing hornfelses and garnet-free staurolite-bearing metapelites mark the garnet and staurolite zones within the BC contact aureole of the studied area. The poly-metamorphic history of the BC contact aureole is not recorded by all samples and pressure had more influence on the tow stage development of the aureole than temperature. Therefore, the different magma pulses from the LZ-CZ and MZ-CZ had different thermal histories which might have also been influenced by the assimilated country rocks. This further implies that the BC evolved over two major stages which were influenced by two major magma pulses.

References

Alexandre, P., Andreoli, M.A.G., Jamison, A. and Gibson, K.L. (2006). $^{40}Ar/^{39}Ar$ age constraints on low-grade metamorphism and cleavage development in the Transvaal Supergroup (central Kaapvaal craton. South Africa): implications for the tectonic setting of the Bushveld Igneous Complex. *South African Journal of Geology*, **109**, 393-410.

Andreoli. M.A.G, (1988a). The discovery of a hidden and strange African orogeny; the Transvaalide Fold Belt, *Tectonic Division of the Geological Society of South Africa*, Abstracts Volume, 4th Annual Conference, l-2.

Andreoli. M.A.G, (1988b). Evidence for thrust tectonics in the Transvaal sequence based on geophysical profiles. Extended Abstracts, *Geocongress 88*, Geological Society of South Africa, 3-6.

Barboza, S.A. and Bergantz, G.W. (2000). Metamorphism and anatexis in the Mafic Complex Contact Aureole, Ivrea Zone, Northern Italy. Journal of Petrology, **48**, 1307-1327.

Bestel, M., Gawronski, T., Abart, R. and Rhede, D. (2009). Compositional zoning of garnet porphyroblasts from the polymetamorphic Wölz Complex, Eastern Alps. *Miner Petrol*, **97**, 173–188.

Blichert-Toft, J., Chauvel, C. and Albare'de, F. (1997). Separation of Hf and Lu for high-precision isotope analysis of rock samples by magnetic sector-multiple collector ICP-MS. *Contributions to Mineralogy and Petrology*, **127**, 248-260.

Bowlen et al. (1983; cited in Engelbrecht, J.P. (1990). Contact metamorphic processes related to the aureole of the Bushveld Complex in the Marico District, western Transvaal, South Africa. *South African Journal of Geology*, **93**, 339-349.

Buick, I.S., Maas, R. and Gibson, R. (2001). Precise U-Pb titanite age constraints on the emplacement of the Bushveld Complex, South Africa. *Journal of the Geological Society*, London, **158**, 3–6.

Burt, D.M. (1971). The system Fe-Si-C-O-H: A model for metamorphosed iron formations. Yearbook, Carnegie Inst., Washington, **71**, 435-443.

Büttner, S.H. (2012). Rock Maker: an MS Excel spread sheet for the calculation of rock compositions from proportional whole rock analyses, mineral compositions, and modal abundance. *Mineralogy and Petrology*, **104**, 129-135.

Campbell, G. (2011). Exploration Geophysics of the Bushveld Complex in South Africa. The leading edge, **30** (6), 622-638.

Carlson, W. D. (2006). Rates of Fe, Mg, Mn and Ca diffusion in garnet. *American Mineralogist*, **91**, 1-11.

Castro, A., Fernández, C., El-Hmidi, H., El-Biad, M. Díaz, M., de la Rosa, J. and Stuart, F. (1999). Age constraints to the relationships between magmatism, metamorphism and tectonism in the Aracena metamorphic belt, southern Spain International Journal of Earth Sciences, **88**, 26–37.

Cawthorn, R.G. and Walraven, F. (1998). Emplacement and crystallization time for the Bushveld Complex. *Journal of Petrology*, **39**, 1669-1687.

Cawthorn, R.G., Eales, H.V., Walraven, F., Uken, R. and Watkeys, M.K. (2006). The Bushveld Complex, Geological Society of South Africa, Johannesburg and Council for Geoscience, Pretoria, ,in: M.R. Johnson, C.R. Anhaeusser, R.J. Thomas, Editors , *The Geology of South Africa*, 261–281.

de Capitani C. and Petrakakis K. (2010). The computation of equilibrium assemblage diagrams with Theriak/Domino software. *American Mineralogist*, **95**, 1006-1016.

Droop, G.T.R. (1987). A general equation for estimating Fe^{3+} concentrations in ferromagnesian silicates and oxides using stoichiometric criteria. *Mineralogical Magazine*, **51**, 431-437.

Dymoke, P. and Sandiford, M. (1992). Phase relations in Buchan facies series pelitic assemblages: calculations with application to andalusite–staurolite paragenesis in the Mount Lofty Ranges, South Australia. *Contributions to Mineralogy and Petrology*, **110**, 121–132.

Eales, H.V., Cawthorn, R.G., 1996. The Bushveld Complex. In: Cawthorn, R.G. (Ed.), Layered Intrusions. Elsevier Science B.V., pp. 181–229.

Engelbrecht, J.P. (1976). Meta-sediments of the Pretoria Group in the Enzelsberg area, Marico District. *Trans. Geol. Soc. S. Afr.*, **79**, 1, 61-75.

Engelbrecht, J.P. (1986). Die Bosveld kompleks en sy vloergesteentes in die omgewing van Nietverdiend, Wes-Transvaal: Ph.D. thesis (unpublished), University of Pretoria, Pretoria, South Africa, 327pp.

Engelbrecht, J.P. (1990). Contact metamorphic processes related to the aureole of the Bushveld Complex in the Marico District, western Transvaal, South Africa. *South African Journal of Geology*, **93**, 339-349.

Eriksson, P.G., Mazumder, R., Roy, K.K., Bose, P.K., Altermann, W., and van der Merwe, R. (1999). The 2.7–2.0 Ga volcano-sedimentary record of Africa, India and Australia: evidence for global and local changes in sea level and continental freeboard. *Precambrian Research*, **97**, 269–302.

Eriksson, P.G., Altermann, W., Catuneanu, O., van der Merwe, R. and Bumby, A.J. (2001). Major influences on the evolution of the 2.67–2.1 Ga Transvaal basin, South Africa, *Sediment. Geol.*, **141–142**, 205–231.

Evans, B.W. (1965). Application of a reaction-rate method to the breakdown equilibria of muscovite and muscovite plus quartz. *American Journal of Science*, **263**, 647-667.

Evans, T. P. (2004). Reconciling the structural and metamorphic record of orogeny in the central western hemisphere through microstructure and garnet isopleth thermobarometry. PhD. thesis (unpublished), James Cook University of North Queensland, Australia, 159pp.

Ferry, J.M., and Spear, F.S. (1978). Experimental calibration of the partitioning of Fe and Mg between biotite and garnet. *Contribution to Mineralogy and Petrology*, **66**, 113-117.

Fuhrman, M. L. and Lindsley, D. H. (1988). Ternary-feldspar modelling and thermometry. American Mineralogist, **73**, 201–215.

Gaidies F., Abart R, de Capitani C, Schuster R, Connolly J.A.D, Reusser, E. (2006). Characterisation of polymetamorphism in the Austroalpine basement east of the Tauern Window using garnet isopleth thermobarometry. Journal of Metamorphic Geology, 24, 451–475.

Grambling, J.A. and Williams, M.L. (1985). The effects of Fe^{3+} and Mn^{3+} on aluminium phase relations in north-central New Mexico, USA. Journal of Petrology, **26**, 324 - 354.

Gerdes, A., Zeh, A. (2009). Zircon formation versus zircon alteration – new insights from combined U–Pb and Lu–Hf in-situ LA-ICP-MS analyses, and consequences for the interpretation of Archean zircon from the Limpopo Belt. *Chemical Geology*, **261**, 230–243.

Gibson. R.L., Courtnage, P.M., and Charlesworth, E.G. (1999). Bedding parallel shearing and deformation in the lower Transvaal Supergroup north of the Johannesburg Dome, South Africa. *South African Journal of Geology*, **102**, 99-108.

Ghent, E.D. (1976). Plagioclase – garnet – Al2SiO5 – quartz: a potential geobarometer – geothermometers. *American Mineralogist*, **61**, 710-714.

Green, N.L. and Usdansky, S.I. (1986). Toward a practical plagioclase - muscovite thermometer. American Mineralogist, **71**, 1109-1117.

Hall, A. L. (1932). The Bushveld Igneous Complex of the Central Transvaal: *Mem. Geol. Surv. South Africa*, **28**, -560 pp.

Hammerbeck, E.C.I. (1986). Andalusite in the metamorphic aureole of the Bushveld Complex. In*: Mineral Deposits of Southern Africa*. C.R. Anhaeusser and S. Maske (Editors). Geol. Soc. S. Afr., Johannesburg, I&II, 993-1004.

Hannah, J.L., Bekker, A., Stein, H.J., Markey, R.J. and Holland, H.D., (2004). Primitive Os and 2316 Ma age for marine shale: implications for Paleoproterozoic glacial events and the rise of atmospheric oxygen. *Earth Planet. Scientific Letters*, **225**, 43–52.

Harris, N., McMillan, A., Holness, M., Uken, R., Watkeys, M., Rogers, N. and Fallick, A. (2003). Melt generation and fluid flow in the thermal aureole of the Bushveld Complex. *Journal of Petrology*, **44** (6), 1031-1054.

Hartzer, F. J. (1987). Die geologie van die Krokodilrivierfragment, Transvaal. M.Sc. thesis (unpublished), Rand Afrikaans University, Johannesburg, South Africa, -201pp.

Hartzer, F. J. (1994). Transvaal inliers: geology and relationship with the Bushveld Complex. PhD. Thesis (unpublished), Rand Afrikaans University, Johannesburg, South Africa, -415pp.

Hartzer, F.J. (1995). Transvaal Supergroup inliers: geology, tectonic development and relationship with the Bushveld complex, South Africa. *Journal of African Earth Sciences*, **21**, 521-547.

Hatton, C. J. and Schweitzer, J. K. (1995). Evidence for synchronous extrusive and intrusive Bushveld magmatism. *Journal African Earth Sciences*, **21**, 579-594.

Hirsch, D.M., Prior, D.J. & Carlson, W.D. (2003). An overgrowth model to explain multiple, dispersed high-Mn regions in the cores of garnet porphyroblasts. *American Mineralogist*, **88**, 131–141.

Hodges, K.V. and Spear, F.S. (1982). Geothermometry, geobarometry and the Al_2SiO_5 triple point at Mt. Moosilauke, New Hampshire. *American Mineralogist*, **67**, 175-198.

Hoisch, T.D. (1989). A muscovite-biotite geothermometer. American Mineralogist, **74**, 565-572.

Hoisch, T. D. (1990). Empirical calibration of six geobarometers for the mineral assemblage quartz + muscovite + biotite + plagioclase + garnet. Contributions to Mineralogy and Petrology, **104**, 225–234.

Hoisch, T. D. (1991). Equilibria within the mineral assemblage quartz + muscovite + biotite + garnet + plagioclase, and implications for the mixing properties of octahedrally-coordinated cations in muscovite and biotite. Contributions to Mineralogy and Petrology, **108**, 43–54.

Holdaway, M.J. and Lee, S.M. (1977). Fe-Mg cordierite stability in high-grade politic rocks based on experimental, theoretical and natural observations. *Contribution to Mineralogy and Petrol*ogy, **63**, 175-198.

Holdaway, M. J. (2000). Application of new experimental and garnet Margules data to the garnet–biotite geothermometer. American Mineralogist, **85**, 881–892.

Holland, T.J.B. and Powell, R. (1998). An internally-consistent thermodynamic dataset with uncertainties and correlations: the system Na_2O-K_2O-CaO-MgO-MnO-FeO-Fe_2O_3-Al_2O_3-SiO_2-TiO_2-C-H_2-O_2. *Journal of Metamorphic Geology*, **8**, 89-124.

Hulbert, L.J. and Sharpe, M.R. (1981). Andalusite-biotite-cordierite-muscovite hornfels, Faugha Ballagh. In: C.F. Vermaak, and G. Vongrunewladt, (Editors). *3rd International Platinum Symposium, Executive guide book*, 39-41.

Human, D.R. (1975). The geology and metamorphic petrology of part of the basal argillaceous zone, Daspoort Stage, Pretoria Series of the Farm Havercroft, North Eastern Transvaal. *Petros*, **6**, 25-43.

Human, D.R. and Collins, L.A. (1986). The Havercroft-Streatham Andalusite Deposit, Eastern Transvaal. In: Anhaeusser, C.R. & Maske, S., (Eds.), *Mineral Deposits of Southern Africa*. I. Geol. Soc. S. Afr., Johannesburg, 1005-1008.

Johnson, T.E., Gibson, R.L., Brown, M., Buick, I.S. and Cartwright, I. (2003). Partial melting of metapelitic rocks beneath the Bushveld Complex, South Africa. *Journal of Petrology*, **44** (5), 789-813.

Johnson, T.E.and Brown, M. (2004). Quantitative constraints on metamorphism in the Variscides of Southern Brittany – a complimentary pseudosection approach. *Journal of Petrology*, **45**, 1237–1259.

Johnson, T.E., Brown, M., Gibson, R. and Wing, B., (2004). Spinel-cordierite symplectites replacing andalusite: evidence for melt-assisted diapirism in the Bushveld Complex, South Africa. *Journal of Metamorphic Geology*, **22**, 529-545.

Johnson, T. E., Brown, M. AND White, R. W. (2010). Petrogenetic modelling of strongly residual metapelitic xenoliths within the southern Platreef, Bushveld Complex, South Africa. *Journal of metamorphic Geology*, **28**, 269–291.

Kaneko, Y. and Miyano, T. (1990). Contact metamorphism by the Bushveld Complex in the north-eastern Transvaal, South Africa. Journal of Mineralogy, *Petrology and Economic Geology*, **85**, 66-81.

Kaneko, Y., Miyano, T. and van Reenen, D.D. (2000). Pseudomorphs and ghost structures of some aluminous silicate minerals in pelitic hornfelses of the Timeball Hill Formation, Transvaal Supergroup, in the north-eastern Transvaal, South Africa. Ann. Rep., *Inst. Geosci., University Tsukuba*, **26**, 41-46.

Koziol, A.M. and Newton, R.C. (1988). Redetermination of the anorthite breakdown reaction and improvement of the plagioclase-garnet-Al_2SiO_5-quartz geo-barometer. *American Mineralogist*, **73**, 216-223.

Kretz, R. (1982). Transfer and exchange equilibria in a portion of the pyroxene quadrilateral as deduced from natural and experimental data. *Geochiica et Cosmochimica Acta.*, **46**, 411-421.

Kretz R. (1983). Symbols for rock-forming minerals. *American Mineralogist*, **68**, 277–279.

Lagos, M., Scherer, E. E., Tomaschek, F., Münker, C., Keiter, M., Berndt, J. and Ballhaus, C. (2007). High precision Lu-Hf geochronology of Eocene eclogite-facies rocks from Syros, Cyclades, Greece. *Chemical Geology*, **243**, 16-35.

Likhanov, I.I., Reverdatto, V.V., Sheplev, V.S., Verschinin, A.E. and Kozlov P.S. (2001). Contact metamorphism of Fe- and Al-rich graphitic metapelites in the Transangarian region of the Yenisei Ridge, eastern Siberia, Russia. Lithos, **58**, 55–80.

Ludwig, K. (2007). Isoplot/Ex version 3.41b, a geochronological toolkit for Microsoft Excel. *Berkeley Geochronology Center*, Special Publication 4.

Mahar, E.M., Baker, J.M., Powel, R., Holland, T.J.B. and Howell, N. (1997). The effect of Mn in mineral stability in metapelites. Journal of Metamorphic Petrology, 15, 223-238.

Millonig, L., Zeh, A., Gerdes, A. and Klemd, R., (2008). Late Archean high-grade metamorphism in the Central Zone of the Limpopo Belt (South Africa): Petrological and geochronological evidence from the Bullae Pluton. *Lithos*, **103**, 333–351.

Miyano, T., Beaks, N.J. and van Reenen, D.D. (1987). Metamorphic evidence for early post-Bushveld sills in the Penge Iron Formation, Transvaal Sequence, Eastern Transvaal. *South African Journal of Geology*, **90**(1), 37-43.

Münker, C.,Weyer, S., Scherer, E. E. and Mezger, K. (2001). Separation of high field strength elements (Nb, Ta, Zr, Hf) and Lu from rock samples for MC-ICPMS measurements. *Geochemistry, Geophysics, Geosystems*, **2**.

Nell, J. (1985). The Bushveld Metamorphic aureole in the Potgietersrus Area: Evidence for a Two-Stage Metamorphic Event. *Economic Geology*, **80**, 1129-1152.

Newton, R.C. and Haselton, H.T. (1981). Thermodynamics of the garnet-plagioclase-Al_2SiO_5-quartz geobarometer. In R.C. Newton, A. Navrotsky, and B.J. Wood (Editors). *Thermodynamics of Minerals and Melts*, Springer, New York. pp. 131-147,

Newton, R.C. and Perkins, D. (1982). Thermodynamic calibration of geobarometers based on the assemblages garnet-plagioclase-orthopyroxene (clinopyroxene)-quartz. *Amer. Miner.*, **67**, 203-222.

Pattison, D. R. M., Spear, F. S. and Cheney, J. T. (1999). Polymetamorphic origin of muscovite + cordierite + staurolite + biotite assemblages; implications for the metapelitic petrogenic grid and for P-T paths. *Journal of Metamorphic Geology*, **17**, 685 – 703.

Pattison, D. R. M. and Tinkham, D. K. (2009). Interplay between equilibrium and kinetics in prograde metamorphism of pelites: an example from the Nelson aureole, British Columbia. *Journal of metamorphic Geology*, **27**, 249–279

Perchuk, L.L. (1977). Thermodynamic control of metamorphic processes. In: S.K. Saxena and S. Bhattacharji (Editors.), Energetics of Geological Processes. Springer and Verlag, New York.-352pp.

Perchuk, L.L., Podlesskii, K.K. and Aranovich, L.Ya. (1981). Thermodynamic properties of end-member minerals from natural paragenesis. In: R.C. Newton, A. Navrotsky, and Woods, B.J. (Eds.*). Thermodynamics of minerals and melts*.- 304pp.

Perkins and Chipera (1985). Garnet-orthopyroxene-plagioclase-quartz barometry: refinement and application to the English River sub-province and the Minnesota River valley. *Contr. Mineral. Petrol.*, **89**, 69-80.

Pitra, P. and De Waal, S.A., (2001). High-temperature, low-pressure metamorphism and development of prograde symplectites, Marble Hall Fragment, Bushveld Complex (South Africa). *Journal of Metamorphic Geology*, **19**, 311-325.

Pouchou, J.L. and Pichoir, F. (1991). Quantitative analysis of homogeneous or stratified micro volumes applying the model "PAP". In: K.F.J. Heinrich, and D.E. Newbury (Editors.), *Electron Probe Quantitation*. Plenum Press, New York, 31-76

Powell, R. and Holland, T.J.B. (2008). On thermobarometry. *Journal of Metamorphic Geology*, **26**, 155–179.

Rajesh, H.M., Chisonga, B.C., Shindo, K., Beukes, N.J. and Armstrong, R.A. (2013). Petrographic, geochemical and SHRIMP U–Pb titanite age characterization of the Thabazimbi mafic sills: Extended time frame and a unifying petrogenetic model for the Bushveld Large Igneous Province. Precambrian Research 230, 79 – 102.

Raubenheimer, D. (2012). Peak estimates of the peak Bushveld metamorphism in the eastern Bushveld Complex, Limpopo province, South Africa: Constraints from P-T pseudosections. Master's thesis (unpublished), University of Pretoria, Pretoria, South Africa, - 176pp.

Reczko, B.F.F. (1994). The geochemistry of the sedimentary rocks of the Pretoria Group, Transvaal Sequence. PhD Thesis (unpublished), University of Pretoria, Pretoria, South Africa, -385 pp. (Volume 1 = 385 pp.)

Robb, L. J., Robb, V. M. and Walraven, F. (1994). The Albert Silver Mine revisited: towards a model for polymetallic mineralization in granites of the Bushveld Complex, South Africa. Economic Geology Research Unit (EGRU), University of the Witwatersrand. Information Circular, 277, 25pp.

SACS (South African Committee for Stratigraphy) (1980). Stratigraphy of South Africa Part 1: Lithostratigraphy of the Republic of South Africa, South West Africa/Namibia and the Republics of Bophuthatswana, Transkei and Venda, L.E. Kent, Editor, *Handbook Geological Survey South Africa*, **8** , 690pp.

Saggerson, E.P. and Turner, L.M. (1995). A review of Metamorphism in the Republic of South Africa and the Kingdoms of Lesotho and Swaziland. Council for Geoscience. *Geological survey of South Africa*, Pretoria. - 285pp.

Schmidt, A., Weyer, S., Mezger, K., Scherer, E.E., Xiao, Y., Hoefs, J. and Brey, G.P. (2008). Rapid eclogitisation of the Dabie–Sulu UHP terrane: Constraints from Lu–Hf. *Earth and Planetary Science Letters*, **273**, 203–213.

Scherer, E. E., Münker, C. and Mezger, K. (2001). Calibration of the lutetium-hafnium clock. *Science*, **293**, 683-687.

Schreiber, U.M. (1990). A paleo-environmental study of the Pretoria Group in the eastern Transvaal. PhD thesis (unpublished), University of Pretoria, 308pp.

Scoates, J.S., Wall, C.J., Friedman, R.M., VanTongeren, J.A., Mathez, E.A., 2012. Age of the Bushveld Complex. In: Goldschmidt 2012 Conference Abstracts, 22nd V.M. Goldschmidt Conference "Earth in Evolution", Montreal, Quebec, Canada June, 24–29, -234 pp.

Scherstén, A., Årebäck, H., Cornell, D., Hoskin, P., Åberg, A and Armstrong, R. (2000). Dating mafic-ultramafic intrusions by ion-microprobing contact-melt zircon: examples from SW Sweden. Contribution to Mineralogy and Petrology 139, 115-125.

Schmid, R. and Wood, B.J. (1976). Phase relationships in granulite metapelites from the Ivrea-Verbano zone (northern Italy). *Contrib. Mineral. Petrol.*, **54**, 255-279.

Schreyer, W. (1976). Experimental metamorphic petrology at low pressures and high temperatures, in Bailey, D.K. and MacDonald, R,. eds., *The evolution of crystalline rocks*. Academic Press, London, pp. 261-331.

Schweitzer, K, Hatton, C.J. and de Waal, S.A. (1995). Economic potential of the Rooiberg Group: volcanic rocks in the floor and roof of the Bushveld Complex. *Mineralium Deposita*, **30**, 168–177

Sharpe, M.R. (1982). The floor contact of the eastern Bushveld Complex: field relations and petrography. Inst. Geol. Res. Bushveld Complex, Univ. Pretoria, *Res. Rept.*, **36**, 43 pp.

Sharpe and Chadwick (1982), Structures in Transvaal Sequence rocks within and adjacent to the Eastern Bushveld Complex. *Transactions of the Geological Society of South Africa*, **85**, 29-41.

Sharpe, M.R. (1985). Strontium isotope evidence for preserved density stratification in the main zone of the Bushveld Complex, South Africa. *Nature*, **316**, 197-203.

Söderlund, U., Patchett, J. P.,Vervoort, J. D. and Isachsen, C. E. (2004). The ^{176}Lu decay constant determined by Lu-Hf and U-Pb isotope systematics of Precambrian mafic intrusions. *Earth and Planetary Science Letters*, **219**, 311-324.

Spear, F. S. and Selverstone, J. (1983). Quantitative P-T paths from zoned minerals: theory and tectonic applications. *Contributions to Mineralogy and Petrology*, **83**, 348-357.

Spear, F. S. (1993). *Metamorphic Phase Equilibria and Pressure-Temperature-Time Paths*. Mineralogical Society of America, Washington DC. -799pp.

Tankard, A. J., Jackson, M. P. A., Eriksson, K. A., Hobday, D. K., Hunter, D. R. and Minter, W. E. L. (1982). Crustal Evolution of Southern Africa. Springer-Verlag. New York. United State of America. -523pp.

Thompson J.B. Jr (1957). The graphical analysis of mineral assemblages in pelitic schists. *American Mineralogy*. **42**, 842–858.

Thompson, A.B. (1976). Mineral reactions in pelitic rocks: II. Calculation of some P-T-X (Fe-Mg) phase relations. *Amer. J. Sci.*, **276**, 425-454.

Tracy, R.J., Robinson, P. and Thompson, A.B. (1976). Garnet composition and zoning in the Determination of temperature and pressure of metamorphism, central Massachusetts. *American Mineralogist*, **61**, 762-775.

Uken, R. (1998). The geology and structure of the Bushveld Complex metamorphic aureole in the Olifants River area. PhD thesis (unpublished), University of Natal, Durban. South Africa. 277pp.

Van Biljon, S. (1936). Limestones in the upper part of the Pretoria series. *Transaction of geological society of South Africa*, **39**, 45-76.

Vance, D. and Holland, T.J.B. (1993). A detailed isotopic and petrological study of a single garnet from the Gassetts Schist, Vermont. *Contribution to Mineralogy and Petrology*, **114**, 101–118.

Vervoort, J. D., Patchett, P. J., Söderlund, U. and Baker, M. (2004). Isotopic composition of Yb and the determination of Lu concentrations and Lu/Hf ratios by isotope dilution using MC ICPMS. *Geochemistry, Geophysics, Geosystems*, **5**, doi:10.1029/2004GC000721

Wallmach, T., Hatton, C.J. and Droop, G.T.R. (1989). Extreme facies of contact metamorphism developed in calc-silicate xenoliths in the eastern Bushveld Complex. *Canadian Mineralogist*, **27**, 509-523.

Wallmach, T., Hatton, C.J., De Waal, S.A. and Gibson, R.L. (1995). Retrogressive hydration of calc-silicate xenoliths in the eastern Bushveld complex: evidence for late magmatic fluid movement. *Journal of African Earth Sciences*, **21**, 633-646.

Walraven, F., Armstrong, R. A. & Kruger, F. J. (1990). A chrono-stratigraphic framework for the north–central Kaapvaal Craton, the Bushveld Complex and Vredefort structure. *Tectonophysics*, **171**, 23–48.

Wang, P., Spear, F.S., 1991. A field and theoretical analysis of garnet + chlorite + chloritoid + biotite assemblages from the tri-state (MA, CT, NY). area, U. S. A. Contributions to Mineralogy and Petrology, **106**, 217–235.

Waters, D.J. and Lovegrove, D.P. (2002). Assessing the extent of disequilibrium and overstepping of prograde metamorphic reactions in metapelites from the Bushveld Complex aureole, South Africa. *Journal of Metamorphic Geology*, **20**, 135-149.

Wells (1979; cited in Uken, R. (1998). The geology and structure of the Bushveld Complex metamorphic aureole in the Olifants River area. PhD thesis, University of Natal, Durban. 277pp.

Wood and Fraser (1976, cited in Hulbert, L.J. and Sharpe, M.R. 1981). Andalusite-biotite-cordierite-muscovite hornfels, Faugha Ballagh. In: C.F. Vermaak, and G. Vongrunewladt, (Editors). *3rd International Platinum Symposium, Executive guide book*, 39-41.

Wolf D. E., Andronicos, C.L., Vervoort, J.D., Mansfield M.R. and Chardon D. (2010). Application of Lu–Hf garnet dating to unravel the relationships between deformation, metamorphism and plutonism: An example from the Prince Rupert area, British Columbia. *Tectonophysics*, **485**, 62–77.

Wu, C. M., Zhang, J. and Ren, L.D. (2004b). Empirical garnet–biotite–plagioclase–quartz (GBPQ) geobarometry in medium- to high-grade metapelites. *Journal of Petrology*, **45**, 1907–1921.

Wu, C.M. and Zhao, G. (2006). Recalibration of the Garnet–Muscovite (GM) Geothermometer and the Garnet–Muscovite–Plagioclase–Quartz (GMPQ) Geobarometer for Metapelitic Assemblages. *Journal of Petrology*, **47**, 2357–2368.

Appendix A

Mineral modes calculations and bulk rock re-calculation

An independent method of modal estimation was utilised on scanned polished thin sections and back scattered images using adobe Photoshop CS2. Because in the scanned images some of the minerals like garnet and andalusite have the same colours, the phases had to be picked one by one using the magic wand tool in Photoshop (e.g. Figure 2-1) and thereafter the picture is edited in quick mask mode (Figure 2-2).

Since phases like biotite show a range of colours (e.g. dark to greenish), while other phases could not be easily distinguish from a scanned image, the amount of garnet and andalusite obtained were then subtracted from 100% ((e.g. 100 – (4 + 2) = 96)) and the remainder was said to represent the matrix phases which could be easily distinguished on a backscattered image.

Once the picture is opened, on the tool bar there's a select option where colour range can be chosen, thereafter a selection tool can be used to select the phase of interest at least four different grains of the same phase, automatically the grains will be assigned the same colour, then press ok to get the number of pixels. These pixel sizes can then be divided by the total number of pixels multiply by 100 to obtain the percentage of the percentage of that phase within the representative chosen area.

Once all the mineral modes have been calculated, they were then be inserted on the phase rock maker sheet, mode column in accordance with the stoichiometric mineral formula calculations from EPMA data (e.g. Figure 2-4), for more information on rock maker application the reader is referred to Büttner, (2012).

P-T error estimate calculation

Errors in calculating pseudosections and isopleth thermobarometry can be subdivided into thermodynamic, analytical and geological errors. Errors attributed to thermodynamic data represent systematic errors which affect the overall accuracy of the pseudosection, whilst analytical and geological errors represent random errors which affect the precision of the results. For a more detailed explanation of errors associated with thermodynamic data the reader is referred to (Powel and Holland, 1988; Powell and Holland, 1994; Holland and Powell, 1998; Worley and Powell, 2000).

The errors resulting from the thermodynamic data are constant throughout the pseudosection calculations (Evans, 2004) and the activity composition (a-X) models also introduce constant errors between different calculations of the same type (Worley and Powel, 2000).

The errors of the estimated P-T conditions for sample DY954 and DY956 in chapter 4, were calculated from the isopleth intersections of biotite (Mg#), garnet (X_{alm}) and plagioclase (X_{ab}) occurring within a P-T field that represent equilibrium conditions. The estimated errors for DY954 are actually 30 ^{0}C at 0.35 kbar (Figure 2-5) and 13 ^{0}C at 0.3 kbar for DY956 (Figure 2-6), whilst the estimated error for DY918 calculated from the isopleth intersections of chlorite (Mg#), garnet (X_{prp}) and plagioclase (X_{ab}) are 13 ^{0}C at 0.2 kbar (Figure 2-7).

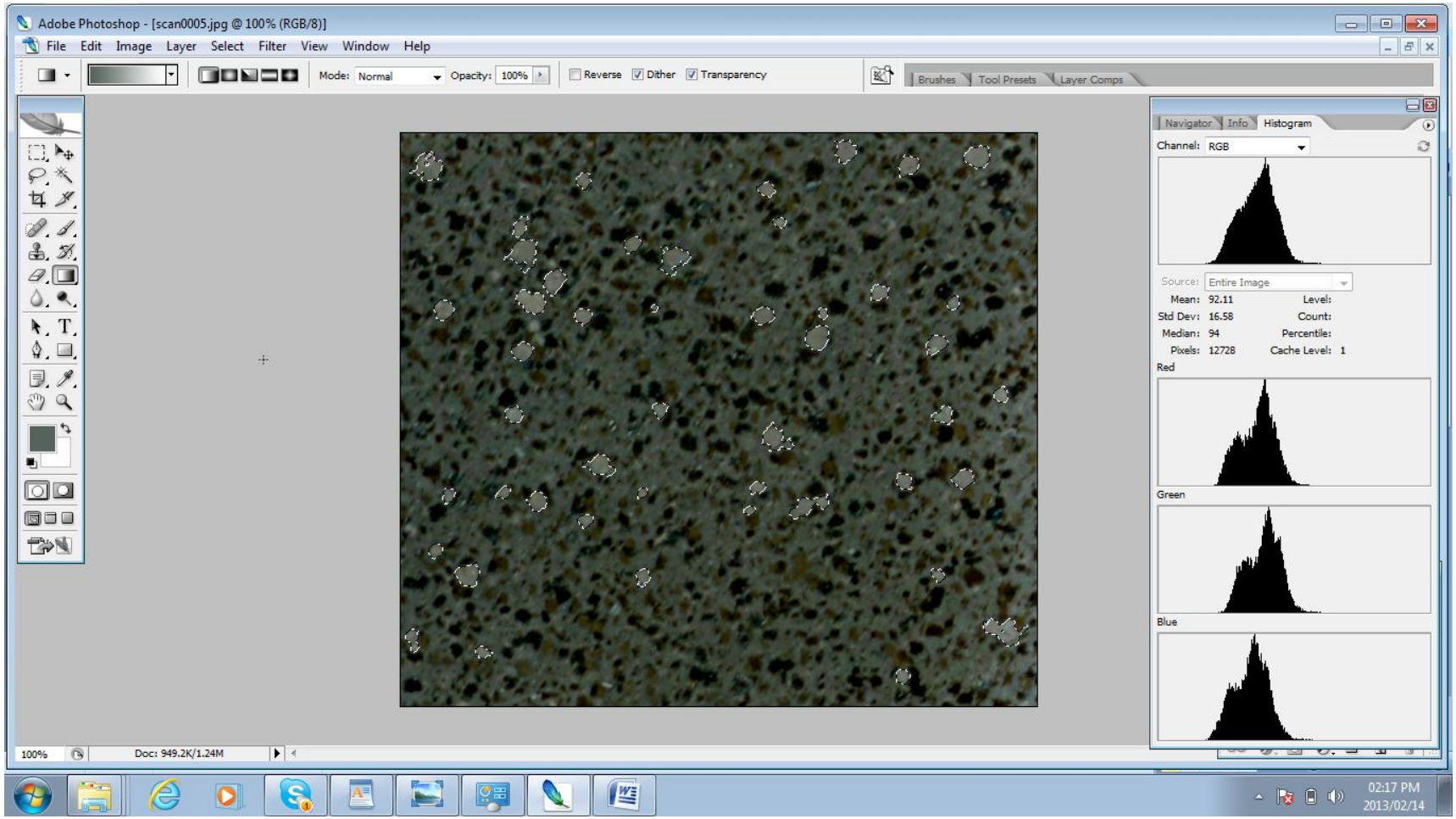

Figure A-1. Section of a polished thin-section showing distribution of phases and the selection of garnet porphyroblasts, selected by magic wand tool.

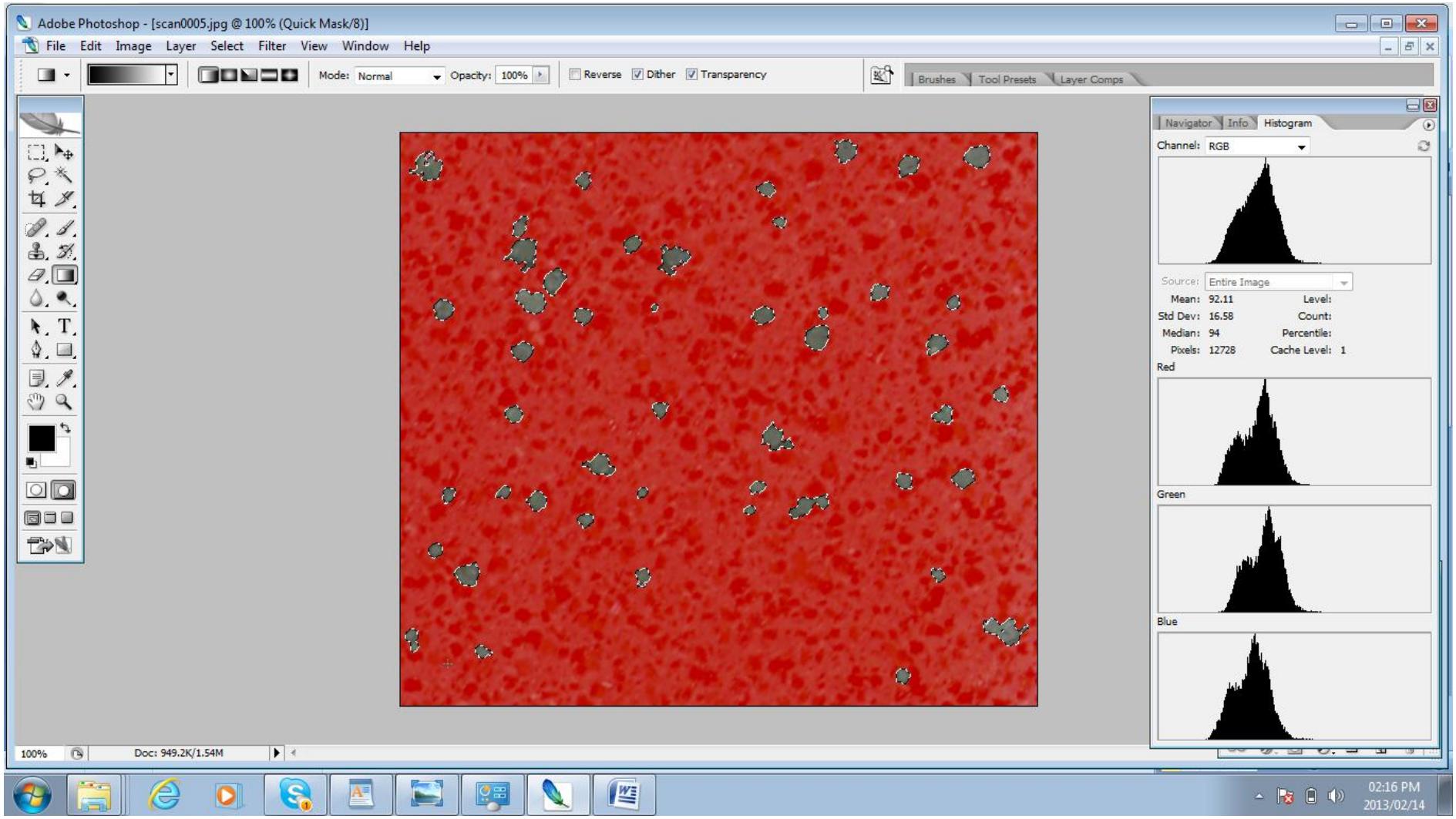

Figure A -2. Section of a polished thin-section showing distribution of garnet porphyroblasts edited in quick mask mode, The right hand side shows the normal distribution of garnet within this field and number of pixel sizes that it account for with respect to the other phases.

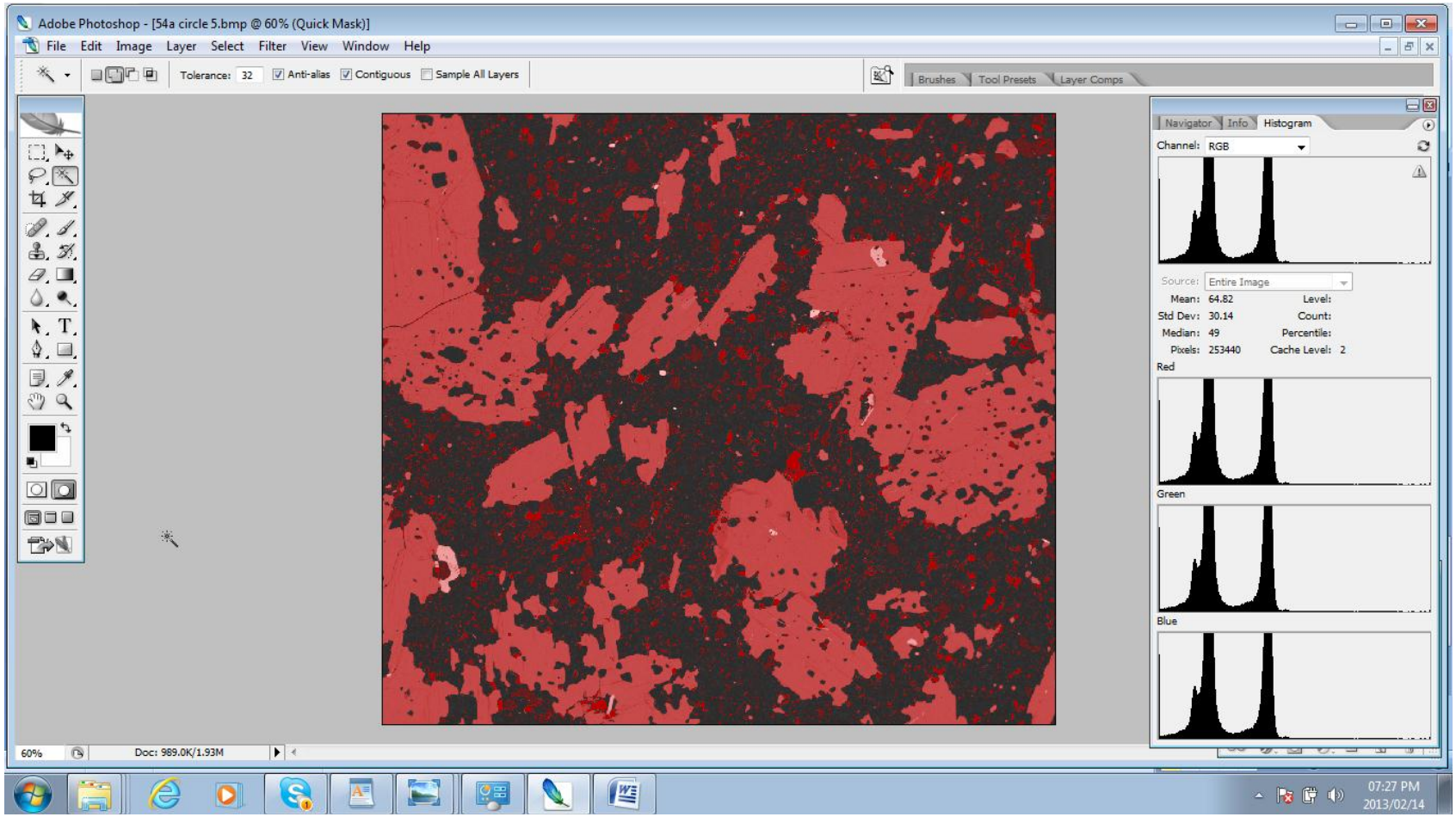

Figure A-3. Back scattered image showing colour contrast of the different mineral phases with the rock, The orange colour represent biotite flakes, pinkish represent ilmenite, black represent plagioclase and reddish is quartz The right hand side shows the total number of pixel sizes with respect to all the phases.

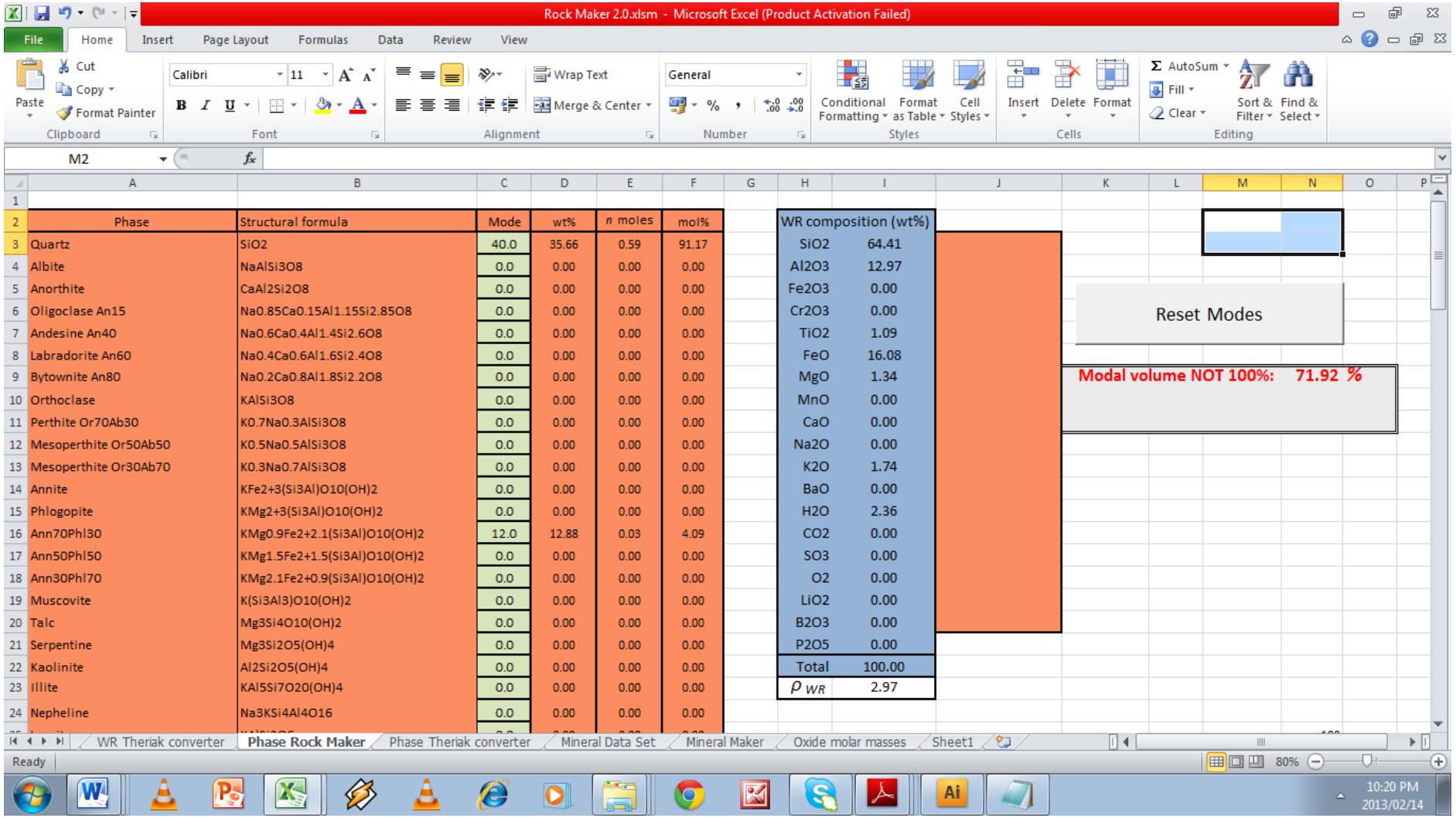

Phase	Structural formula	Mode	wt%	n moles	mol%
Quartz	SiO2	40.0	35.66	0.59	91.17
Albite	NaAlSi3O8	0.0	0.00	0.00	0.00
Anorthite	CaAl2Si2O8	0.0	0.00	0.00	0.00
Oligoclase An15	Na0.85Ca0.15Al1.15Si2.85O8	0.0	0.00	0.00	0.00
Andesine An40	Na0.6Ca0.4Al1.4Si2.6O8	0.0	0.00	0.00	0.00
Labradorite An60	Na0.4Ca0.6Al1.6Si2.4O8	0.0	0.00	0.00	0.00
Bytownite An80	Na0.2Ca0.8Al1.8Si2.2O8	0.0	0.00	0.00	0.00
Orthoclase	KAlSi3O8	0.0	0.00	0.00	0.00
Perthite Or70Ab30	K0.7Na0.3AlSi3O8	0.0	0.00	0.00	0.00
Mesoperthite Or50Ab50	K0.5Na0.5AlSi3O8	0.0	0.00	0.00	0.00
Mesoperthite Or30Ab70	K0.3Na0.7AlSi3O8	0.0	0.00	0.00	0.00
Annite	KFe2+3(Si3Al)O10(OH)2	0.0	0.00	0.00	0.00
Phlogopite	KMg2+3(Si3Al)O10(OH)2	0.0	0.00	0.00	0.00
Ann70Phl30	KMg0.9Fe2+2.1(Si3Al)O10(OH)2	12.0	12.88	0.03	4.09
Ann50Phl50	KMg1.5Fe2+1.5(Si3Al)O10(OH)2	0.0	0.00	0.00	0.00
Ann30Phl70	KMg2.1Fe2+0.9(Si3Al)O10(OH)2	0.0	0.00	0.00	0.00
Muscovite	K(Si3Al3)O10(OH)2	0.0	0.00	0.00	0.00
Talc	Mg3Si4O10(OH)2	0.0	0.00	0.00	0.00
Serpentine	Mg3Si2O5(OH)4	0.0	0.00	0.00	0.00
Kaolinite	Al2Si2O5(OH)4	0.0	0.00	0.00	0.00
Illite	KAl5Si7O20(OH)4	0.0	0.00	0.00	0.00
Nepheline	Na3KSi4Al4O16	0.0	0.00	0.00	0.00

WR composition (wt%)	
SiO2	64.41
Al2O3	12.97
Fe2O3	0.00
Cr2O3	0.00
TiO2	1.09
FeO	16.08
MgO	1.34
MnO	0.00
CaO	0.00
Na2O	0.00
K2O	1.74
BaO	0.00
H2O	2.36
CO2	0.00
SO3	0.00
O2	0.00
LiO2	0.00
B2O3	0.00
P2O5	0.00
Total	100.00
ρ_{WR}	2.97

Figure A-4. Example of the whole rock calculation from Rock maker 2.0 (after Büttner, 2012).

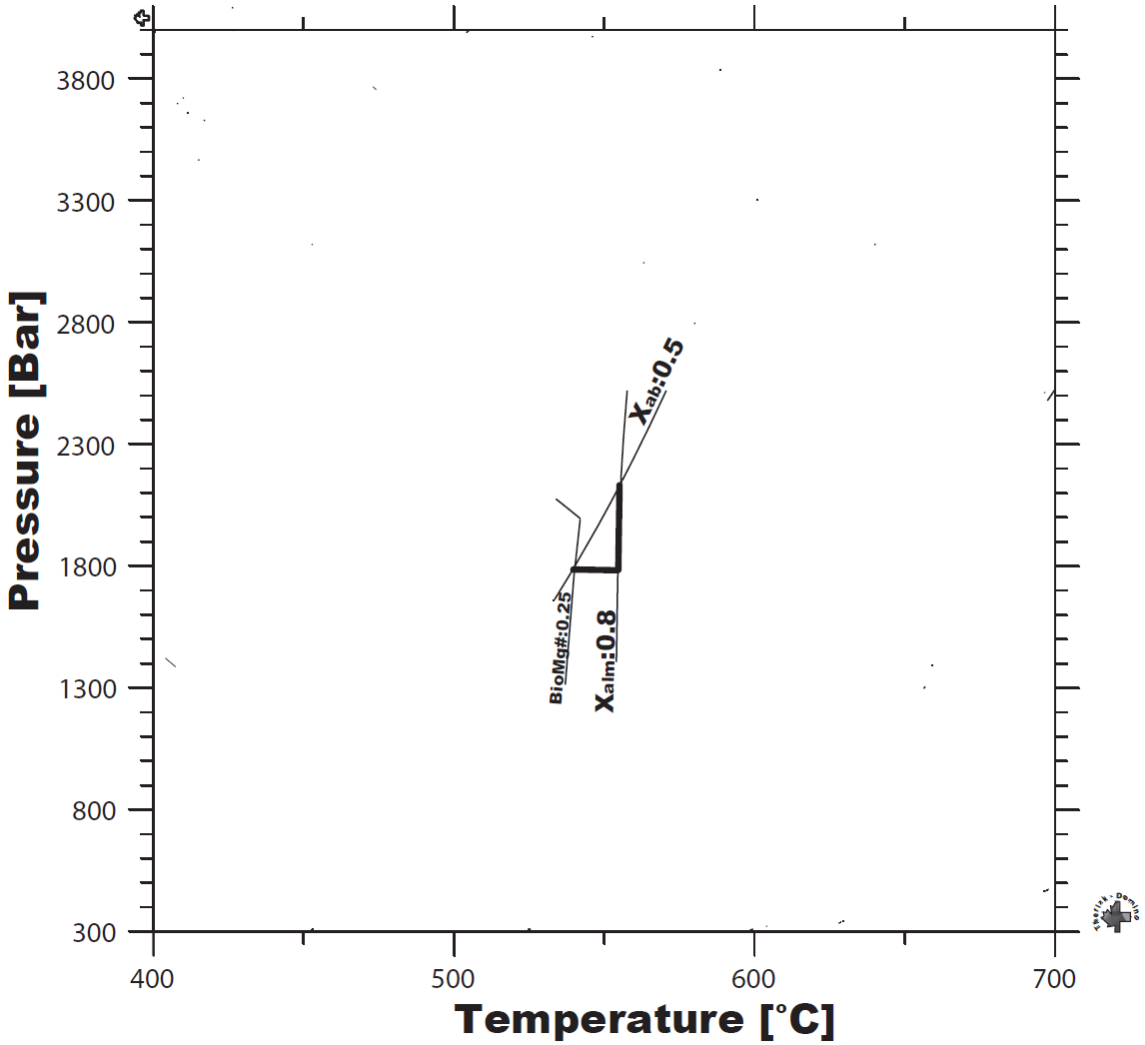

Figure A-5. Isopleth intersections of biotite, plagioclase and garnet showing the error associated with the estimated equilibrium P-T conditions for sample DY954.

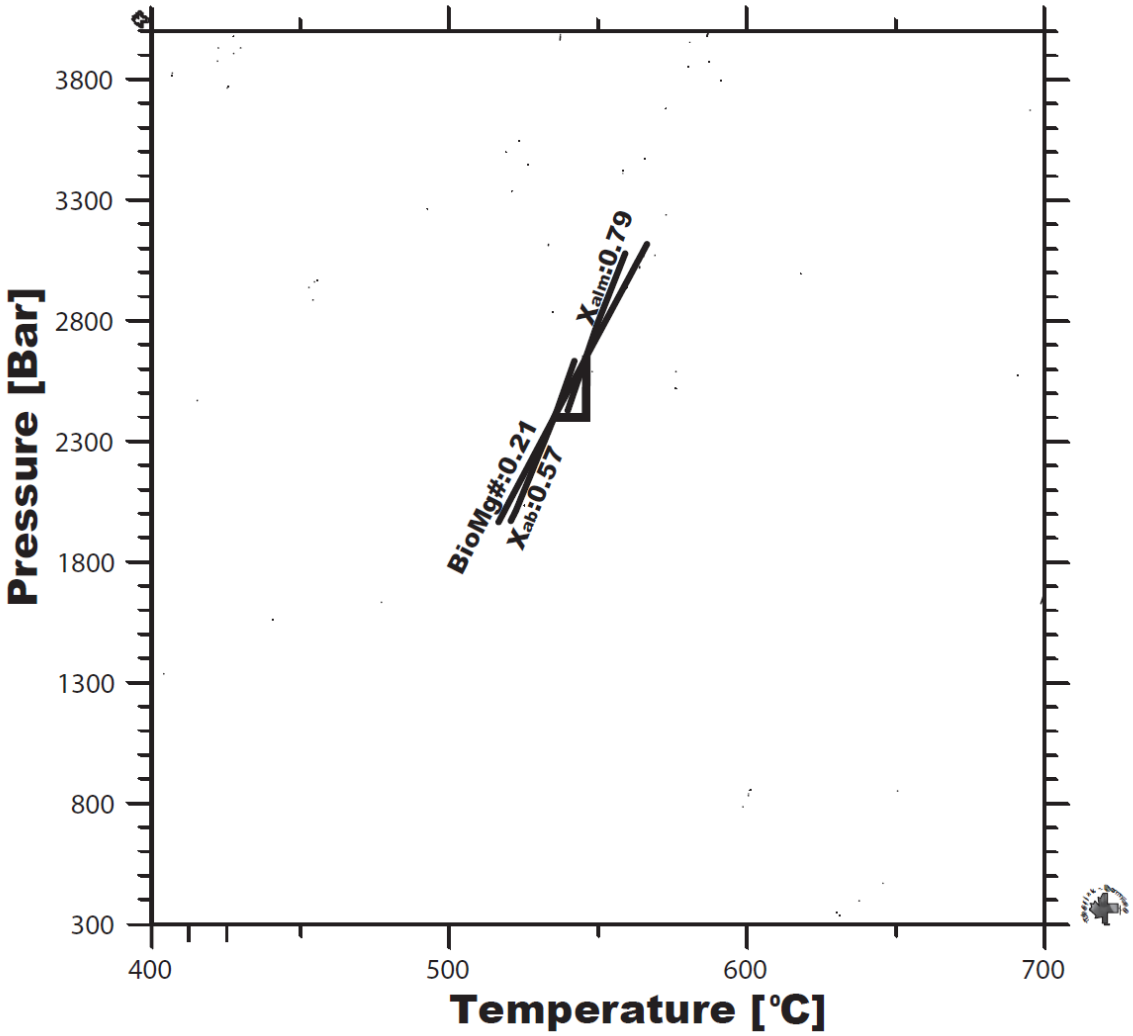

Figure A-6. Isopleth intersections of biotite, plagioclase and garnet showing the error associated with the estimated equilibrium P-T conditions for sample DY956.

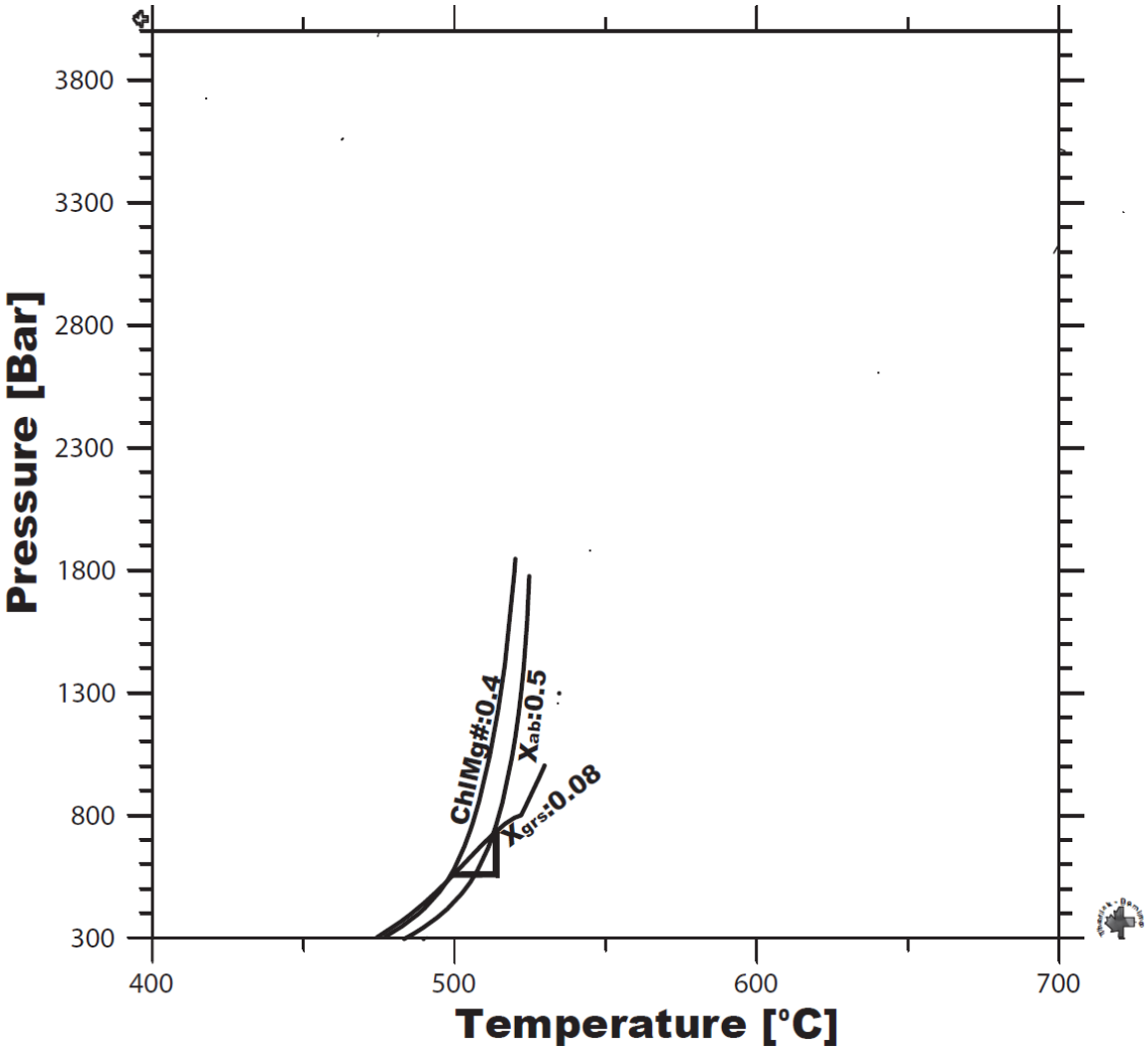

Figure A-7. Isopleth intersections of biotite, plagioclase and garnet showing the error associated with the estimated equilibrium P-T conditions for sample DY918.

Appendix B

Electron probe analysis data is available on a disc accompanying this thesis